HYGROTHERMAL EFFECTS OF AIR CAVITIES BEHIND CLADDINGS ON BUILDING ENVELOPES

A Dissertation
Submitted to the Graduate Faculty
of the
North Dakota State University
of Agriculture and Applied Science

By

Yanmei Xie

In Partial Fulfillment of the Requirements
for the Degree of
DOCTOR OF PHILOSOPHY

Major Department:

Civil, Construction and Environmental Engineering

August 2022

Fargo, North Dakota

North Dakota State University

Graduate School

Title

HYGROTHERMAL EFFECTS OF AIR CAVITIES BEHIND SIDING ON BUILDING ENVELOPES

By

Yanmei Xie

The Supervisory Committee certifies that this ***disquisition*** complies with

North Dakota State University's regulations and meets the accepted standards

for the degree of

DOCTOR OF PHILOSOPHY

SUPERVISORY COMMITTEE:

Huojun Yang
Chair

Jerry (Zhili) Gao

Eric Asa

Yao Yu

Xiangfa Wu

Approved:

November 14, 2022
Date

Xuefeng Chu
Department Chair

ABSTRACT

Air cavity behind claddings within building envelope provides an approach to mitigating building moisture-related issues as well as improving the building's thermal performance. However, studies in literature commonly assume the cavity air as still and thus neglect the influence of mixed convection on the performance of building envelope. In addition, the drying performance of the air cavities remains unknown, and commonly a rectangular unicellular cavity is improperly assumed to simplify the investigation of the hygrothermal performance of a cladding system. Moreover, the literature lacks a study of the effect of humid air in the air cavity on heat and mass transfer. Therefore, it necessitates advanced problem formulation and solving to comprehensively study the effects of air cavities behind claddings on the performance of building envelope.

The specific objectives are to 1) investigate potential of self-drying siding with raised air cavities for building envelopes; 2) study the effects of the cavity depth in mixed convection of air cavity for building envelopes; 3) analyze the effects of humid air in an air cavity on mass and heat transfer with phase change at the wall. To achieve these objectives, firstly, this study redefines the drying potential of air cavity taking into account the air cavity depth related to the shape irregularity and the inlet and outlet uncertainties. Then the formulated problems of mixed convection of air cavities behind sidings are solved with a perturbation method and SIMPLER algorithm. The results show that the drying performance is found to be heavily dependent on the cavity depth. Further, increasing the ratio of the siding depth to the air cavity depth amplifies the cavity air's velocity, temperature, and mass fraction at cavity walls, as well as the heat and mass transfer across cavities. Consequently, this study demonstrated that humid air with the phase change and the cavity depth have significant effects on the hygrothermal performance of

building envelopes. The outcome of this study provides valuable guidance on the thermal performance evaluation of air cavity and has the potential of improving the design of claddings for the overall hygrothermal performance of building envelope.

ACKNOWLEDGMENTS

First, I would like to thank my academic advisor Dr. Huojun Yang. I would not have been able to complete my dissertation without his considerable and consistent support, helpful suggestions, and valuable encouragement on my research during my Ph.D. study. In addition, I would like to thank my committee members: Dr. Jerry Gao, Dr. Eric Asa, Dr. Yao Yu, and Dr. Xiangfa Wu. They provide their expert suggestions on my research, which allows me to further improve my dissertation

Furthermore, I would like to thank the Department of Civil, Construction and Environmental Engineering and College of Engineering at North Dakota State University for financial support during this research and my master program.

Finally, it is a pleasure to thank all graduate students in my office. They provide me with a pleasant working environment. I would like to extend my gratitude to all my family who kept caring and supporting me during my progress.

TABLE OF CONTENTS

LIST OF TABLES

LIST OF FIGURES

NOMENCLATURE

V	Wind velocities at height z
V_0	Wind velocities at the reference height z_0
n	An exponent dependent on the stability of the atmosphere
ρ	Fluid density
t	Time
v	Flow velocity vector field
$\sum Q$	Sum of volume flow rate into the cavity
p	The pressure in moving air
g	Gravitational
P_e	Outside opening pressures
P_i	Inside opening pressures
c	Loss coefficient,
l_e	Effective length through the inlet or outlet
Q	Air flow rate through the opening
A	Area of the opening
ΔP_f	Pressure gradient across the opening caused by the wall friction
f	Friction factor
h	Cavity height
D_h	Hydraulic diameter
P_1	Entrance pressure of the cross sections
P_2	Exit pressure of the cross sections
V_1	Entrance velocity

V_2	Exit velocity
C_c	Coefficient of contraction
K	Coefficient caused by the concentrations.
$\Delta P_{unsteady}$	Air differential pressures across the cavity's segment caused by unsteady flow
m	Number of the sudden enlargement and contraction of cross-section
P_{c1}	Air pressure at the closest points from the cavity opening along the air flow direction
P_{cf}	Air pressure at the farthest points from the cavity opening along the air flow direction
P_i	The external pressures at the ith opening
P_{i+1}	The external pressures at the (i+1) th opening
V_i	Inlet velocity at the ith opening
V_{i+1}	Inlet velocity at the (i+1) th opening
$P_{i,i}$	Internal pressure at the ith openings in the cavity
$P_{i,i+1}$	Internal pressure at the (i+1) th openings in the cavity
d	Air cavity depth
l	Grove width
s	Groove depth
λ	Period of the groove
U	Velocity components along X axis
V	Velocity components along Y axis
β	Coefficients of thermal expansion without mass fraction
β^*	Coefficients of thermal expansion with mass fraction

T	Fluid temperature
$\bar{T}$	Average of temperature at the wall sheathing and vinyl siding
w	Mass fraction (kg of vapor/kg of mixture)
$\bar{w}$	Average of mass fraction at the wall sheathing and vinyl siding
μ	Dynamic viscosity of fluid
k	Thermal conductivity
C_p	Specific heat at constant pressure
D_m	Coefficient of mass diffusivity
T_0	Temperature at the wall sheathing
T_1	Temperature at the vinyl cladding
U_∞	Air velocity at the inlet
R_e	Reynolds number
P_r	Prandtl number
g_t	Local temperature Grashof number
g_c	Local mass Grashof number
S_c	Schmidt number
a	Dimensionless groove depth of vinyl siding
ε	Dimensionless air cavity depth
τ	Dimensionless shear stress
τ^0	Dimensionless shear stress at the flat wall
τ^1	Dimensionless shear stress at the groove wall
Nu	Dimensionless Nusselt number
Nu^0	Dimensionless Nusselt number at the flat wall

Nu^1	Dimensionless Nusselt number at the groove wall
Sh	Dimensionless Sherwood number
Sh^0	Dimensionless Sherwood number at the flat wall
Sh^1	Dimensionless Sherwood number at the groove wall
n	Dimensionless temperature
m	Dimensionless mass fraction
v	Kinematic viscosity
Φ	Humidity ratio
Ve	Transverse velocity at the interface
C	Fluid concentration
$\bar{C}$	Average of concentration at the wall sheathing and brick veneer

1. INTRODUCTION

1.1. Background

People living in Northern American spend more time of their lives in buildings due to the cold weather in the winter and spring. Therefore, the environmental conditions of the buildings affect their life's quality and productivity. Moreover, the connection between, the construction and maintenance of buildings, and the energy consumptions and climate change, are stronger and stronger over time (Straube, 1999).

Buildings play a significant role in human activities. However, most of the buildings in the period of service life have defects, which decreases the lifespan of the building, dissatisfies the in-service performance, and fails of the building enclosures. The building enclosures failure mainly include roof and façade failures that account for the large portions of American building defect (Straube, 1999). Moisture is one of the leading factors to cause the failure of the building enclosures, especially in the cold States of United States. The majority of time and effort is spent to control the moisture for the building enclosures in North America. Therefore, full understanding of the moisture movement inside/outside the building enclosure is significantly important to control and avoid the moisture related issues.

Additionally, people are concerned more and more about climate changes because greenhouse gas warms the Earth's surface. However, the building energy consumption contributes to 43.6% of total energy consumption and building carbon dioxide emission accounts for 23% (Berger et al. 2015). Therefore, it is necessary to improve the energy efficiency of building, in order to decrease the energy consumption and CO2 emissions.

In the literature, there have been many technical renovations of buildings to improve the energy efficiency and control the moisture, such as improving the insulations, installing the

ventilation devices to ventilate the wall through proposing net zero buildings, etc. (Ghrissi et al. 2021). Among them, air cavity between the cladding and wall sheathing are used as the ventilation system to improve the energy efficiency and control the moisture of the building envelopes.

1.2. Objectives

Studies in literature commonly assume the cavity air as still and thus neglect the influence of mixed convection on the performance of building envelope. In addition, the drying performance of the air cavities behind the siding remains unknown, and commonly a rectangular unicellular cavity is improperly assumed to simplify the investigation of the hygrothermal performance of a siding system. Moreover, the literature lacks a study of the effect of humid air in the air cavity between the siding and wall sheathings on heat and mass transfer in a cavity with evaporation or condensations. Therefore, it necessitates advanced problem formulation and solving to comprehensively study the effects of air cavities behind siding on the performance of building envelope.

The main objective of this study is to investigate the hygrothermal performance of the wall claddings. Increasing the understanding of interaction of the heat, air, and moisture in the air cavity is of special interest. Vinyl siding wall systems and masonry wall systems are the two focuses of the study because of their widespread use.

1.3. Outlines

This thesis consists of seven chapters. Chapter 1 introduces the backgrounds, objectives, and the outlines.

Chapter 2 introduces air cavity behind claddings, the function of the air cavity, comparing the effects of air cavity on different types of the claddings, and effects of the air cavity in the building envelopes.

Chapter 3 studies the air flow within air cavities behind a residential vinyl siding, analyzes the effects of moist in air cavities on the hygrothermal performance of building envelopes, evaluates the drying potential of a siding system through the air flow rate within the cavities, and proposes a new self-drying siding with optimally raised air cavities for residential building envelopes.

Chapter 4 studies ratios of vinyl siding depth to air cavity depth in mixed convection of air cavity behind vinyl siding for building envelopes and adopts the perturbation technique to solve the governing equations with specified boundary conditions. The effects of the critical parameters, including the Reynolds number, the air cavity depth, the dimensionless temperature on the walls, and the dimensionless air mass fraction, on the velocity, temperature, and mass fraction distribution of the fluid motion as well as the skin friction and the rate of heat and mass transfers at the walls are discussed.

Chapter 5 redefines the heat and mass transfer problem in air cavity with humid air considering condensation or evaporation at the interface between the film and air. To analyze this, the partial differential equations are solved using the SIMPLER algorithm with considering the axial diffusion terms. The effect of inlet air conditions (the inlet air temperature, inlet air vapor content, and Reynolds numbers) on the axial evolutions of the transverse velocity at the interface, average air temperature, average air vapor content, friction factors, the sensible and latent Nusselt number, and the Sherwood number are investigated. The results of heat and mass transfer analysis

approve the significant effects of convection on the comprehensive performance of building envelopes with sidings.

Chapter 6 analyzes the heat and mass transfer problem in the air cavity considering the effects of condensation or evaporation of humid air and the depth of the air cavity, based on the mathematical model built in Chapter 5. The effect of inlet air conditions (the inlet air temperature, inlet air vapor content) on the axial evolutions of the transverse velocity at the interface, average air temperature, average air vapor content, the sensible and latent Nusselt number, and the Sherwood number are investigated.

Finally, Chapter 7 presents the critical findings of this dissertation and Chapter 8 proposes idea thoughts for future research on hygrothermal performance of the wall claddings related to this dissertation.

2. AIR CAVITY BEHIND CLADDINGS

This chapter will introduce air cavity behind claddings, the function of the air cavity behind claddings, the effects of air cavity on types of the claddings, and effects of the air cavity in the building envelopes.

2.1. Air Cavity

The movement of moisture or water vapor includes 1) moving with the air, 2) diffusing through materials, 3) moving with heat transfer, etc. Among them, air movement accounts for more than 98% of vapor movement in air cavity of buildings (Straube, 1999). Moreover, air moves due to the pressure gradient through holes and cracks into the building envelopes. Compared to moisture transfer by heat transfer and diffusion through materials, moisture transfer by air is a quick process.

Controlling moisture not only can solve the moisture related issues but also can make the building more energy efficient. Air cavities between the exterior and interior walls are designed to reduce environmental loads, and thus preventing moisture into the buildings. Air cavities are formed after the cladding is installed (shown in Figure 1). The cavities are a tiny space providing the path of the gravity and air flow. There are four types of air cavities: unvented, vented, pressure moderated, and ventilated air cavity.

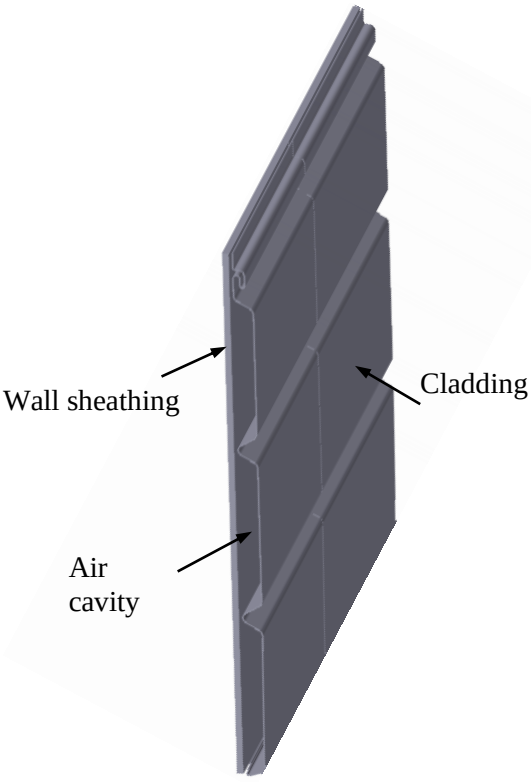

Figure 1. Air cavity

An Unvented air cavity (shown in Figure 2) can be developed in 1800s with the material of walls having the higher strength with the less weight. An unvented cavity has no path which allows air to enter the cavity. Claddings or finishes works as the barrier (Salonvarra et al., 2007). However, this type of cavities has the moisture issues due to that it cannot move the moisture outside of the cavity or cannot dry itself quickly.

Some moisture control designs for the wall systems are evolved, for example pressure-equalized cavity walls. The pressure-equalized cavity walls allow the exterior air into the cavity walls to create the pressure, which helps reduce or remove the moisture in the cavity against the veneer (Kumar, 2000). In reality, there are too many restricted requirements to satisfy a true net-zero pressure differential across a veneer, such as rigidity of the support wall, continuity and tightness air barrier, airtight wall cavity baffles, etc.

Ventilated or vented cavity wall was proposed by Birkeland. A ventilated or vented cavity wall is a more realistic and economical strategy to solve the moisture problems in wall systems. A vented wall system allows water to vapor diffusion air exchange between the cavity and exterior. The vented cavity wall lets the exterior air into the cavity or inside air out of the cavity through vents located at the veneer panels. The vented walls have less moisture related issues such as cracking, spalling, staining, etc. (Rahiminejad & Khovalyg, 2021). In some cases, the vented or ventilated cavity wall helps prevent chronic efflorescence compared to the unvented cavity wall.

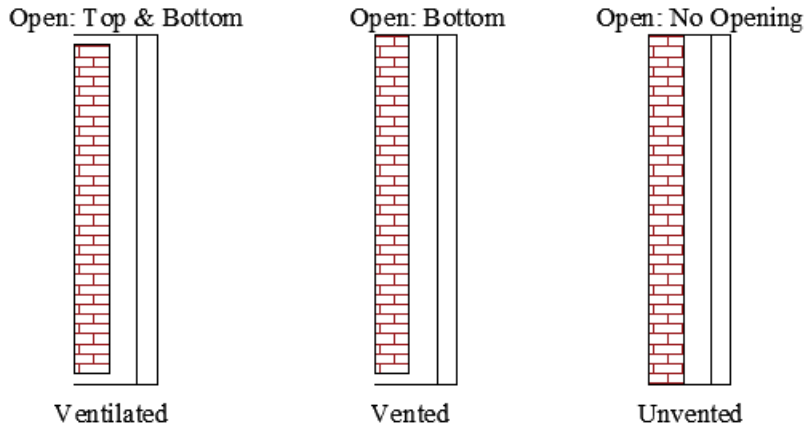

Figure 2. Air cavity ventilation systems

In order to have more water vapor diffusion and more air exchange between the cavity and exterior, the ventilated cavity is proposed. This type of wall system not only can provide the mechanism for drying the inner wythe and the claddings, but also can diffuse the moisture out of the inner wythe. Compared to the vented cavity, the ventilated cavity allows a remarkable airflow in or out of the cavity. Ventilated air cavities would be a most welcomed method to provide free drying.

2.2. Functions of Air Cavity

Air cavities provide functions listed as follows:

1) prevent both bulk water and capillary moisture flow into the wall cavity,

2) provide a drainage for incidental rain, water or condensation water

3) remove evaporated/ desorbed moisture from the inner wall or absorptive claddings through ventilation,

4) can potentially permit pressure equalization of the system to prevent water infiltration through the inner wythe and into the inner wall structure.

While the capillary break and drainage functions are obvious, research about the drying effects of ventilation have had contradictory findings. Field and laboratory research has shown that the use of ventilated air spaces behind claddings has the potential to increase drying and reduce wetting from absorptive claddings and sun-driven moisture. However, some mentioned that the ventilated air layer behind claddings does not significantly accelerate drying of a capillary veneer wetted by rain. In the study of full-scale insulated wall assemblies with stucco cladding, the authors concluded that drying was slow for all wall types and that the ventilated rainscreen wall design did not enhance drying of water that penetrates into the stud cavity. Although the cavity ventilation was reported in that study not providing a benefit to moisture reduction, it is well accepted that higher ventilation rates behind the cladding will increase the drying rate of an initially wetted wall. The study also indicated that the ventilation plays a significant role to remove the moisture in the cavity between the vinyl siding and sheathing walls. Once the moisture enters the cavity in a form of bulk liquid and water, the condensation will occur in hot and humid climates. Moreover, higher air exchange will introduce more moisture into the cavity, which leads to reduction of the drying efficiency. The cavity behind the claddings affects the

building performance in several ways. In winter or cold climates, the moisture content of the sheathing increases due to that the vapor moisture migrates from indoor to the outdoor and condenses on the sheathings. Vapor migration helps to remove the moisture generated by occupants and their activities from housing. However, moisture can accumulate on the sheathing during cold weather or even hot weather when the material outside of the wall is impermeable. Therefore, the vapor moisture traps in the air cavity behind cladding and sheathings. Because the walls cannot dry out as readily in warm weather in such cases, moisture contents in the sheathing and other components remain elevated into warm weather. That can lead to staining, mold, and decay. Claddings, especially vinyl sidings, have multiple air paths as the joints are intentionally installed loose to allow for thermal expansion.

The studies of air cavity in the moisture removal have a significant dilemma. Some research shows that the ventilation of air cavity has a positive effect on the drying. Popp indicated that the ventilation of the cavity has the potential to increase the drying and reduce wetting from absorptive claddings (Popp & Mayer, 1981). Straube et al. studied the impact of cavity ventilation on the building performance. The results show that the ventilation has the positive effect on the moisture drying (Mortgage, Corporation, Straube, & Burnett, 1995). Burnett et al. investigated the effect of the opening area on the drying potential. The large opening area, the more drying potential obtain. Canada Mortgage and Housing Corporation (CMHC) investigated the characteristics of ventilation of the cavity behind the claddings including retaining moisture, the rate at which moisture can be dissipated and factors which affect this process, air flow resistance within drainage channels, and air flow water vapor resistance of intermediate joints in the cladding. They concluded that the ventilation helps remove the moisture. Bassett and McNeil (Bassett & McNeil, 2020), and Kristin Nore (Nore, 2010), etc. also obtained the same results that

the ventilation has a positive effect on the drying the moisture for the building envelopes. However, the contractional results are found by other researchers. Kuenzel (Künzel, 1995) measured several of different walls assembled with the brick claddings and concluded that the effect of the ventilation on drying the moisture can be neglected because the moisture content of the veneer walls did not change with the ventilation cavities. TenWolde et al. (TenWolde, Carll, & Malinauskas, 1995) analyzed the multilayer walls and the effect of the air leakage. The results indicated that ventilation or air leakage may lead to the moisture accumulated and has a negative effect on the drying the moisture in the veneers. Hansen et al. (Hansen & Nicolajsen, 2002) conducted the experiment with different walls with different types of cladding and indicated that dry airflow helps remove the moisture out the cavity whereas humid airflow adds the moisture into the cavity. They also found that the moisture content of wood frame walls without a ventilated cavity is as the same as the moisture content with a ventilated cavity. Therefore, they concluded that the ventilation had no significant effect on drying potentials. Lawton et al (Lawton, Brown, & Lang, 1999). obtained the same results through the lab study. Based on the previous studies, it can be found that the field and theoretical studies support that the ventilated cavity has a positive effect on drying whereas the lab tended to show that the ventilated cavity has no effect on drying. Even though the researchers did not obtain the consistent results of the function of the function of the ventilated cavity on the drying, most researcher thought the ventilated cavity has a positive effect on the drying.

The ventilated cavity not only influences drying, but also has an effect on the thermal performance of building envelopes. The studies of air cavity in the thermal performance for building envelopes also have a significant dilemma. Hens (Hens, 1984) conducted the field and lab experiments and indicated that the effect of ventilated air cavity on the heat transmission is

not significant. Jung also obtained the same results that the effect of the higher air flow rate in the air cavity in the heat performance can be ignored (Jung, 1985). These findings challenged the benefits of the ventilated cavity in thermal performance for the building envelopes. However, Uslokk showed that the ventilation of the cavity behind the cladding can reduce the heat loss caused by convection (Uvsløkk, 1988). Some research also indicated that the ventilated air cavity decreases the condensation on the wall sheathings. Moreover, the vent size has a significant influence on the cooling load. Furthermore, under the certain climate conditions, the ventilation air cavity wall has an importunate effect on thermal and moisture performance for the building envelops. Pressnail et al. (Pressnail, Timusk, Kan, Dong, & Kan, 2003) conducted the climate chamber drying study and found that the ventilation significantly reduces the condensation with the air cavity behind the claddings.

2.3. Air Cavity in Types of the Claddings

According to the U.S. Census Bureau statistics (Bureau, 2011), over 60% of all new homes are clad with absorptive materials such as brick, stucco, wood, fiber cement, and stone, etc.

2.3.1. Vinyl siding

According to Figure 3, siding with irregular shape (including wood, fiber cement, and vinyl siding) accounts for over half of all residential claddings, yet the cavities behind this siding have historically had less research focus compared to other cladding types. Despite the extensive use of irregular-shape siding, little research has been focused on the mechanisms of exploiting ventilation air flow within the cavities behind it. This may be due to irregular and complex cavity created behind the siding. Commonly this siding has two installation methods: one with furring strips between the siding and wall sheathing for connections, and the other (i.e., also called as the contact-applied siding) directly attached on the surface of wall sheathing. Due to the simplicity

installation and low cost, the siding without furring is more common in the U.S., and it is the cladding system selected for this research. Then, vinyl siding is selected as the study example as it is the most common residential cladding in the U.S., and its non-absorptivity facilitates further investigating the hygrothermal performance of air cavities behind siding because moisture transfer through the siding can be neglected.

vinyl siding accounts for 37% of the wall cladding for new buildings (Bureau, 2011). Vinyl siding is a type of cladding material used for decorating and weatherproofing with its alternates been aluminum or fiber cement or stucco or any other suitable material. It is manufactured from polyvinyl chloride (PVC) resin by co-extrusion process.

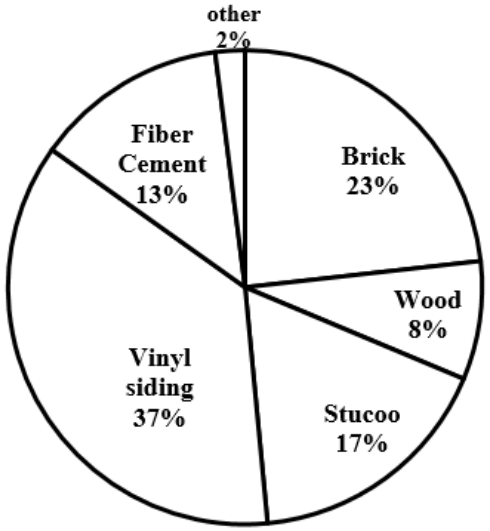

Figure 3. Principal type of exterior wall cladding on new construction

Vinyl siding is the most popular cladding type in residential buildings in North America, because it provides a durable, long lasting, aesthetically pleasing finish as well as low cost. Vinyl siding comes in a variety of shapes, textures, and colors, creating a wide array of looks for different houses. It is manufactured primarily from durable polyvinyl chloride in several different profiles, including single, double, triple, vertical, and Dutch lap (Figure 4)

Single Double Triple Vertical Double dutch lap

Figure 4. Types of vinyl siding

For a contact-applied vinyl siding with irregular shape, since it is directly attached to the surface of wall sheathing through a nailed connection, the small gap attaching the siding with sheathing greatly limits the aforementioned drying functions of air cavity: capillary break, drainage, and ventilation drying. Although moisture may not be absorbed in or penetrate through a non-absorptive material like vinyl siding, it can exist within the cavity behind siding through the siding cracks and the installation joints between two connecting pieces of siding. Moisture issues may further occur within the exterior envelope when the bulk water from incidental leaks or condensed from moisture vapor is stuck within the gap between the siding and the sheathing for an enough long time. Even though a siding system may provide gravity drainage channels to remove bulk water, they are not effective to remove water adhering within the small gap between the siding and the sheathing and it takes a long time for enough water to accumulate to be removed. On the other hand, the cavity behind irregular-shape siding is composed of many small air cavity cells, and each cell is interconnected with another through a small gap between the siding and the wall sheathing. Air leakage occurs at the siding cracks and/or the installation joints of siding pieces, and the air flow paths within the cavity cell can be either vertical (upward, downward) or horizontal. Previous research lacks in the hygrothermal performance of the multicellular cavity, and a rectangular unicellular cavity behind claddings

2.3.2. Brick

Brick is a common cladding material, accounting for 23% of wall cladding for new buildings (shown in Figure 3). Brick claddings have several types, single slots, multiple slots, rectangular, circular, etc. Due to that brick is a hygroscopic porous material, it can store very significant quantities of water. Once bricks reach its saturation moisture content, it will stop to absorb the water. Therefore, the moisture or water will stay at the surface of the brick when brick reaches the saturation moisture content. If the moisture at the surface of brick cannot dry out in time, it may enter the wall sheathings and cause the moisture related issues as described previously. On the other hand, brick has a high thickness that is up to 0.39ft, high conductivity, and high heat cavity. Therefore, bricks have a significant effect on thermal performance for building envelopes.

Different methods are proposed to study the thermal behavior of the air cavity behind the brick cladding. Among them, CFD is the most common used method in the previous studies. For example, Balocco (Balocco, 2009) used the CFD method to develop the 3-D model and investigated the thermal behavior of a ventilated brick walls. Based on CFD models, Van Belleghem et al. (Van Belleghem, Steeman, Janssens, & De Paepe, 2015) proposed a coupled computational Fluid Dynamics and Heat, Air, and Moisture model. It indicted that the stack effect can cause the reversed flow in the air cavity behind bricks under certain climate conditions. Stazi et al. (Stazi, Ulpiani, Pergolini, Di Perna, & D'Orazio, 2020) conducted the experiment to study the variation of heat flows and thermal performance. They found that an external massive brick claddings can reduce both the income and outgoing heat flux.

Ventilated air cavities behind brick claddings plays an important role in dryings. As known, ventilation is mainly driven by the pressure differential and thermal buoyance. The

opening position had a significant effect on the ventilation. The openings at the top and bottom of the cavity will cause the most ventilation (Rahiminejad & Khovalyg, 2021). A very well-ventilated cavity walls provide the small amount of cooling. Moreover, the drying rate depends on the ventilation flow rate. the higher ventilation flow rate, the higher drying rate will obtain (Salonvarra et al., 2007). The high permeance causes the high relative humidity at the surface of sheathing. The consistent of moisture contents of the sheathing cause less dimensional change, which will reduce cracking. Therefore, it is important to keep the moisture content of the sheathing the same. Furthermore, solar heating helps increase the ventilation flow rate, which indirectly affects the drying rate.

2.3.3. Stucco

Stucco is an exterior plaster, which can be directly applied to masonry or concrete walls and wood-framed walls. Stucco is traditionally made with lime, sand, water, and fibers. Modern stucco typically contains Portland cement, sand, and water. Acrylic stucco (sometimes called synthetic stucco) is sometimes used to provide a crack resistant finish over cement. Stucco cladding is found on low to mid rise buildings, uncommon to find on tall stories buildings.

Compared to the brick claddings, the use of stucco trended upward in recent years. That is because stucco has several advantages listed as follows(Rahiminejad & Khovalyg, 2021). :

1) A durable, energy-efficient siding material
2) Tight sealing properties make it a great noise barrier
3) A fire retardant
4) Resistant to mold, mildew, and rot
5) Little maintenance throughout its long-life expectancy

However, it also has several significant disadvantages(Salonvarra et al., 2007):

1) Expensive installation costs as it often requires multiple layers
2) Not suitable for extremely wet climates or frequent heavy rains
3) Time-consuming for repainting stucco

Compared to the brick cladding wall, the thickness of stucco is small which reaches up to 0.16ft (0.05 m) (Rahiminejad & Khovalyg, 2021), and the thermal conductivity of stucco cladding is high. Therefore, the temperate gradient of the stucco cladding is less than the brick claddings. Because stucco is a thin cladding, its water storage capacity can quickly be reached in rainy climates. Stucco is a porous building material as brick. Therefore, the drainage cannot start until the stucco reaches the saturation moisture content or the rate of wetting is larger than the rate of absorption. Ge and Ye (Ge & Ye, 2007) studied the effect of ventilation on the cavity wall and showed that the ventilation has a small influence on the temperature profile in the air cavity behind stucco claddings. The moisture flux across the cladding is greater than the other part of the wall, especially for the absorbed cladding materials.

2.3.4. Fiber cement

Fiber Cement was invented by Czech engineer Ludwik Hatschek and has been used for over 100 years. It is produced in sheets and fabricated into finished panels. Fiber cement boards are made of 50%-70% cement, fibers, and fillers. It has several advantages listed as follows (Rahiminejad & Khovalyg, 2021):

1) High bending strength
2) Moisture resistance
3) Biological corrosion
4) Fire resistance
5) Environment friendly

6) Low cost

Fiber cement is sensitive to moisture change in both material and the external environment. The strength of fiber cement decreases with the increase of water content. Because the bond between cement and fiber is weak when the moisture content is large. Therefore, it is significant to keep the fiber cement dry. Langmans and Roles (Langmans & Roels, 2015) investigated brick and fiber cement cladding systems, and indicated that the pressure differential of fiber cement cladding system is much higher than the brick cladding systems. Therefore, ventilation rate of the fiber cement is higher than brick cladding, and the potential drying of the fiber cement is better than brick claddings.

2.4. Conclusions

This chapter introduces the air cavity behind claddings, the function of the air cavity behind claddings, and the types of claddings. The main results are listed as follows:

1) The field and theoretical studies support that the ventilated cavity has a positive effect on drying whereas the lab tended to show that the ventilated cavity has no effect on drying. Even though the researchers did not obtain the consistent results of the function of the function of the ventilated cavity on the drying, most researchers accept the ventilated cavity has a positive effect on the drying.
2) The ventilated cavity not only influences drying, but also has an effect on the thermal performance of building envelopes. The ventilation of the cavity behind the cladding can reduce the heat loss caused by convection.
3) The depth of cavity plays a more significant role than the vent size, and the moisture in the air cavity behind the vinyl siding claddings is more difficult to dry out than other types of claddings.

4) Compared to the water non-absorptive cladding (vinyl siding), ventilation is significant for walls with water absorptive claddings, such as bricks, woods, stucco, etc.
5) The temperate gradient of the stucco and fiber cement cladding is less than the brick claddings. The pressure differential of fiber cement cladding system is much higher than the brick cladding systems

3. POTENTIAL OF SELF-DRYING SIDING WITH RAISED AIR CAVITIES FOR BUILDING ENVELOPES[1]

Cladding is an external finishing system which functions as the structural protection and a decorative finish. The cladding includes several types: stucco, masonry veneer, aluminum siding, vinyl siding, fiber cement, wood cladding, et. (Radhi, 2010). Among these types, the vinyl siding is the most widely used type with a 37% share according to the U.S. Census Bureau statistics (Bureau, 2011). The vinyl siding has significant advantages in the less life cycle cost of a building considering the maintenance, durability, aesthetic features, and various shapes of vinyl siding. It has a variety of shapes and textures, creating a wide array of looking for different houses. It is manufactured primarily from durable polyvinyl chloride in several different profiles, as shown in Figure 4, including single, double, triple, vertical, and dutch lap. The configuration of one piece of a common vinyl siding is shown in Figure 5, where the nail hem is the area, directly attaching to the wall sheathing and helping fasten the nail to the wall sheathing through the fastening holes. The top lock is the portion that can be used to lock its next upper piece of siding. The center butt is the bend in the siding's center that makes the siding appear to be two or more pieces instead of one, and it also directly attaches to the wall sheathing. The buttlock or butt hook is the opposite side to the fastening strip, which locks in the preceding under piece of siding or trim. The panel projection is the size of the center butt or the butt at the siding bottom.

[1] The material in this chapter was co-authored by Yanmei and Huojun Yang. Yanmei Xie had primary responsibility for collecting samples in the field and for interviewing users of the test system. Yanmei Xie was the primary developer of the conclusions that are advanced here. Yanmei Xie also drafted and revised all versions of this chapter. Huojun Yang served as proofreader and checked the math in the statistical analysis conducted by Yanmei Xie.

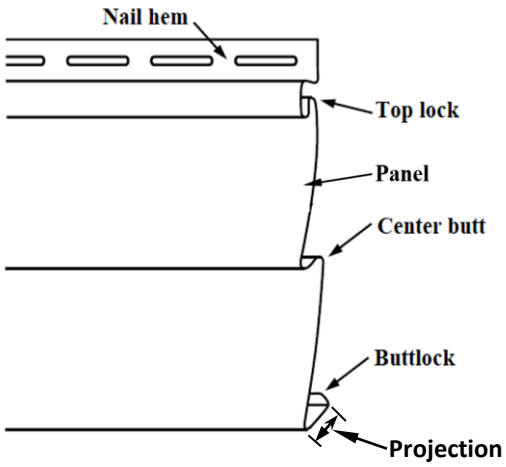

Figure 5. Configuration of a vinyl siding

After the installation of vinyl siding, the cavity between the vinyl siding and wall sheathings is formed. Air leakage occurs at the joints of siding panels. Then the cavity, vinyl siding, and the wall sheathing form the ventilation enclosure system (Davidovic, Srebric, & Burnett, 2006). Canada Mortgage and Housing Corporation (CMHC) comprehensive examined the ventilation cavity system behind the vinyl siding and reported that the vinyl lap-siding with its inter-locking system has the lowest flow rate. Additionally, Straube and Smegal found that the moisture trapped in the gap of vinyl siding due to the intermittent gap behind the siding (John Straube & Smegal, 2007). Once the moisture penetrates into the wall sheathing, moisture-related issues for building envelops will occur, such as frost damage, erosion, mold growth, etc. (shown in Figure 6). The findings about the effect of the ventilation on the cavity drying are contradictory. Lawton et. al. (Lawton, Brown, & Lang, 2001) reported that the ventilated wall system cannot help increase the drying rate of cavity moisture. Moreover, Lstiburek et. al. indicated that the water entering the cavity is more than its removal for the ventilation wall (Lstiburek, Karagiozis, & Ueno, 2002). However, the other experimental research showed that the ventilation cavity has a positive effect on the drying moisture in the cavity (Mayer & Künzel, 1983; Popp & Mayer, 1981; John Straube & Finch, 2009). Even though some researcher indicated that the ventilation wall

system does not provide a benefit to drying moisture, higher ventilation rates behind the cladding will increase the drying rate of an initially wetted wall (Ge & Ye, 2007; John Straube & Finch, 2009).

Crumbing plaster behind rain penetration

Frost damage

Erosion

Mould growth

Figure 6. Moisture-related issues for building envelops

In addition, the existence of moisture vapor and bulk water in the siding system significantly affects the thermal performance of the building envelops. First, moisture vapor has much lower thermal conductivity than the dry air, and the thermal conductivity of the saturated air is 22% lower than that of the dry air when the air temperature is 100 ºC, as shown in Figure 7. Second, in terms of convection heat transfer, the convection coefficient of the liquid or bulk water can be 50-80 times as that of air, and forced convection has much higher heat transfer rate than the natural convection, as shown in Table 1. Third, when a phase change occurs between bulk water and moisture vapor, such as evaporation of bulk water or condensation of moisture vapor, the heat loss or gain is much higher (up to 20 times as the forced convection method as shown in Table 1). The condensed water is like a bead with its diameter larger than the tiny gap attaching the siding with the wall sheathing. The moisture-related issues may occur due to the absorbed water by the wall wood sheathing if the condensed water cannot be dried out in time. Furthermore, the condensed water may obstruct the air flow through the gaps, decreasing the ventilation drying in each cavity cell behind siding. The radiation can be neglected because it is beyond this research focus. Therefore, the aforementioned heat transfer modes regarding water, including convection,

condensation and evaporation, greatly reduce the energy efficiency of the air cavity behind siding and thus the whole wall envelop system. Keeping the air cavity drying between the siding and the wall sheathing is an effective way to improve the energy efficiency of the siding system. However, as described above, the gaps between the wall sheathing and the nail hem or center butt can easily trap water, and they are too small to dry moisture efficiently; increasing the gap can improve the energy efficiency of building envelops.

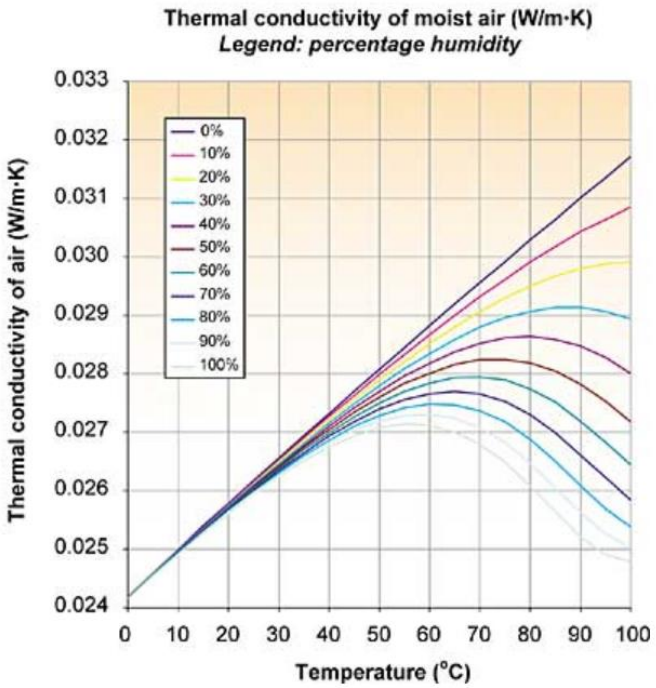

Figure 7. Thermal conductivity of air (Beirão, Ribeiro, Lourenço, Santos, & Nieto de Castro, 2012)

Table 1. Typical ranges for convection coefficient (Mitchell & Braun, 2012)

Mode	$h_c(^{W}/_{m^2} - {}^{0}C)$
Nature convection	
Gases	1-25
Liquids	50-1,000
Forced convection	
Gases	25-250
Liquids	50-20,000
Condensations/ boiling	1,000-100,000

Although there is multiple research that has studied the ventilation wall system, most of them assumed the vinyl siding as rectangular and neglects the effect of the geometry on the moisture drying in the cavity (Desta, Langmans, & Roels, 2011; Kumar, 2000; Suárez, Joubert, Molina, & Sánchez, 2011). Additionally, in order to simplify the numerical calculation, our previous research has assumed the outlets and inlets are certain. However, the inlets and outlets with multiple opening for the ventilation system are not determined. Thus, the previous results are not precise. Therefore, it is necessary to study the potential drying performance or air flow rate in the air cavity with the comprehensive consideration of irregular shape of air cavity, and inlets and outlets uncertainty.

To address the issues mentioned above, this paper provides a novel design of vinyl siding with the increase of the cavity depth. This study redefines the drying potential of air cavity between the vinyl siding and wall sheathing taking into account the air cavity depth related to the shape irregularity and the inlets and outlet uncertainty. Based on the discharge equations, the equations for the one-story building ventilation are derived. Furthermore, the effect of air cavity depth is investigated on the drying potential. The findings can potentially improve the accuracy and creditability of future related analysis and provide practical guidance on engineering designs of building envelopes.

3.1. Air Flow through a Siding System

There are several driving forces to induce the air flow through the opening and the air cavity behind vinyl siding, such as mechanical methods (operating an electric or manual funs) and pressure differential present in the environment (winds and temperature buoyance) (Womble, Yeatts, Cermak, & Mehta, 1995). This paper mainly studies self-drying potential performance in the air cavity induced by the wind because the air cavity behind vinyl siding is easily susceptible to wind compared to other factors. The air flow in this paper is divided to two parts: air leakage through the openings and air flow in the air cavity behind vinyl siding. Based on the wind power law and continuity equations, a mathematic model as follows with the consideration of the irregular shape of vinyl siding and the unknown inlets and outlets is developed to evaluate the drying potential performance of the air cavity behind the vinyl siding for the low-rise building envelop.

3.1.1. Single piece of vinyl siding

3.1.1.1. Wind induced pressure on building

Wind is generated by air flow due to the gradient of the atmospheric pressure. Air moves from the higher to the lower pressure area, resulting in winds of various speeds. The wind power law is the relationship between the air velocity and the altitude, described as

$$\frac{V}{V_0} = \left(\frac{z}{z_0}\right)^n \tag{1}$$

V_0 is assumed as the wind speeds measured at $z_0 = 10\ m$ $(32.8\ ft)$. The value of exponent n ranges from 1/3 to 1/4 in urban area.

3.1.1.2. Continuity equation

The continuity equation (Holmes, 1980) can be written as

$$\frac{\partial \rho}{\partial t} + \nabla \cdot (\rho v) = 0 \tag{2}$$

For incompressible fluid as the density is constant and is independent of space and time, and the mass continuity equation can be simplified as

$$\nabla \cdot (v) = 0 \tag{3}$$

The Equation (3) also can be written as

$$\sum Q = 0 \tag{4}$$

3.1.1.3. Air leakage

Single piece of vinyl siding has an inlet and outlet. Therefore, this situation can be used as a single discharge equation. The Bernoulli equation for unsteady fluid flow along a streamline can be determined by Equation (5) (Oh, Kopp, & Inculet, 2007):

$$\rho \int_1^2 \frac{\partial V}{\partial t} ds + \rho \int_1^2 dp + \frac{1}{2}\rho(V_2^2 - V_1^2) + \rho g(z_2 - z_1) = 0 \tag{5}$$

Considering the flow through an opening, with P_e and P_i which are the outside and inside the opening pressures, respectively, neglecting the effects of gravitational acceleration, the Bernoulli equation above becomes:

$$|\Delta \mathrm{p}| = \mathrm{C}\frac{1}{2}\,\rho \mathrm{V}^2 + \rho \mathrm{l_e}\frac{\partial \mathrm{V}}{\partial \mathrm{t}} \tag{6}$$

The effective length through the inlet or outlet is calculated as follow (Vickery, 1985)

$$\mathrm{l_e} = \mathrm{l} + \mathrm{H} \tag{7}$$

or

$$\Delta \mathrm{p} = \mathrm{c}\frac{1}{2}\,\rho \mathrm{V}|V| + \rho \mathrm{l_e}\frac{\partial \mathrm{V}}{\partial \mathrm{t}} \tag{8}$$

For steady and incompressible flow ($\frac{\partial \mathrm{V}}{\partial \mathrm{t}} = 0$), Equation (8) can be rearranged as

$$\Delta \mathrm{p} = \mathrm{c}\frac{1}{2}\,\rho \mathrm{V}|V| \tag{9}$$

The Equation (9) with the flow rate Q through the opening can become as

$$|\Delta \mathrm{p}| = \mathrm{c}\frac{1}{2}\,\rho(\frac{Q}{A})^2 \tag{10}$$

The roughness of the surface of the wall or pipe have a significant impact on the friction which can cause the pressure loss. The pressure differential caused by the friction can be calculated using Darcy-Weisbach equation (White, 1979).

$$\Delta P_f = f \frac{h}{D_h} \frac{1}{2} \rho V^2 \tag{11}$$

The total pressure differential caused by the air flow through the opening is rewritten as

$$|\Delta \mathrm{p}| = \mathrm{c} \frac{1}{2} \rho \mathrm{V}^2 + \rho \mathrm{l_e} \frac{\partial \mathrm{V}}{\partial \mathrm{t}} + f \frac{h}{D_h} \frac{1}{2} \rho V^2 \tag{12}$$

The length of the opening has an impact on the pressure loss. The longer the length of the opening, the higher the pressure differential will be. Since the length of the inlet or outlet is much small, the pressure differential caused by the wall friction can be neglected, while the air flow pass through the opening. Thus, for the steady and incompressible flow, the pressure differential as shown in Figure 8 can be simplified as

$$\Delta \mathrm{p} = \mathrm{c} \frac{1}{2} \rho \mathrm{V} |V| \tag{13}$$

or

$$|\Delta \mathrm{p}| = \mathrm{c} \frac{1}{2} \rho (\frac{Q}{A})^2 \tag{14}$$

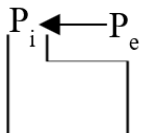

Figure 8. Leaked air flowing through an opening

The value of loss coefficient (c) varies with the configuration of opening and the air velocity, and cannot be simply determined by a generally accepted model. Different loss coefficient equations were investigated, for example, by Idelchik et al. (Idelchik, 1986)and Straube et al. (J Straube & Burnett, 1995). In addition, Straube et al. (John Straube & Burnett, 1999)used $c = 0.5$ and $c = 1$ for the entrance and exit of 90° elbows in their ventilation model,

respectively. The loss coefficient c was reported between 1.041 and1.085, when the air flows through a thin and thick wall orifice with a well-rounded entrance (Hutcheon, Handegord, & Hutcheon, 1983). For a sharp-edged or square-edged orifice of a thin and thick wall, the loss coefficient could be about 2.5 (R. Van Straaten, 2004), and thus the loss coefficient is assumed to be 2.5 in this paper due to the analogous research background (i.e., the square-edged orifice of a thin wall).

3.1.1.4. Cavity flow

The cavity geometry between the wall sheathing and vinyl siding is complex, because the panel types of the vinyl siding are various. The change of the air cavity's section has an impact on the pressure differential. Thus, the pressure loss of air flow through the cavity not only results from the wall friction and unsteady air flow velocity, but also from the cavity geometry. The major pressure loss due to cavity geometry includes sudden enlargements and concentrations along the cavity. Therefore, this paper first analyzes the air pressure loss due to sudden enlargements and concentrations, then summarizes the total pressure loss for the air flow through the cavity.

1) Sudden enlargements and contractions

When the cross-section of a cavity is abruptly enlarged or contracted, the air flow cannot follow the sudden change of geometry. This creates pockets of turbulent eddies in the corners, resulting in the dissipation of mechanical energy into intermolecular energy and thus a pressure drop.

As shown in Figure 9, the head loss ("Losses due to sudden enlargement. ,") for a sudden enlargement can be calculated as

$$h_l = {(1 - \frac{A_1}{A_2})^2 \, {U_1}^2} \Big/ {2g} \tag{15}$$

Based on Bernoulli's equation, the according pressure loss can be expressed as

$$P_1 - P_2 = \frac{1}{2}\rho V_2|V_2|(2 - 2\frac{A_2}{A_1}) \quad (16)$$

where P_1 and P_2 are the entrance and exit pressure of the cross sections, V_2 is the entrance and exit velocity, and A_1 and A_2 are the entrance and exit area, respectively.

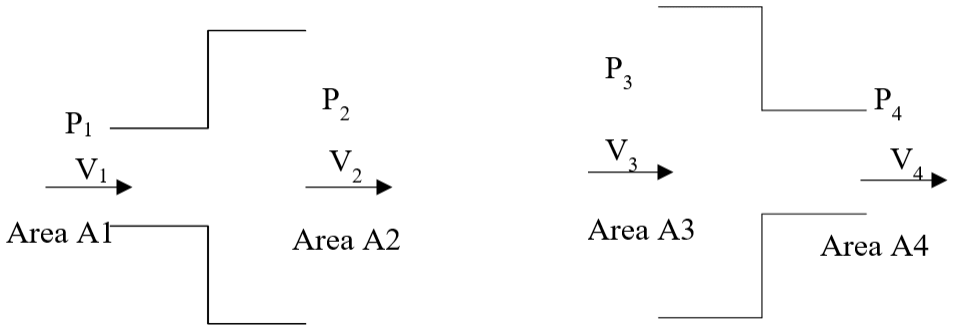

(a) Sudden enlargement (b) Sudden contraction

Figure 9. Pressure gradient due to sudden change in cross-section

On the other hand, the head loss ("Losses due to sudden contraction,") for a sudden contraction shown in Figure 9 can be calculated as

$$h_l = {(1 - \frac{1}{C_c})^2 V_3^2}\Big/{2g} \quad (17)$$

where C_c is the coefficient of contraction. Also, $(1 - \frac{1}{C_c})^2$ is usually replaced by a coefficient K, which is listed in Table 2 for a different $\frac{A_4}{A_3}$, and Eqn. (18) is simplified by,

$$h_l = {KV_3^2}\Big/{2g} \quad (18)$$

Table 2. K value at an ${A_4}/{A_3}$ (Mamourian, Shirvan, Ellahi, & Rahimi, 2016)

${A_4}/{A_3}$	0	0.0	0.16	0.36	0.64	1.0
K	0.5	0.45	0.38	0.28	0.14	0

Based on Bernoulli's equation, the pressure loss for the sudden contraction can be expressed as

$$P_3 - P_4 = \frac{1}{2}\rho \mathrm{V}_4|\mathrm{V}_4|(1 + K - \left(\frac{A_4}{A_3}\right)^2) \tag{19}$$

where P_3 and P_4 are the entrance and exit pressure of the cross section, V_4 is the exit velocity, A_3 and A_4 are the entrance and exit area, respectively; K is the coefficient caused by the concentrations.

2) Friction

$$\Delta P_f = f\frac{h}{D_h}\frac{1}{2}\,\rho \mathrm{V}|V| \tag{20}$$

3) Unsteady flow

Moreover, the unsteady flow in the cavity can be calculated as,

$$\Delta P_{unsteady} = \rho l_e \frac{\partial V}{\partial t} \tag{21}$$

Thus, for one piece of siding shown in Figure 10, the total air differential pressure through the cavity is the sum of the aforementioned three components, and it can be expressed as

$$P_{c1} - P_{cf} = \sum_{j=1}^{n}\frac{1}{2}\rho V_{j+1}\left|V_{j+1}\right|\left(2 - 2\frac{A_{i+1}}{A_i}\right) + \sum_{j=1}^{m}\frac{1}{2}\rho V_{j+1}\left|V_{j+1}\right|\left[1 + K_j - \left(\frac{A_{j+1}}{A_j}\right)^2\right] +$$

$$\left(f\frac{h}{D_h}\frac{1}{2}\,\rho V_i|V_i| + \rho l_{e,l}\frac{\partial U_l}{\partial t}\right) \tag{22}$$

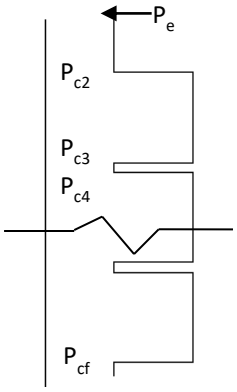

Figure 10. Air pressure in a cavity behind a single piece of vinyl siding

Van Straaten found that the wall friction is about 0.044 (R. A. Van Straaten, 2017), when the air flow rate is high. Therefore, the friction coefficient ($f\frac{h}{D_h}$) shown in Equation (11) for the air cavity is below 0.125. while the sum of the a sudden contraction coefficient ($1+K-\left(\frac{A_3}{A_2}\right)^2$) and a sudden enlargement coefficient ($2-2\frac{A_2}{A_1}$) is 1.4, which is as 11 times as the friction coefficient. Meanwhile, as the lower air flow rate, the friction coefficient induced the pressure differential is less than 0.044, and thus the sum of a sudden concentration and enlargement is larger than 11 times of pressure differential. Therefore, the pressure differential caused by the change of the cross section of the air cavity is the major factor, and the pressure differential caused by the wall friction can be neglected. Furthermore, for the steady and impressible flow with neglecting the friction, Equation (22) can be simplified as

$$P_{c1}-P_{cf}=\sum_{j=1}^{n}\frac{1}{2}\rho V_{j+1}\left|V_{j+1}\right|\left(2-2\frac{A_{i+1}}{A_i}\right)+\sum_{j=1}^{m}\frac{1}{2}\rho V_{j+1}\left|V_{j+1}\right|\left[1+K_j-\left(\frac{A_{j+1}}{A_j}\right)^2\right] \quad (23)$$

or

$$P_{c1}-P_{cf}=V_{j+1}\left|V_{j+1}\right|\left\{\sum_{j=1}^{n}\frac{1}{2}\rho\left(2-2\frac{A_{i+1}}{A_i}\right)+\sum_{j=1}^{m}\frac{1}{2}\rho\left[1+K_j-\left(\frac{A_{j+1}}{A_j}\right)^2\right]\right\} \quad (24)$$

When the air velocity is replaced with air flow rate Q, the above Equation (18) can be rearranged as

$$\left|P_{c1} - P_{cf}\right| = Q^2 \left\{ \sum_{i=1}^{m} \frac{1}{2}\rho \left(\frac{1}{A_{i+1}}\right)^2 \left(2 - 2\frac{A_{i+1}}{A_i}\right) + \sum_{j=1}^{m} \frac{1}{2}\rho \left(\frac{1}{A_{j+1}}\right)^2 \left[1 + K_j - \left(\frac{A_{j+1}}{A_j}\right)^2\right] \right\}$$

3.1.2. Multiple pieces of siding

There are multiple pieces (e.g. n) of vinyl siding for the low-rise building envelopes as shown in Figure 11. Therefore, it has n+1 opening or leaks caused by the installation. Based on the single discharge equation shown above, the multiple discharge equations are determined with unknown the inlet and outlet openings. For the ith piece of the vinyl siding, the air pressure differential through the opening and air cavity behind vinyl siding can be rewritten by combined Equations (13) and (24)

$$P_i - P_{i,i} = c\frac{1}{2}\rho V_i |V_i| \tag{25}$$

$$P_{i,i} - P_{i,i+1} = \left|\sum_i V_i\right| \sum_i V_i \left\{ \sum_{l=1}^{m} \frac{1}{2}\rho \left(2 - 2\frac{A_{l+1}}{A_l}\right) + \sum_{j=1}^{m} \frac{1}{2}\rho \left[1 + K_j - \left(\frac{A_{j+1}}{A_j}\right)^2\right] \right\} \tag{26}$$

$$P_{i+1} - P_{i,i+1} = c\frac{1}{2}\rho V_{i+1} |V_{i+1}| \tag{27}$$

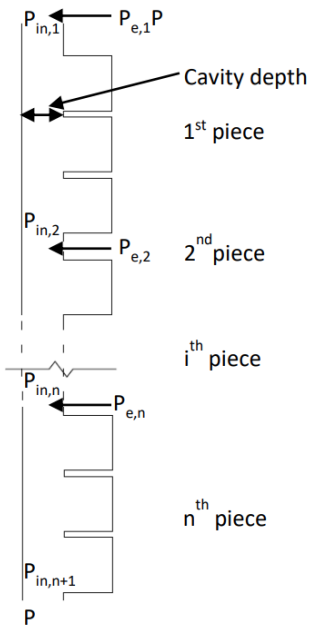

Figure 11. Air pressure in a cavity behind N pieces of vinyl siding

Further, the coefficients for the air flow pressure loss through the opening and air cavity behind the vinyl siding are certain while neglecting the effects of wall friction and air slug. Therefore, Equations (25) and (26) can be rearranged as

$$P_i - P_{i,i} = R^2 V_i |V_i| \tag{28}$$

$$P_{i,i} - P_{i,i+1} = H^2 R^2 |\sum_i V_i| \sum_i V_i \tag{29}$$

where $c\frac{1}{2}\rho = R^2$ and $\sum_{l=1}^{m} \frac{1}{2}\rho\left(2 - 2\frac{A_{l+1}}{A_l}\right) + \sum_{j=1}^{m} \frac{1}{2}\rho\left[1 + K_j - \left(\frac{A_{j+1}}{A_j}\right)^2\right] = H^2 R^2$.

Since the leaks or the openings are multiple, it is very difficult to determine which opening or leak is the inlet or outlet. The multiple discharge equations (Equations 25 to 27) need to solve and further determine the inlets and outlet. In the simultaneous equations, there are 2n+2 unknowns ($P_{i,1}$,…, $P_{i,i}$, …, $P_{i,n+1}$, V_1,…, V_i, …, V_{n+1}), while the number of equations is 2n+1. Thus, there is an additional equation required to solve them.

$$\sum_{i=1}^{n+1} V_i = 0 \tag{30}$$

3.2. Analytic Model

The ventilated wall systems for one-story building covered the vinyl sidings as the cladding is used for the study. Its height is about 2.54m (8 ft), which is the height of the ten pieces of the tripe dutch lap vinyl siding. As mentioned in the Introduction section, since the gap between vinyl siding and wall sheathing is tiny, the air flow rate is much small. In other word, this gap has negative effect on the drying potential for the ventilation wall system. Therefore, an increase of the air cavity depth between vinyl siding and wall sheathing can help increase the drying rate of the air cavity. Furthermore, an optimal depth of the air cavity can be obtained through evaluating the maximum air flow rate or the drying potential of air cavity behind the vinyl siding.

The loss coefficient (c) through the opening varies with different types of openings or cracks. There is some research studied the effect factors on the loss coefficeint. For example, $c = 0.5$ and $c = 1$ for entrance and exit of 90° elbows in their ventilation model, respectively, and C is between 1.041 and 1.085 for a thin and thick walled orifice (Hutcheon & Handegord, 1983). Additionally, c is about 2.5 for a sharp-edged or square-edged orifice of a thin and thick wall (R. Van Straaten, 2004) (R. Van Straaten, 2004). This paper assumes c is 2.5 as the joist of ventilation system belongs to square-edged orifice of a thin wall.

In addition, some research reported that the air flow from the orifice opening to the air cavity is turbulence and not laminar. However, in order to simply the simulation, most studies still consider the flow through the opening and the air cavity behind vinyl siding to be laminar. Therefore, this paper assumes the air flow is laminar. The analytic model is used for the vinyl siding with several assumption as follows:

1) The air leakage at the horizontal connections between two siding pieces is neglected;

2) A constant loss coefficient for the orifice opening of 2.5 and no wall friction;
3) Rigid vinyl siding and wall sheathing, and airtight sheathing;
4) No air temperature difference at the air cavity opening and within the cavity. The air temperature is assumed to be 20 ℃ (room temperature); the humidity ratio at the opening inlet be 50%;
5) Fully developed laminar flow.

The mathematic model developed in Section 3.2 is validated by the computational fluid dynamics (CFD). To build the CFD model, the commercial software Ansys Workbench is used, because it is the state-of-art technique in engineering simulation. The CFD model is composed of 10 pieces of vinyl siding with eleven opening joists, as while as the cavity depth is 30% of the siding panel projection. Both the mathematic model and CFD model have the same environment condition (air flow velocity at 10m, air density and air moisture content) and boundary conditions.

Figure 12 shows the comparison results of the mathematic model and CFD model. The air flow velocity at 10m (8 ft) is as the same as the certain day in Fargo, ND. It is indicated that the air flow rate in the cavity used the mathematic method is less than CFD results. That is because the mathematic model neglects the effect of friction of the wall. Consequently, the air flow resistance through the air cavity for the mathematic model is less than CFD model. However, the difference between both models is much small, and it is below 10%. Therefore, the effects of friction on the air flow rate is not significant compared to the irregular shape. Furthermore, the mathematic model proposed in this paper is acceptable to calculate the air flow behind the vinyl siding.

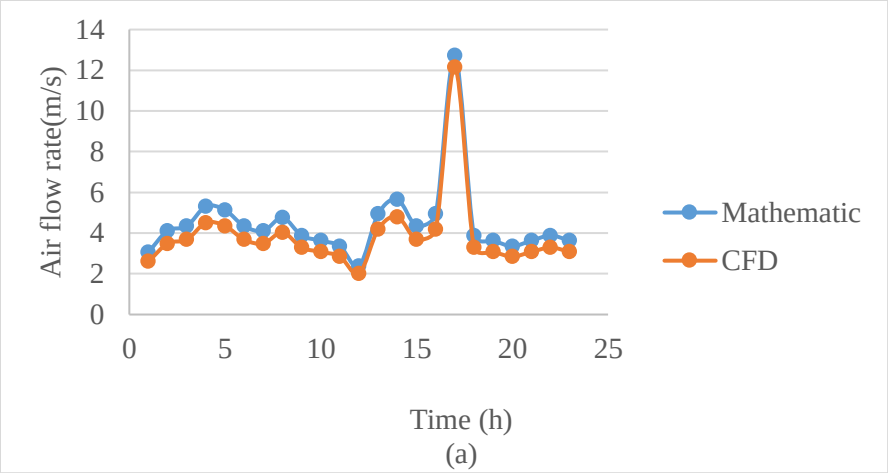

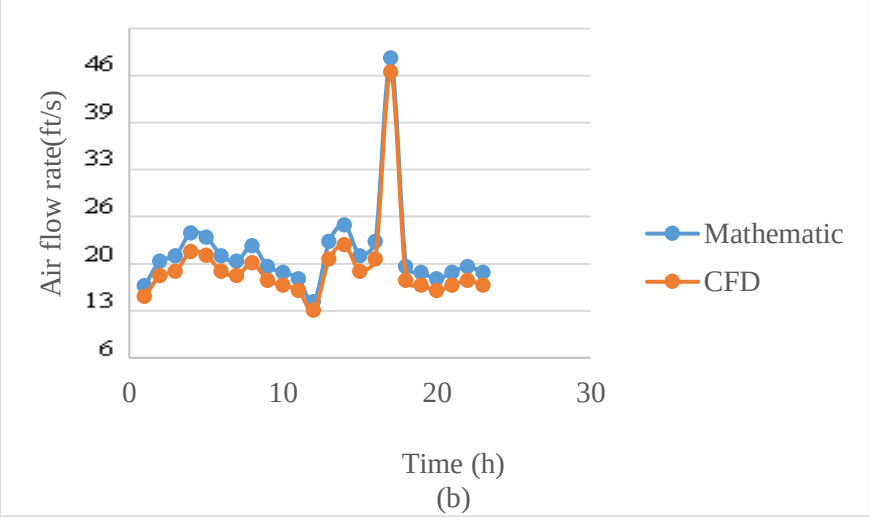

Figure 12. Comparative results of air flow rate in air cavity between mathematic model and CFD model (unit of (a) is m/s, and unit of (b) is ft/s)

3.3. Evaluating Drying Potential of Cavities Behind Siding

The air flow rate in the cavity behind vinyl sidings can denote their drying potential as mentioned in the Introduction section. The higher the air flow rate, the larger drying potential. Therefore, the air flow rate can be used to evaluate the drying potential in the cavity at the optimal depth of the cavity.

According to Equation 25, the cavity depth has a significant effect on the air flow velocity in the cavity behind vinyl siding because the cavity depth plays a critical role in determining the flow resistance. Due to that it is complicate to solve the Equations 28 and 29, sensitivity analysis

is used to investigate the effects of the cavity depth on the air velocity. Sensitivity can be defined as a response derivative with regards to a design variable. This derivative can be understood as the expected change in the response when the considered design variable is perturbed (Nieto, Hernández, & Jurado, 2009). Sensitivity analysis is an important part to help the designer to follow a guided design process avoiding unfruitful design modifications (Tan, 1989; R. Yang, 1989).

Increasing the gap between the vinyl siding and wall sheathing may mitigate the moisture-related issue of building envelopes, as mentioned in Introduction. The sensitivity analysis is used to evaluates the relationship between the cavity depth and air flow velocity in the cavity. In the sensitivity study, the siding's panel projection is used as a benchmark to define the cavity depth which is between 1% and 100% of the benchmark in increments of 1%, and there are 100 scenarios in total.

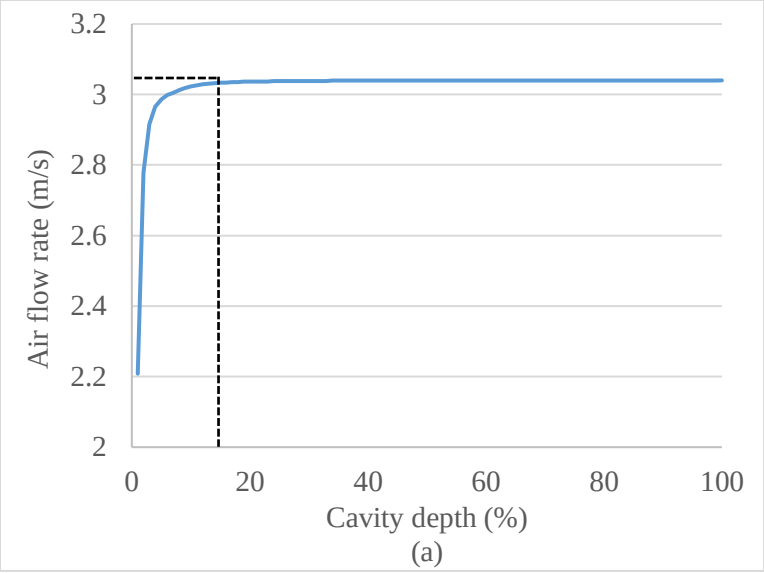

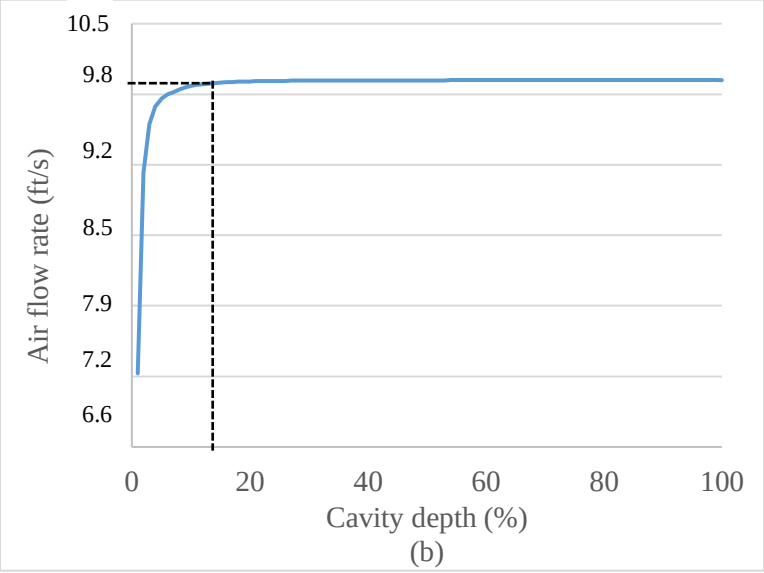

Figure 13. Air flow velocity with the increase cavity depth (unit of (a) is m/s, and unit of (b) is ft/s)

Figure 13 shows the relationship between the cavity depth and the air flow rate at the given air flow velocity of 2m/s (6.56 ft/s) at the height of 10m in the environment. With the increase of the cavity depth, the air flow rate increases with the given air flow velocity. Meanwhile, the air flow rate fast increases to a maximum value, then converged to a constant value. When the cavity depth increases to 20% of the panel projection, i.e. 0.33cm (0.13in), for the triple dutch lap vinyl siding, the cavity air flow rate reaches its maximal value. However, the

value 0.33cm (0.13in), is less than the largest droplet diameter of 0.5cm (0.2in). In order to avoid the moisture condensed or accumulated at the tiny gap between the vinyl siding and wall sheathings, the optimal cavity depth for the vinyl siding system should be no less than value of 0.5cm (0.2in).

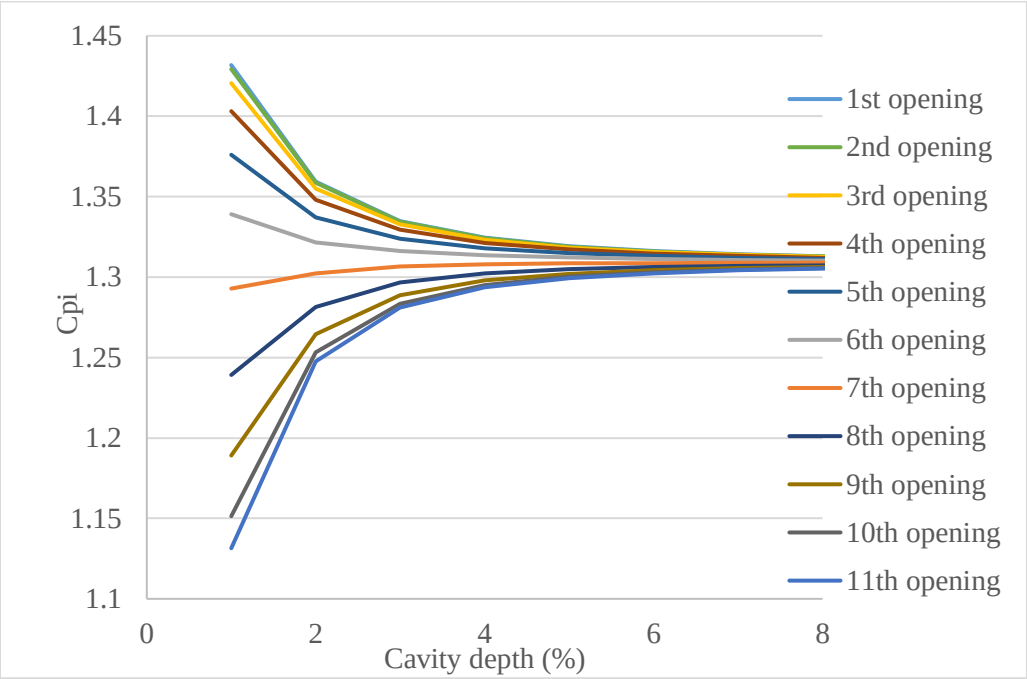

Figure 14. Pressure coefficients for the openings (Cpi) vs cavity depth

Figure 14 shows the relationship between the cavity depth and the pressure coefficient in the cavity (Cpi) for the total 11 openings at the given air flow velocity of 2m/s (6.56 ft/s) at the height of 10m in the environment. For the 1st opening to the 6th opening, Cpi first decreases with the increase of the cavity depth, and then converges to the minimum value. On the contrary, for the 7th opening to the 11th opening, Cpi first increases, and then converged to the maximum value, with the increase of the cavity depth. Meanwhile, pressure coefficient in the cavity (Cpi) decreases with the increases of the height of opening, and the closer the two adjacent openings are to the middle of opening, the greater difference those pressure coefficients (Cpi) in the cavity.

Therefore, the location of the opening or the height of the opening has an effect on the pressure coefficient in air cavity.

3.4. New Siding Design

Based on the results above, an optimal air cavity depth for a vinyl siding can be obtained to maximize the air flow rate. Consequently, the maximum air flow rate can provide the high air cavity drying performance through the ventilation as mentioned in Introduction part. Moreover, the optimal cavity depth also avoids the moisture attaching to the wall sheathing and vinyl siding, because it is not less than the largest droplet diameter. A new vinyl siding design is needed to satisfy the optimal cavity's requirement, such as its manufacture, installation, and maintenance, and structural function. Figure 15 is proposed as a new siding with a beam, which helps to increase the gap between the vinyl siding and wall sheathing. A series of paralleled holes are punched on the beams to provide the passage of air flow in the cavity. Therefore, this beam not only can increase the ventilation in the cavity, but also makes the installation of the vinyl siding as simple as the traditional ones.

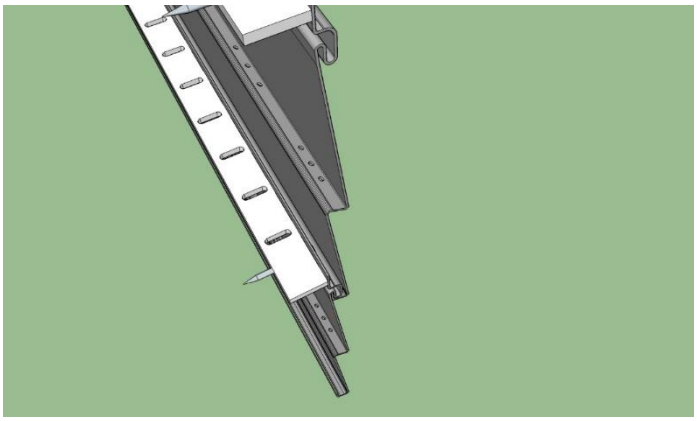

Figure 15. Details of installation connections for a new vinyl siding

3.5. Conclusion

This paper mainly studies the drying potential through the air flow in the air cavity behind the vinyl siding, develops the mathematic models with the considering the effects of openings and

the irregular shapes, evaluates the effects of air cavity depth with the siding panel projection as benchmark on the drying potential, and finally proposes a new design of vinyl siding. The main results of this paper are listed as follows.

1) Since the gap between the vinyl siding and wall sheathing is much small, moisture may be trapped in the air cavity, which may cause the moisture-related issues such as the rain penetration, frost damage, and short life span of structure. Moreover, an increase of this gap is found to have a positive effect on the drying performance of air cavity behind vinyl siding. These phenomenon helps to propose the new design of vinyl siding with an increase of gap.
2) Instead of the simple rectangular air cavity behind the vinyl siding as most research studied, the irregular shape of the air cavity behind vinyl siding with the unknown inlets and outlets are analyzed. The results show that sudden contractions and enlargements of cross sections of the air cavity behind the vinyl siding have a significant effect on the air flow rate or drying performance for the air cavity. It also indicates that the shape of vinyl siding plays a major role in the drying potential of the air cavity, compared to the other factors such as wall frictions.
3) Based on the discharge equation and equation for flow in the cavity, the mathematic model for the one-story building ventilation with multiple discharges is developed. Compared to the CFD model, the result shows the air flow rate in the air cavity behind vinyl siding calculated by the mathematic model is small, due to that the mathematic model neglects the wall friction in air cavity. However, the difference between both models is much small. Therefore, this mathematic model is acceptable to evaluate the drying performance of the air cavity behind vinyl siding.

4) Through sensitivity analysis, the effects of the air cavity depth on the air flow rate within a cavity are evaluated. The results show the air flow rate increases at the given air flow velocity, with the increase of air cavity depth. Meanwhile, the air flow rate fast increases to a maximum value, then converged to a constant value. When the cavity depth increases to 20% of the siding panel projection, i.e. 0.33cm (0.13in), for the triple dutch lap vinyl siding, the cavity air flow rate reaches its maximum value. However, the value 0.33cm (0.13in), is less than the water droplet diameter of 0.5cm (0.2in). In order to avoid the moisture trapped in the air cavity, the optimal depth of air cavity should be not less than 0.5cm (0.2in). Additionally, the location of the opening or the height of the opening plays an important role in the pressure coefficient Cpi. pressure coefficient in the cavity (Cpi) decreases with the increases of the height of opening, and the closer the two adjacent openings are to the middle of opening, the greater difference between those pressure coefficients in the cavity.
5) As the optimal cavity depth is found for a maximized drying potential in the air cavity behind vinyl siding, the beams with punched holes between vinyl siding and the wall sheathing are introduced to the traditional siding systems as a new siding system. this new design not only can improve the ventilation or the drying potential in the cavity behind vinyl siding, but also can make the installation of the vinyl siding as simple as the traditional ones. Furthermore, this paper provides design guidance for the new siding system.

4. RATIOS OF SIDING DEPTH TO CAVITY DEPTH IN MIXED CONVECTION OF AIR CAVITY BEHIND VINYL SIDING FOR BUILDING ENVELOPES[2]

Cladding is an important component of building envelope, providing a skin or layer for thermal insulation and weather resistance in addition to improving the appearance of buildings (Chew, Tan, & Kang, 2005). Vinyl siding with a 37% share is the most widely used type of building cladding according to U.S. Census Bureau statistics (Bureau, 2011). It has advantages in durability, aesthetics, economy, variety in shapes, textures, and profiles compared with other cladding types. Without designed openings, vinyl siding has ventilation through air leakage at its joints (Karagiozis & Kuenzel, 2009; R. Van Straaten, 2004). Figure 16 illustrates the details of vinyl siding installation including the joints and air cavity. The air cavity behind the vinyl siding alleviates moisture-related issues including rain penetration, frost damage, etc., in addition to benefitting building's thermal performance directly. Actually, moisture significantly affects the energy performance of building envelope as well, as it can decrease the heat conduction resistance and increase the convection coefficient (H. Yang et al., 2019). Moreover, heat loss happens once the moisture condenses (Karagiozis & Kuenzel, 2009). Additionally, air cavities prevent the wall sheathing from absorbing moisture and provide drainage space.

[2] The material in this chapter was co-authored by Yanmei, Zhiming Zhang and Huojun Yang. Yanmei Xie had primary responsibility for collecting samples in the field and for interviewing users of the test system. Yanmei Xie was the primary developer of the conclusions that are advanced here. Yanmei Xie also drafted and revised all versions of this chapter. Huojun Yang served as proofreader and checked the math in the statistical analysis conducted by Yanmei Xie.

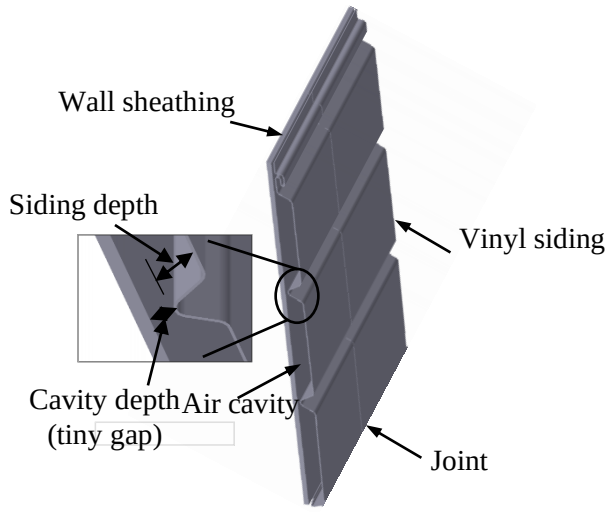

Figure 16. Details of vinyl siding

As shown in Figure 16, adjacent cavity cells are connected through the tiny gap. The tiny gap may limit the cells' ventilation despite the ventilating effects of leaky openings at the joints. On the other hand, this tiny gap can accumulate bulk water from accidental leaks or condensation, which may further obstruct the ventilation of air cavities and cause moisture-related issues. Hence, increasing the gap size has the potential of improving ventilation, mitigating moisture-related issues, and increasing the energy efficiency of building envelops. An improved configuration of the vinyl siding as well as the traditional design is shown in Figure 17.

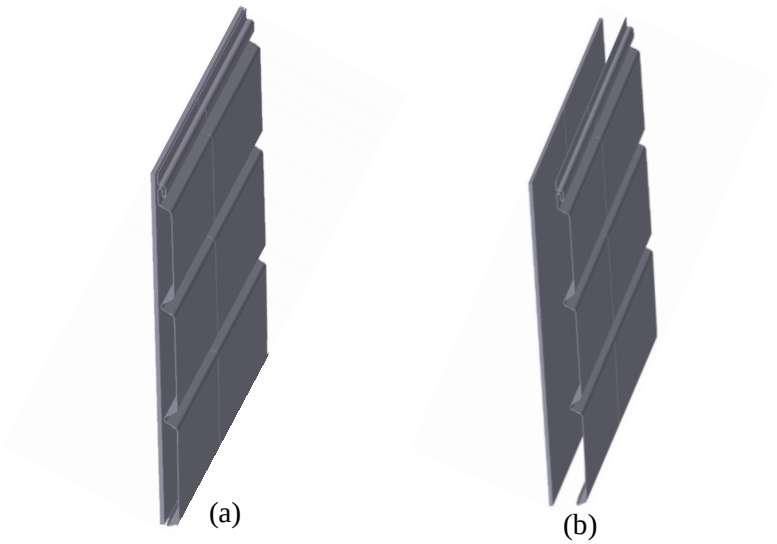

Figure 17. Vinyl siding configurations: (a) traditional; (b) improved

The energy performance analysis of building envelopes have important value, as building sector consumes the largest end energy in the United States with 60% attributed to building envelopes (Hinojosa, Orozco, & Xaman, 2020; Nwaji, Okoronkwo, Ogueke, & Anyanwu, 2021). However, there are limited studies in literature on heat, air and moisture modelling (HMA) of the cavity behind vinyl siding. Previous studies assume the air in cavities as still and thus omit the effects of mixed convection on heat and mass transfer (Finch & Straube, 2007b; Ouf, O'Brien, & Gunay, 2018; John Straube & Finch, 2009). For example, Straube and Finch (Finch & Straube, 2007b; John Straube & Finch, 2009) studied the impact of cavity on the building performance using the commercial software WUFI, ignoring the ventilation by assuming the air as still. In reality, ventilation air is driven through the air cavity by a wind induced air pressure differential and/or thermal buoyancy (stack effect) (El-Sadi, Haghighat, & Fallahi, 2010). The direction as well as the rate of air flow is a combined result of all driving forces, leading to complex flow patterns within the air cavity. Therefore, an advanced analysis considering the effects of mixed convection is necessary for accurate analysis of the energy performance of building envelops with air cavities.

Moreover, previous studies in literature assume the shape of air cavities as rectangular and thus neglect the effects of geometric irregularity and complexity. However, studies on mixed-convection induced heat and mass transfer in areas other than building envelope reveals that shape irregularity has significant effects on the flow pattern and/or energy efficiency of objects such as electrical devices with fan cooling, nuclear reactors, heat exchanger, etc. Cho et al. and Kie et al. (Cho, Kim, & Shin, 1998; Kie, Moon-Uhn, & Hyun, 1998) studied the 2D steady flow's linear stability in wavy-walled channels and found that Reynolds number of wavy-walled channel flow is much lower than the plane channel flow. Gradeck et al. (Gradeck, Hoareau, & Lebouché, 2005) investigated the local heat transfer inside a corrugated channel through the experiment, and the result shows that its heat transfer is higher than in a rectangular channel because of the effects of channel's geometry. Li et al. (Li & Karava, 2014; Li, Karava, Currie, Lin, & Savory, 2014; Li, Karava, Savory, & Lin, 2013) analyzed the energy performance of building-integrated photovoltaic thermal (PV/T) systems with corrugated unglazed transpired solar collectors (UTCs) through experimental modeling and numerical simulations. The results show that geometric parameters, including the slope length, the corrugation wavelength, and the PV panel height, have significant impacts on the energy performance of UTCs. Takaoka et al. (Takaoka, Sano, Yamamoto, & Mizushima, 2009) examined the flow instability in a symmetric spatially periodic channel, and they concluded that the convective instability is related to the Hopf bifurcation in the periodic flow. Ghaddar et al. (Ghaddar, Korczak, Mikic, & Patera, 1986; Ghaddar, Magen, Mikic, & Patera, 1986) numerically investigated the incompressible flow in grooved channels and found that self-sustained flow oscillations are induced by the linear mode's instability. Xie and Xi reported the effects of geometry in unsteady forced convection on heat transfer and flow fluctuation (Xie & Xi, 2017). Yang and Chen investigated the effects of turbulent flow on heat

transfer in a ribbed channel and found that the rib height and thickness significantly affect the friction factor and heat transfer (Y.-T. Yang & Chen, 2015). Other related studies can be found in (Hatami, 2017; Hatami, Zhou, Geng, Song, & Jing, 2017; Rashidi, Nasiri, Khezerloo, & Laraqi, 2016), which also demonstrate the significant effects of shape irregularity on the flow pattern and/or energy efficiency of objects. Considering its significant influence in other areas as indicated in literature, advanced analysis on mixed convection of building envelopes should take into account the effects of shape irregularity instead of assuming a rectangular channel.

In summary, existing studies are limited regarding the effects of air cavity of vinyl sidings on the energy performance of building envelops, as potentially important effects from the mixed convection and geometric irregularities are not sufficiently investigated. Aiming at improving the performance of energy analysis on building envelope especially that regarding the vinyl-siding type of cladding, the present study redefines the heat and mass transfer problem in the air cavity considering the effects of mixed convection and ratios of vinyl siding depth to air cavity depth related to the shape irregularity. The partial differential equations are solved using the perturbation method. The effects of critical parameters (Reynolds numbers, air cavity depth, dimensionless temperature on the walls, and dimensionless air mass fraction) on the velocity, temperature, and mass fraction distribution of the fluid motion as well as the skin friction and heat and mass transfer rate at the walls are investigated. The results show that the increase of the air cavity depth can decrease temperature, mass fraction, heat and mass transfer coefficients, and their amplitudes, which makes their distributions flatter. Therefore, these results of heat and mass transfer analysis approve the significant effects of and the shape irregularity on the building envelopes with vinyl sidings. These findings can potentially improve the accuracy and creditability of future related analysis and provide practical guidance on engineering designs of

building envelopes of this type. Moreover, this study provides an essential supplement to the state of the art of energy performance analysis of building envelopes with a comprehensive analysis of the effects of mixed convection and geometric irregularities. The remaining part of this paper is structured as follows: Section 4.2 introduces the methodology used in this study, including the problem definition of mixed convection heat and mass transfer within air cavities and the problem solving using the perturbation method; Section 4.3 presents the results of analysis including that of parametric analysis; Section 4.4 concludes this study with remarks and recommendations.

4.1. Methodology

This section defines the problem of mixed convective heat and mass transfer within the air cavity behind the vinyl siding of building envelopes, considering the influence of ratios of siding depth to cavity depth related to geometric irregularity and complexity. It contains the effects of fluid continuity and conservation of momentum, energy, and mass fraction. Solutions to the defined problem are pursued using the perturbation method. The equations are derived for calculating the skin friction, heat transfer, and mass transfer at the boundaries. Finally, the accuracy of theoretical derivations and numerical calculations in the developed methodology is validated through comparing with the numerical simulations using the computational fluid dynamics (CFD) method.

4.2. Problem Definition

When analyzing the mixed convective heat and mass transfer in air cavities behind the vinyl siding of building envelopes, this study considers the effects of geometric irregularity and complexity by approximating the geometry of vinyl siding with groove. Compared with the uniform rectangular assumption in literature, this approximation simulates the effects of ratios of siding depth to air cavity depth. Figure 18 shows the defined physical model and corresponding

coordinate system for problem solving. The X axis is set along the flat wall pointing downward, and the Y-axis is perpendicular to the X axis pointing towards the vinyl siding. Air flows into the air cavity along the X axis; within the air cavity, the air flows between two vertical boundaries, namely the corrugated groove at $Y = \eta(X)$ and the flat wall sheathing at $Y = 0$.

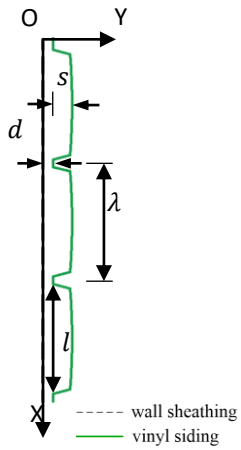

Figure 18. Physical model and coordinate system (d : Air cavity depth; l: Grove width; s: Groove depth; λ: Period of the groove).

With the problem and coordinate system defined, the continuity, momentum, energy, and mass fraction equations governing the system can be written, respectively, in the following form (Hammou, Benhamou, Galanis, & Orfi, 2004; Xu et al., 2019; Xu, Feng, & Zhang, 2017):

$$\frac{\partial U}{\partial X} + \frac{\partial V}{\partial Y} = 0 \tag{31}$$

$$\rho\left(\frac{\partial U}{\partial t} + U\frac{\partial U}{\partial X} + V\frac{\partial U}{\partial Y}\right) = -\frac{\partial P}{\partial X} + \mu\frac{\partial^2 U}{\partial X^2} + \mu\frac{\partial^2 U}{\partial Y^2} + \rho g\beta(T - \overline{T}) + \rho g\beta^*(w - \overline{w}) \tag{32}$$

$$\rho\left(\frac{\partial V}{\partial t} + U\frac{\partial V}{\partial X} + V\frac{\partial V}{\partial Y}\right) = -\frac{\partial P}{\partial y} + \mu\frac{\partial^2 V}{\partial X^2} + \mu\frac{\partial^2 V}{\partial Y^2} \tag{33}$$

$$\frac{\partial T}{\partial t} + U\frac{\partial T}{\partial X} + V\frac{\partial T}{\partial Y} = \frac{k}{\rho C_p}\left(\frac{\partial^2 T}{\partial X^2} + \frac{\partial^2 T}{\partial Y^2}\right) \tag{34}$$

$$\frac{\partial w}{\partial t} + U\frac{\partial w}{\partial X} + V\frac{\partial w}{\partial Y} = D_m\left(\frac{\partial^2 w}{\partial X^2} + \frac{\partial^2 w}{\partial Y^2}\right) \tag{35}$$

where, U and V are the velocity components along X and Y axis, respectively; t is time; ρ is the air flow density which is assumed constant in the flow field; p is the air pressure; g is the acceleration due to gravity; β and β^* are the coefficients of thermal expansion without and with mass fraction, respectively; T is the fluid temperature; $\bar{T}$ is the average of temperature at the wall sheathing and vinyl siding; w is the mass fraction (kg of vapor/kg of mixture); $\bar{w}$ is the average of mass fraction at the wall sheathing and vinyl siding; μ is the dynamic viscosity of fluid; k is the thermal conductivity; C_p is the specific heat at constant pressure; D_m is the coefficient of mass diffusivity.

The boundary conditions of the flow field are defined as follows: the velocity components are zero at the boundaries; the temperature is set as T_0 at the wall sheathing and T_1 at the vinyl cladding; the corresponding mass fractions are w_0 and w_1, respectively. That is, mathematically,

$$U = 0,\ V = 0,\ T = T_0,\ w = w_0 \qquad \text{at } Y = 0 \tag{36}$$

$$U = 0,\ V = 0,\ T = T_1,\ w = w_1 \qquad \text{at } Y = \eta\ (X) \tag{37}$$

Here, $Y = \eta\ (X)$ denotes the surface of the vinyl siding.

Then, dimensionless quantities can be defined as

$$u = \frac{U}{U_\infty},\ v = \frac{V}{\varepsilon U_\infty}, y = \frac{Y}{d},\ x = \frac{X}{\lambda},\ \bar{t} = \frac{U_\infty t}{\lambda},\ p = \frac{d^2 P}{\rho U_\infty \lambda},\ Re = \frac{\rho U_\infty d}{\mu},\ \ \theta = \frac{T-\bar{T}}{T_0-\bar{T}},\ \emptyset = \frac{w-\bar{w}}{w_0-\bar{w}},\ n = \frac{T_1-\bar{T}}{T_0-\bar{T}},\ m = \frac{w_1-\bar{w}}{w_0-\bar{w}},\ P_r = \frac{C_p \mu}{k},\ g_t = \frac{g\beta(T_1-\bar{T})d}{U_\infty^2},\ g_c = \frac{g\beta^*(w_1-\bar{w})d}{U_\infty^2},\ S_c = \frac{\mu}{\rho D_m},\ \overline{\eta} = \frac{\eta}{d},\ a = \frac{s}{d},\ \text{and } \varepsilon = \frac{d}{\lambda}. \tag{38}$$

With dimensionless quantities defined, Equations (31-35) can then be rewritten in the non-dimensional form as follows:

$$\frac{\partial u}{\partial x} + \frac{\partial v}{\partial y} = 0 \tag{39}$$

$$\varepsilon\left(u\frac{\partial u}{\partial x} + v\frac{\partial u}{\partial y}\right) = -\frac{\partial p}{\partial x} + \frac{1}{Re}\left(\varepsilon^2\frac{\partial^2 u}{\partial x^2} + \frac{\partial^2 u}{\partial y^2}\right) + g_t\theta + g_c\emptyset \tag{40}$$

$$\varepsilon^2\left(u\frac{\partial v}{\partial x}+v\frac{\partial v}{\partial y}\right)=-\frac{\partial p}{\partial y}+\frac{1}{Re}\varepsilon^2\left(\varepsilon^2\frac{\partial^2 v}{\partial x^2}+\frac{\partial^2 v}{\partial y^2}\right) \tag{41}$$

$$\varepsilon\left(u\frac{\partial \theta}{\partial x}+v\frac{\partial \theta}{\partial y}\right)=\frac{1}{P_r Re}\left(\varepsilon^2\frac{\partial^2 \theta}{\partial x^2}+\frac{\partial^2 \theta}{\partial y^2}\right) \tag{42}$$

$$\varepsilon\left(u\frac{\partial \emptyset}{\partial x}+v\frac{\partial \emptyset}{\partial y}\right)=\frac{1}{ReS_c}\left(\varepsilon^2\frac{\partial^2 \emptyset}{\partial x^2}+\frac{\partial^2 \emptyset}{\partial y^2}\right) \tag{43}$$

Accordingly, the boundary conditions in Equations (36) and (37) become

$$u=0,\ v=0,\ \theta=1,\ \emptyset=1 \qquad \text{at } y=0 \tag{44}$$

$$u=0,\ v=0,\ \theta=n,\ \emptyset=m \qquad \text{at } y=\overline{\eta} \tag{45}$$

4.3. Problem Solving with the Perturbation Method

The perturbation method is used to solve the problem defined in Equations (39) to (43) with boundary conditions in Equations (44) and (45). Perturbation theory helps to obtain approximate solutions by adding small terms to mathematical problem. It leads to an expression for the pursued solution in the form of a power series in the "small" parameter ε, that is the perturbation series. The perturbation series quantifies the deviation of the target problem from a solvable problem. In this power series, the leading term is the solution to the solvable problem, and the rest evaluates its deviation from the pursued solution. Formally, an approximation to the full solution A is expressed with the following power series:

$$A=\ A_0+\varepsilon A_1+\varepsilon^2 A_2+\cdots \tag{46}$$

where A_0 denotes the solution to a solvable initial problem and A_1 and A_2 represent the higher-order terms that can be solved iteratively. One perturbation solution can be achieved by truncating the series and keeping the first term representing the initial solution and the second term showing the first order correction. That is

$$A\approx A_0+\varepsilon A_1 \tag{47}$$

More details about the perturbation method can be found in (Eldabe, El-Sayed, Ghaly, & Sayed, 2008; Srinivas, Gayathri, & Kothandapani, 2011; Vajravelu & Sastri, 1978).

This study uses first-order perturbations to achieve an approximate solution to the mixed convection problem. The ε defined in Equation (38) is used as the small term to formulate the first order perturbations in this study. Following Equation (47), the distributions of pressure, air flow velocity, temperature, and mass fraction can be written, respectively, in the following form:

$$p(x,y) = p_0(x) + \varepsilon p_1(x,y) \tag{48}$$

$$u(x,y) = u_0(y) + \varepsilon u_1(x,y) \tag{49}$$

$$v(x,y) = v_0(y) + \varepsilon v_1(x,y) \tag{50}$$

$$\theta(x,y) = \theta_0(y) + \varepsilon \theta_1(x,y) \tag{51}$$

$$\emptyset(x,y) = \emptyset_0(y) + \varepsilon \emptyset_1(x,y) \tag{52}$$

where p_0, u_0, v_0, θ_0, and $\emptyset_0$ are the mean or zero-order quantities and p_1, u_1, v_1, θ_1, and $\emptyset_1$ are the first-order perturbation terms.

Substituting Equations (48)– (52) in Equations (39)– (43), collecting the coefficients of zero power of ε, the following equations are obtained

$$-\frac{\partial p_0}{\partial x} + \frac{1}{Re}\frac{\partial^2 u_0}{\partial^2 y} + g_t\theta_0 + g_c\emptyset_0 = 0 \tag{53}$$

$$\frac{1}{PrRe}\frac{\partial^2 \theta_0}{\partial^2 y} = 0 \tag{54}$$

$$\frac{1}{ScRe}\frac{\partial^2 \emptyset_0}{\partial^2 y} = 0 \tag{55}$$

with the following boundary conditions

$$u_0 = 0, \quad \theta_0 = 1, \emptyset_0 = 1 \qquad at\ y = 0 \tag{56}$$

$$u_0 = 0, \quad \theta_0 = n, \emptyset_0 = m \qquad at\ y = \overline{\eta} \tag{57}$$

Collecting the coefficients of 1 power of ε , the following equations are obtained.

$$u_0 \frac{\partial u_0}{\partial x} + v_0 \frac{\partial u_0}{\partial y} = -\frac{\partial p_1}{\partial x} + \frac{1}{Re}\left(\frac{\partial^2 u_1}{\partial^2 y}\right) + g_t\theta_1 + g_c\emptyset_1 \tag{58}$$

$$-\frac{\partial p_1}{\partial y} = 0 \tag{59}$$

$$u_0 \frac{\partial \theta_0}{\partial x} + v_0 \frac{\partial \theta_0}{\partial y} = \frac{1}{PrRe}\frac{\partial^2 \theta_1}{\partial^2 y} \tag{60}$$

$$u_0 \frac{\partial \emptyset_0}{\partial X} + v_0 \frac{\partial \emptyset_0}{\partial Y} = \frac{1}{ScRe}\frac{\partial^2 \emptyset_1}{\partial^2 Y} \tag{61}$$

The corresponding boundary conditions in the groove frame are

$$u_1 = 0, \quad \theta_1 = 0, \emptyset_1 = 0 \qquad at\ y = 0 \tag{62}$$

$$u_1 = 0, \quad \theta_1 = 0, \emptyset_1 = 0 \qquad at\ y = \overline{\eta} \tag{63}$$

After solving the problem defined in Equations (53) to (63). The following equations can be used to solve the skin friction, heat transfer, and mass transfer at the boundaries. Firstly, the dimensionless shear stress can be expressed as

$$\tau = \frac{\partial u}{\partial y} + \frac{\partial v}{\partial x} \tag{64}$$

The dimensionless shear stress at the flat wall and groove wall are

$$\tau^0 = \tau_0^0 + \varepsilon[u_1'(0) + u''_0(0)] \tag{65}$$

and

$$\tau^1 = \tau_0^1 + \varepsilon[u_1'(1) + u''_0(1)] \tag{66}$$

respectively, where,

$$\tau_0^0 = u_0'(0) \text{ and } \tau_0^1 = u_0'(1) \tag{67}$$

The dimensionless Nusselt number in the flow filed can be expressed as

$$Nu = \frac{\partial \theta}{\partial y} = \theta_0' + \varepsilon\theta_1'(y) \tag{68}$$

At the flat wall and groove wall, the dimensionless Nusselt number are

$$Nu^0 = Nu_0^0 + \varepsilon\theta_0'(0) \tag{69}$$

and

$$Nu^1 = Nu_0^1 + \varepsilon[\theta_1'(1) + \theta_0''(1)] \tag{70}$$

respectively, where

$$Nu_0^1 = \theta_0'(1) \text{ and } Nu_0^0 = \theta_0'(0) \tag{71}$$

The dimensionless mass transfer number or Sherwood number Sh in the flow field can be expressed as

$$Sh = \frac{\partial \emptyset}{\partial y} = \emptyset_0' + \varepsilon \emptyset_1'(y) \tag{72}$$

Then at the flat wall and groove wall, the Sherwood numbers are

$$Sh^0 = Sh_0^0 + \varepsilon \emptyset_0'(0) \tag{73}$$

and

$$Sh^1 = Sh_0^1 + \varepsilon[\emptyset_1'(1) + \emptyset_1''(1)] \tag{74}$$

respectively, where,

$$Sh_0^0 = \emptyset_0'(0) \text{ and } Sh_0^1 = \emptyset_0'(1) \tag{75}$$

In summary, the problem firstly defined in Equations (31) to (37) are transformed to the dimensionless form as shown in Equations (39) to (45) via the definitions in Equation (38); following this transformation, the distributions of pressure, air flow velocity, temperature, and mass fraction are written in the form of Equations (48) to (52) via the first-order perturbation method; subsequently, the governing equation are rewritten in the form of Equations (63) to (63); finally, Equation (64) to (75) are used to solve the skin friction, heat transfer, and mass transfer. This section establishes the methodology of solving the mixed convective heat and mass transfer problem in air cavities behind vinyl siding. Section 4.3 will examine the effectiveness of the proposed methodology by presenting and discussing the results of parametric analysis.

4.4. Numerical Validation

In this section, the proposed method is validated by comparing with the results of numerical simulations using the CFD method. A vinyl siding system is built using the Ansys Workbench program with the finite volume method. The CFD model for this system has 11255 elements, which is shown in Figure 19 together with its dimensions.

Figure 19. The CFD model of the vinyl siding system. (l: 2.8 inch, λ: 3.3 inch, s: 0.62 inch, and d: 0.62 inch referring to Figure 18).

The distribution of velocity (u) at x = ½ for the case with a = 1, n = 0, Re = 1, and m = 0 is used for validation. Figure 20 compares the results calculated using the proposed method in this paper and the results from CFD simulations. It shows that the velocity distributions calculated using the two methods are very close to each other, and the relative difference is within 10% along the whole range of y. This comparison validates the accuracy of the proposed method for

mixed convection analysis, which will be used in the rest of this paper for further analysis of the energy performance of building envelopes.

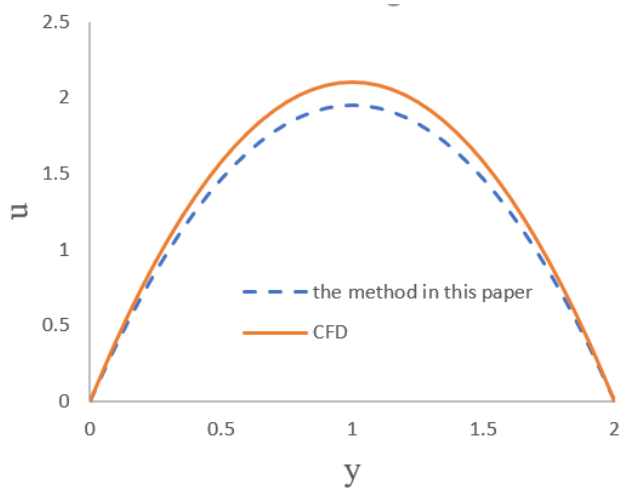

Figure 20. Comparison of the velocity (u) distributions at the location x = 1/2 (a = 1, n = 0, Re = 1, and m =0).

4.5. Results and Discussion

This section presents and discusses the results of mixed convective heat and mass transfer obtained by solving the governing equations with specified boundary conditions using the perturbation method. This study analyzes cases with different values of dimensionless vinyl siding depth (a), dimensionless temperature (n), Reynolds number (Re), and dimensionless mass fraction (m) to investigate the effects of their variations on the distribution of velocity, temperature, mass fracrion, skin friction, Nusselt number, and Sherwood number. When analyzing the effects of a certain variable, the values of other variables are set as constant. The distributions of velocity, temperature, etc. are presented along the wall sheathing (x) and its normal direction (y) respectively. Results discussion will reveal the importance of considering the shape complexity and irregularity of air cavity in analyzing the comprehensive performance of building envelopes with vinyl siding and thus the value of this study.

4.5.1. Effects on velocity distribution

Figure 21 shows the distribution of the non-dimensional velocity (μ) with different values of a, Re, n, m and fixed values of Prandtl number (P_r), Schmidt number (S_c), Grashof number (G_r), and local mass Grash of number (G_c). From Figure 21, it can be seen that u generally increases with the increase of a, Re, n and m . Along the y axis as shown in Figures 21 (a) to (d), u first increases to its maximum and then decreases to zero, yielding parachute-like curves. Figures 21 (f) and (h) depict similar trends along the x axis when n and m vary, respectively. Among these finding, the increase of the dimensionless vinyl siding depth (a) generally amplifies the velocity significantly, indicating the important geometric effects of air cavity. The difference of u between a =1 and a =3 is much smaller than that between a =7 and a =9, which indicates that the increase of vinyl siding depth decreases the velocity, however, the velocity decreases slightly when the air cavity depth increases. It can be seen from Figure 6 that the distribution of u is more affected by the variations of a and Re than by m and n.

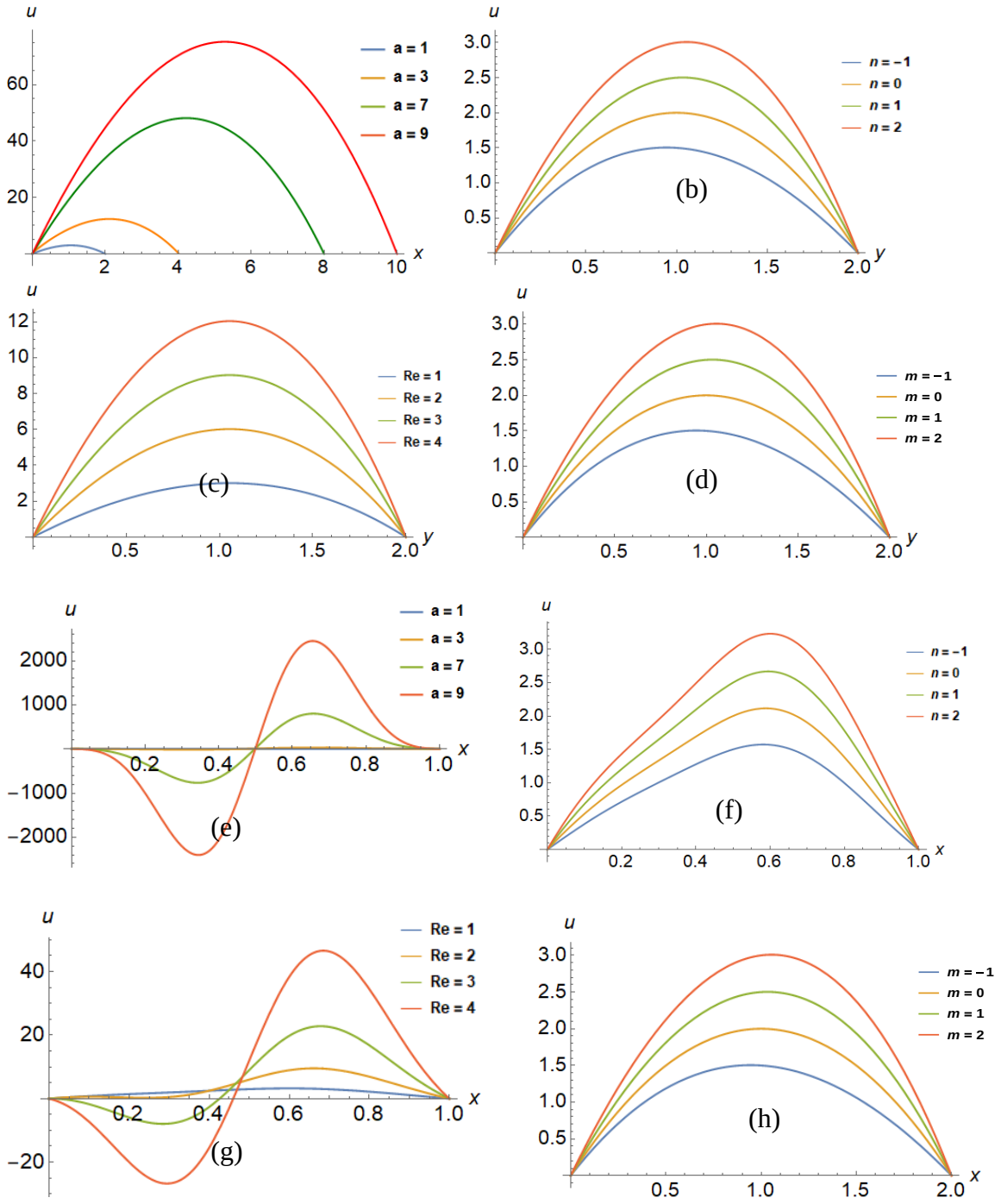

Figure 21. Velocity (u) distribution with the change of variables. (a) distribution along the y axis with different values of a; (b) distribution along the y axis with different values of n; (c) distribution along the y axis with different values of Re; (d) distribution along the y axis with different values of m; (e) distribution along the x axis with different values of a; (f) distribution along the x axis with different values of n; (g) distribution along the x axis with different values of Re; (h) distribution along the x axis with different values of m.

4.5.2. Effects on temperature distribution

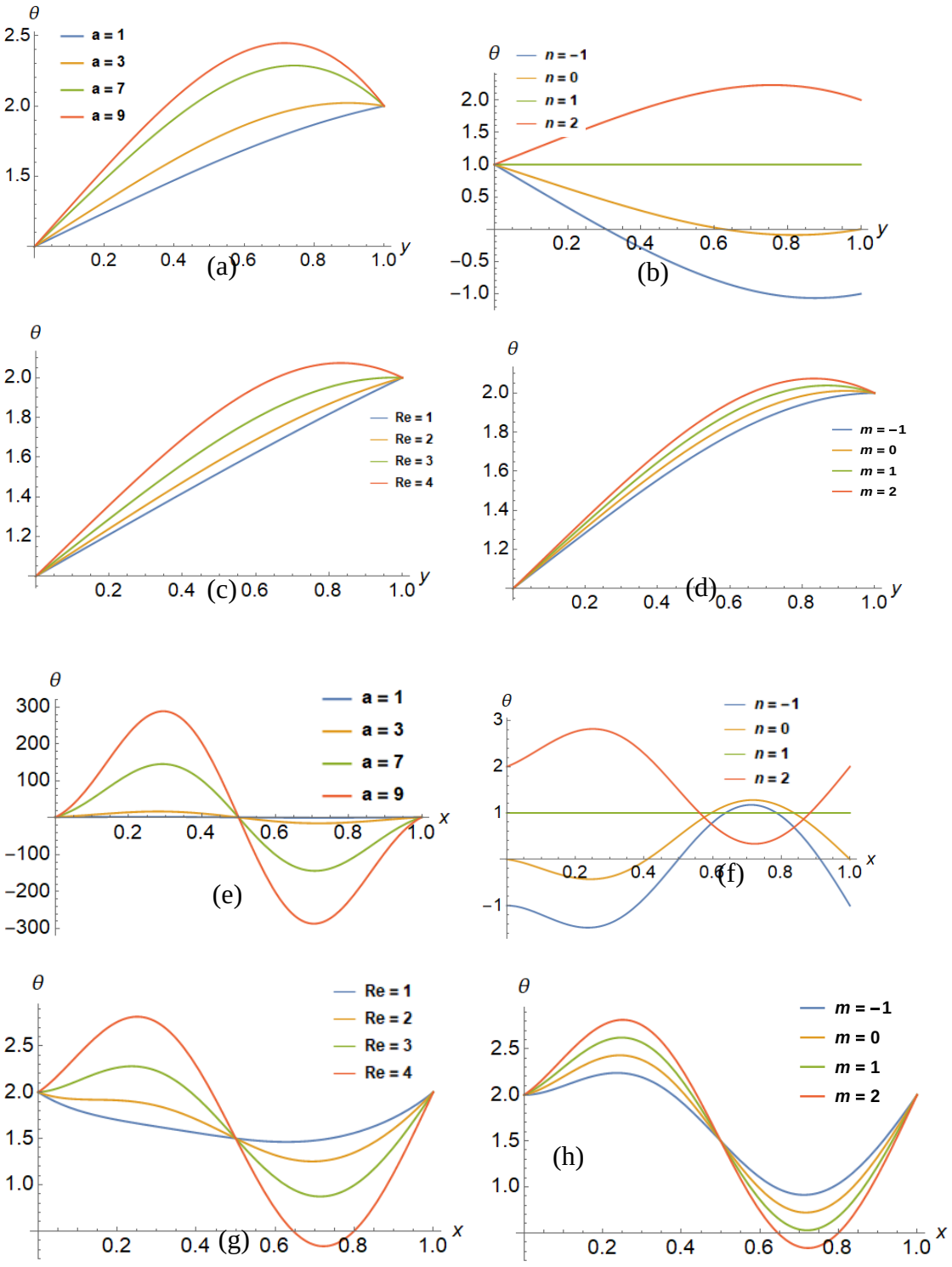

Figure 22. Temperature (θ) distribution with the change of variables. Please refer to Figure 21 for more explanations.

Figure 22 depicts the temperature (θ) profiles for various values of a, n, Re, and m. It shows that θ increases with the increase of a, Re and m at both locations of $x = 1$ (at the first period of grove as shown in Figure 20) and $y = 1$ (at *Y*=*d* as shown Figure 20). In addition, the temperature at first increases to certain value, then decreases slightly as y increases with certain values of a, Re and m, as shown in Figures 22 (a), (c), and (d). Moreover, the increase of the air cavity depth decreases the amplitude of the dimensionless temperature, as shown in Figure 22 (a) and 22(e). Therefore, the increase of the vinyl siding makes the temperature distribution flatter. Figure 22(b) shows significantly different trends for n. It shows that θ increases with the increase of n, and that θ first increases and then decreases slightly along the y axis when $n > 1$; in contrast, when $n < 1$, it first decreases to a certain value and then increases slightly. θ increases with the increase of n along the x axis when $n \leq 0$, and its amplitude increases as well with the increase of n when $n \geq 1$, as shown in Figure 22 (f). These findings indicate that the effects of n and a on the temperature profiles are significantly large compared to other parameters, which again demonstrates the importance of considering the effects of geometric properties.

4.5.3. Effects on mass fraction distribution

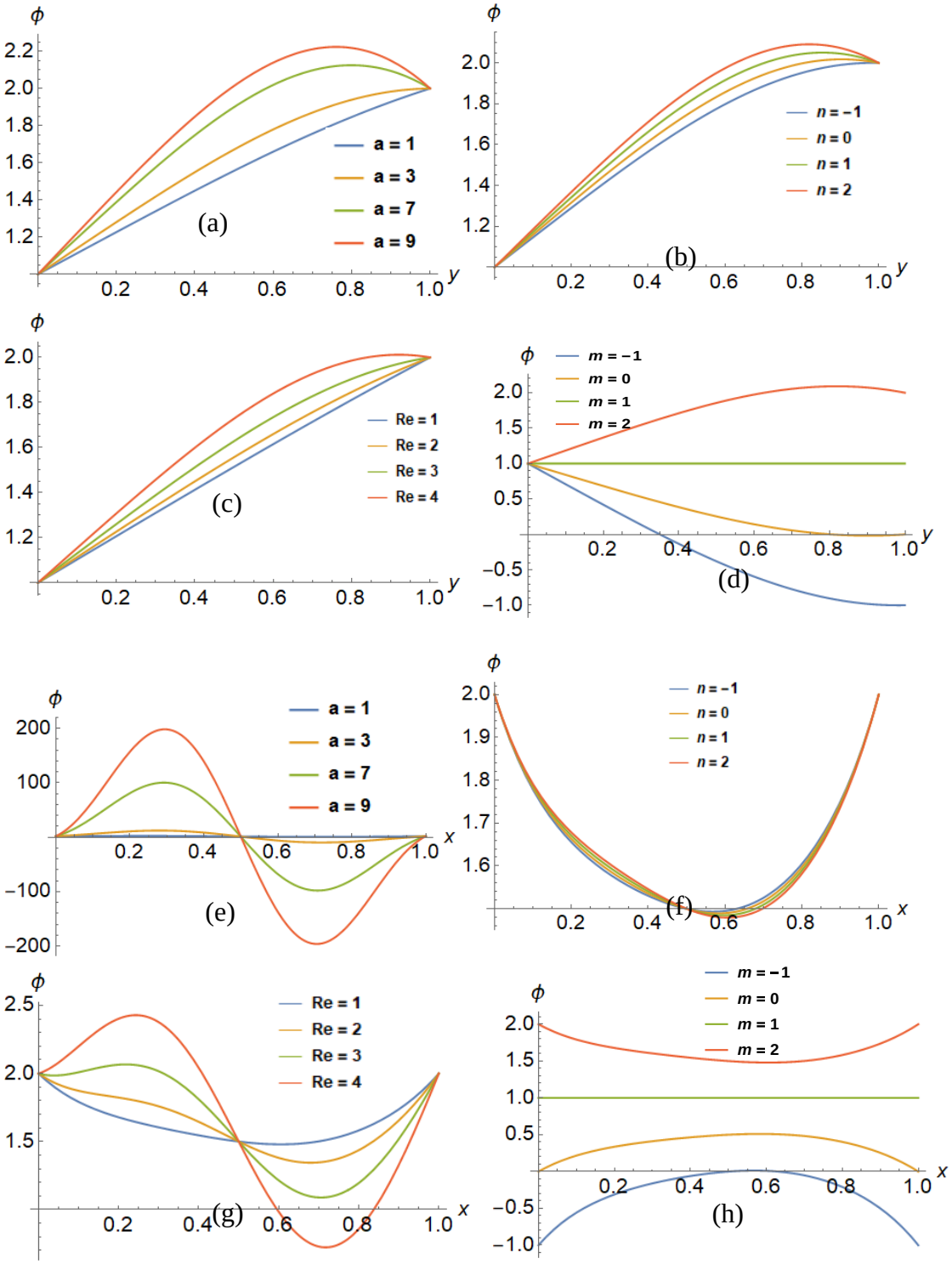

Figure 23. Mass fraction (∅) distribution with the change of variables. Please refer to Figure 21 for more explanations.

Figure 23 shows the distribution of the mass fraction ($\emptyset$) with the change of a, n, Re, and m with other variables fixed (g_t, g_c. P_r, S_c, etc.). Generally, $\emptyset$ increases with the increase of a, n and Re along the y axis as shown in Figures 8 (a) to (c). As shown in Figures 23 (a) and (c), $\emptyset$ increases along the y axis at certain values of a and Re; however, it first increases to its maximum and then decreases slightly as y increases at a certain value of m, as shown in Figure 23 (d). Therefore, the increase of a can increase $\emptyset$ at the location of $x = 1$ and its fluctuation at the location of $y = 1$. Moreover, Figures 23 (d) and (h) show that $\emptyset$ increases with the increase of m at both locations of $x = 1$ and $y = 1$. The mass fraction first increases to certain value and then decreases slightly as y increases when $m > 1$, and it decreases monotonically when $m < 1$. On the contrary, the mass fraction firstly decreases to its minimum and then increases to its maximum when $m > 1$, and it increases to its maximum and then decreases to its minimum when $m < 1$, with the increase of x. From these findings, it can be concluded that a, Re, and m have important effects on the mass fraction profiles compared to n.

4.5.4. Effects on skin friction distribution

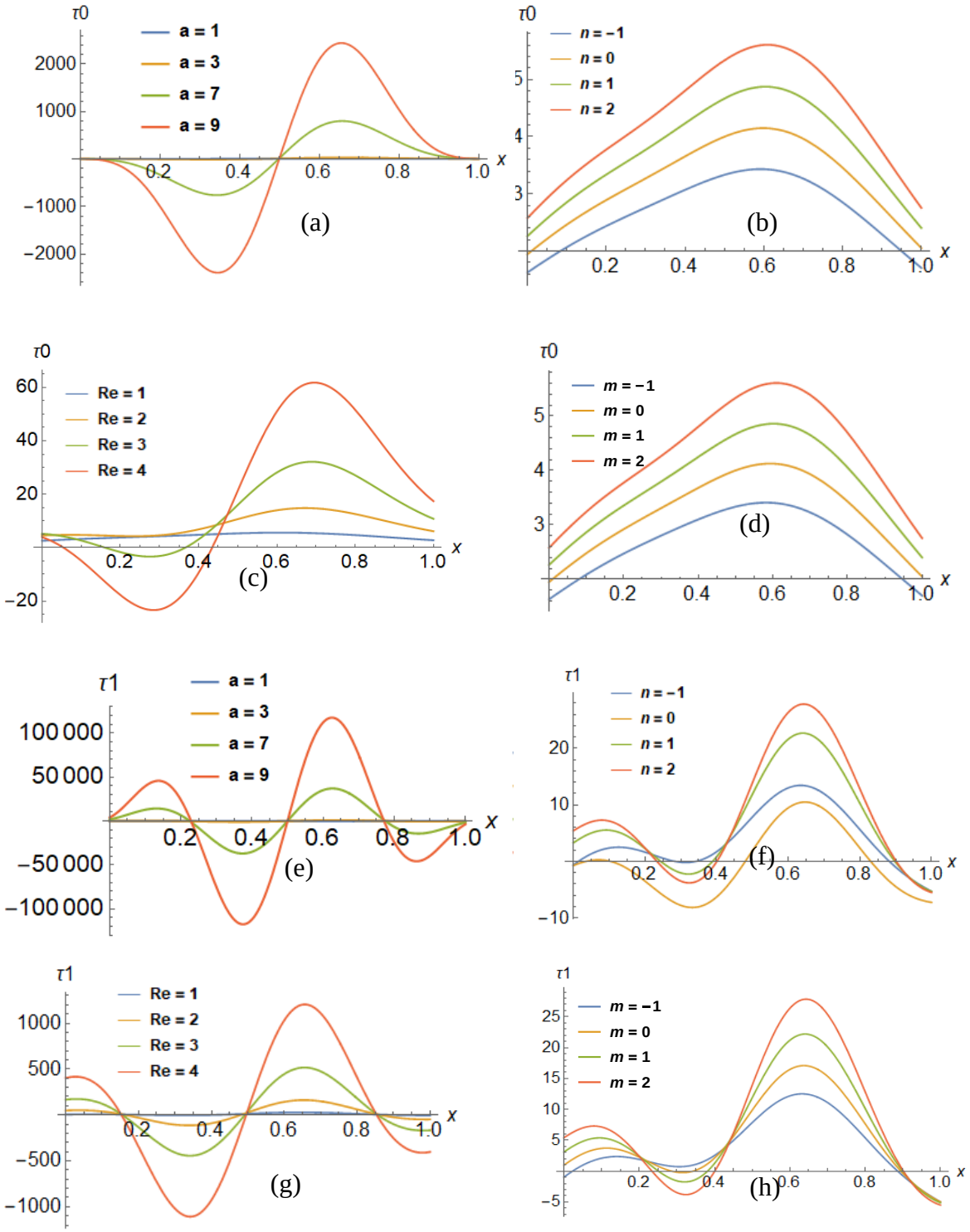

Figure 24. Distribution of the skin friction (τ) with the change of variables. τ_0 is the value of τ at $y = 0$; τ_1 is the value of τ at $y = 1$ Please refer to Figure 21 for more explanations.

The axial shear stress distribution (τ) for different values of a, n, Re, and m is presented in Figure 24. Figures 24 (a) to (h) show that τ generally increases with the increase of a, n, Re, and m. Additionally, an increase of a increases its fluctuation at both walls as shown in Figures 24 (a) and (e). Therefore, the geometry of the air cavity has a significant influence on the skin friction of both walls. It can also be observed that the effects of the parameters of a, n, Re, and m is significantly larger than that on the wall $y = 1$.

4.5.5. Effects on Nusselt number distribution

Figure 25 shows the behavior of Nusselt number distribution, Nu_0 and Nu_1 at the flat wall and the vinyl siding, respectively. Nu_0 and Nu_1 generally increase with the increase of a, Re and m, as shown in Figure 25. Additionally, Figure 25 shows that the effects of a and Re on Nu_0 is opposite to that on Nu_1 with the increase of x. Furthermore, with the increase of the air cavity depth or the increase of a, the heat transfer coefficient decreases. Therefore, the geometry of the air cavity has a significant influence on Nu on both walls. Moreover, the Nu_0 and Nu_1 increase with the increase of n at both walls. It is also observed that Nu_0 and Nu_1 at first decrease to their minimum and then increases to their maximum with the increase of y when $n > 1$. In contrast, they increase to the maximum and then decrease to the minimum with the increase of y when $n \leq 0$. From these results, it can be seen that Nu is affected significantly by an increase in the parameters a, Re and n, compared to m.

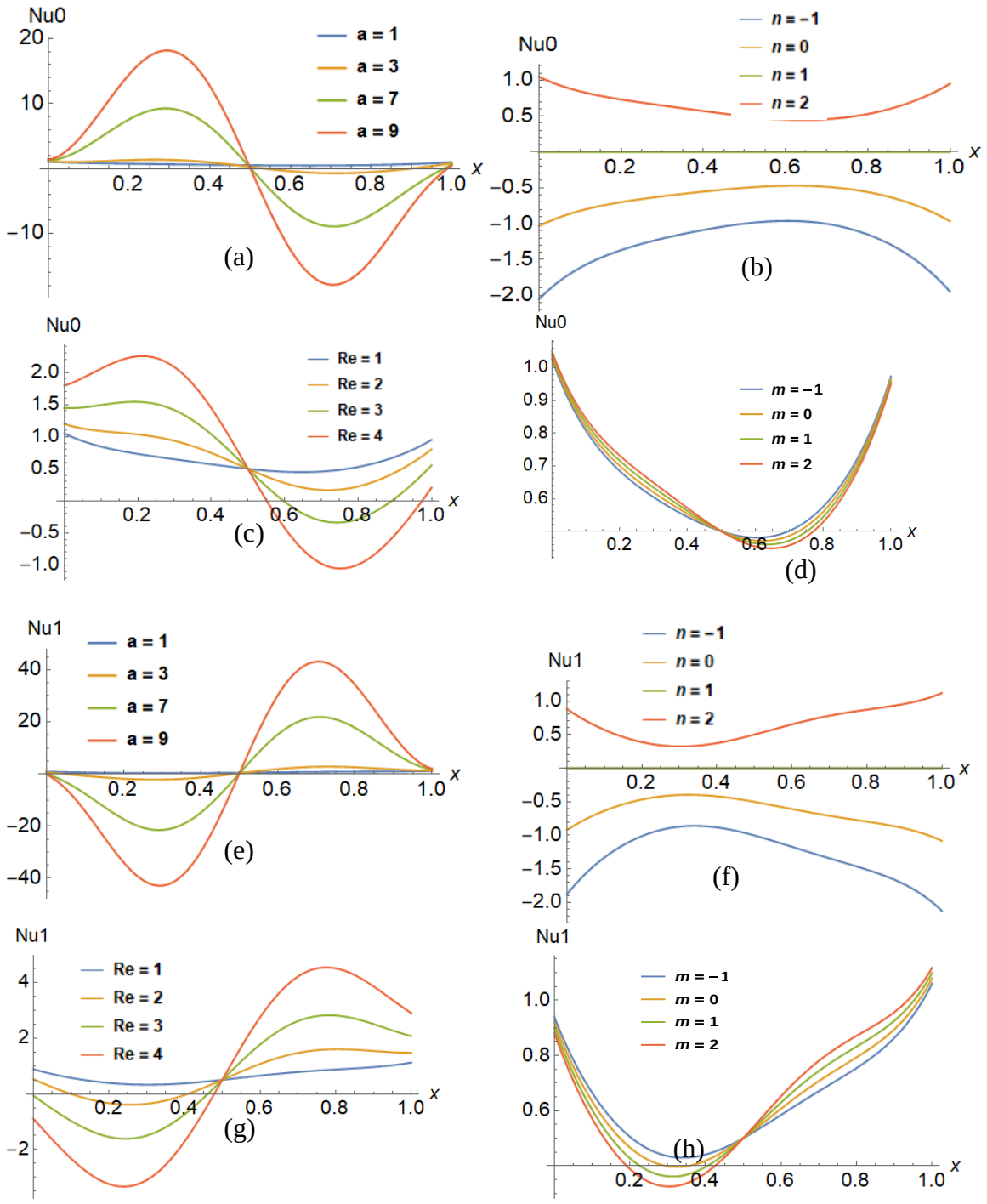

Figure 25. Distribution of the Nusselt number (Nu) with the change of variables. Nu_0 is the value of Nu at $y = 0$; Nu_1 is the value of Nu at $y = 1$. Please refer to Figure 21 for more explanations.

4.5.6. Effects on Sherwood number distribution

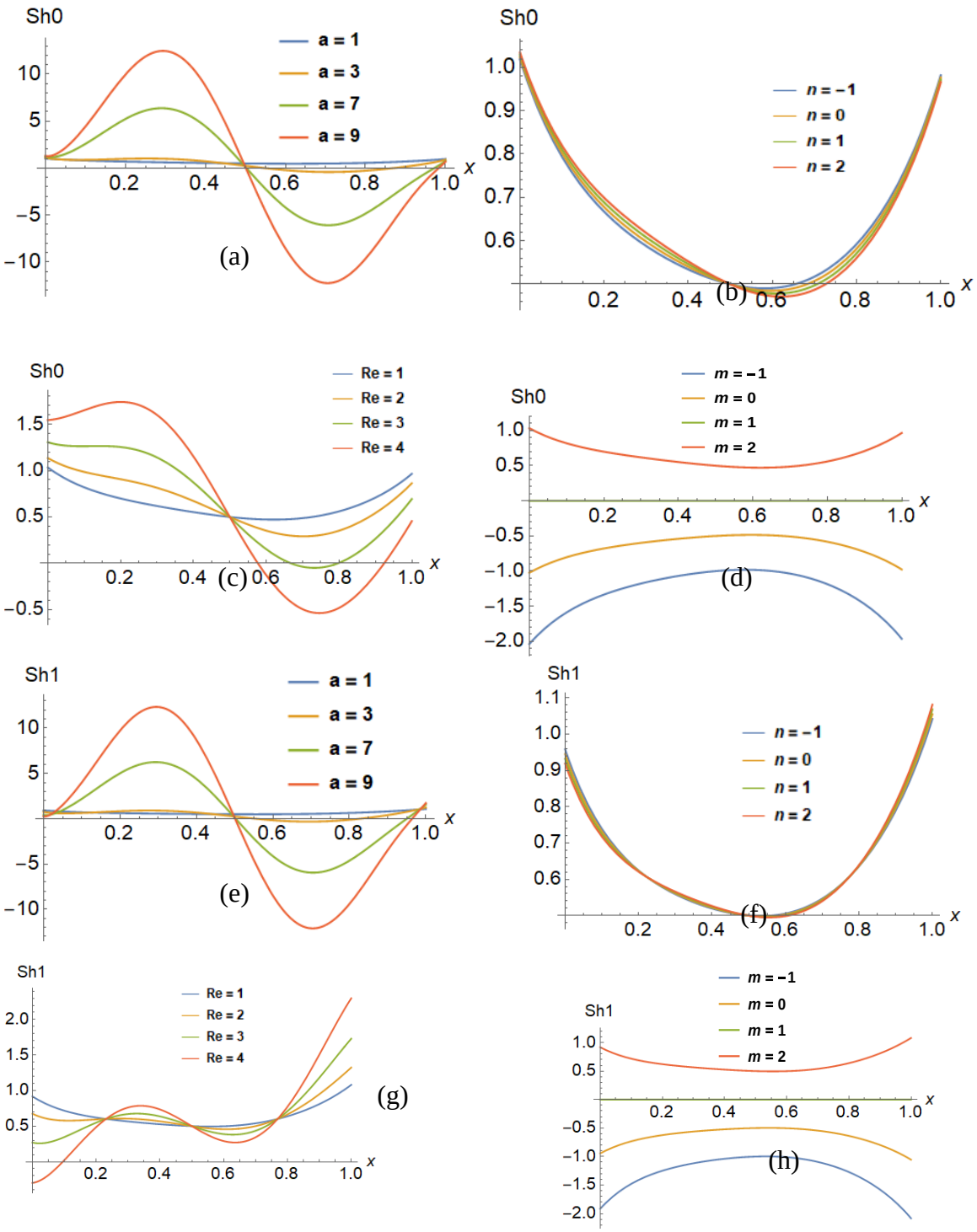

Figure 26. Distribution of the dimensionless Sherwood number (Sh) with the change of variables. Sh_0 is the value of Sh at $y = 0$; Sh_1 the value of Sh at $y = 1$. Please refer to Figure 21 for more explanations.

Figure 26 shows the distribution of the dimensionless Sherwood numbers (Sh). Figure 26 shows an increase of amplitude of Sherwood numbers with the increase of a, Re and n. Therefore, the geometry of the air cavity has a significant influence on Sh on both walls. Moreover, Sh at the both walls increase with the increase of the m, as shown in Figures 26 (d) and (h). In addition, Sh first decrease to the minimum and then increases to its maximum with the increase of y when $m > 1$. In contrast, it increases to the maximum and then decrease to its minimum with the increase of y when $m \leq 1$. Additionally, the effect of n is negligible as shown in Figures 26 (b) and (f), compared with that of other variables.

4.5.7. Summary

This section presents the results of mixed convection analysis and investigated the effects of shape parameter (a) of the air cavity as well as other parameters on the important metrics related to the performance of building envelope. It shows that the siding to cavity depth ratio has significant effects on all the metrics compared with other parameters, which verifies the importance of considering its influence in future design and analysis.

4.6. Conclusions

Considering the limitations of existing studies on the air cavity of vinyl sidings for the energy performance of building envelope, this study investigates ratios of vinyl siding depth to air cavity depth in mixed convection of air cavity behind vinyl siding for building envelopes. The results of simulations show that the geometry of air cavity has significant effects on the overall performance of building envelopes, which approves the essential value of this study, especially when compared with existing studies in the literature that omits the effects of geometry. Influential factors affecting important metrics of air cavity regarding its energy performance (i.e., air velocity, temperature, mass fraction, mass transfer rate, shear stress) are evaluated through a

comprehensive parametric analysis. This study is an essential supplement of the state of the art which lacks an extensive analysis of the effects of geometric irregularities and mixed convection. The outcome of this study provides valuable guidance on the thermal performance evaluation of air cavity behind vinyl siding and has the potential of improving the design of vinyl siding for the overall energy performance of building envelope.

5. EFFECT OF HUMID AIR IN AN AIR CAVITY BEHIND SIDING ON MASS AND HEAT TRANSFER WITH PHASE CHANGE AT THE WALL

The building envelopes are exposed to the external environmental conditions including water, air, heat, and noise, etc. A cavity wall is a wide-spread design to block the impact of these conditions on the building and its envelopes. The cavity wall is composed of an outer leaf, a cavity, and an inner leaf. The outer leaf acts as the weather barrier while the cavity acts as a capillary break and drainage to avoid the moisture to penetrate the inner leaf. There are three types of cavities, unvented cavity, vented cavity and ventilated cavity. The difference between those types of cavities is the position of the opening. The opening of the vented cavity is only at the bottom, which provides the drainage. Meanwhile, the openings of the ventilated cavities are at the top and bottom, which improve the airflow rates and drying. In the literature, the studies reported the contradictory finding regarding the benefits of ventilated cavities. Some papers indicated ventilated air cavity did not provide beneficial moisture and thermal performance. For example, the air with high humidity ratio flows into the air cavity, the moisture in the air will lead to a hygroscopic moisture loading. Additionally, the weather conditions or boundary conditions have a significant effect on the performance of an air cavity. The hygrothermal model could help to understand the performance of the air cavity under the different weather conditions.

As mentioned above, once the humid air enters the air cavity through the opening, it can result in a hygroscopic moisture load. Additionally, the moisture can significantly affect the thermal performance of the building envelopes. For example, the moisture can decrease the heat conduction resistance and increase the convection coefficient. Furthermore, the humid air may be condensed or vapored under certain climate conditions at the wall. The phase change of the humid air in the air cavity can affect the heat transfer between the air cavity and the wall of the building,

and between the air cavity and the claddings. Even though the coupling of heat, air and moisture transportation in the air cavity has been proposed, it has the limitations because of the complexity of the building's physical problems. Firstly, previous studies mainly focused on the ventilation of the air cavities, neglecting heat transfer. On the other hand, they neglected the effect of humid air in the cavity on the hygrothermal performance. However, in other areas, plenty of studies has reported the heat and mass transfer process with humid air through studying and experimenting the effect of humid air in a vertical channel by two parallel plates (Cherif & Daïf, 1999; W. Yan & Lin, 1989; W. M. Yan, 1993). Cherf and Daif showed that an increase of inlet air humidity can decrease the sensible heat transfer slightly and increase latent heat transfer (Cherif & Daïf, 1999). Yan indicated that the liquid film thickness can be neglected when the mass flow is small and latent heat transfer depends on the film temperature and inlet flow rate (W. M. Yan, 1993). Ait Hammou et al. has studied the effect of simultaneous heat and mass transfer on downward laminar flow of humid air in a channel (Hammou et al., 2004). They found that an increase of inlet air temperature can significantly affect the latent Nusselt number. They also proved that the buoyance force has an important effect on the hydrothermal filed, while the effect on the average air temperature and mass friction can be neglected. Based on the study of Hammou et al., Oulaid et al. added the flow reversal in their study. They indicated that buoyance force not only has a significant influence on the hydrothermal field, but also on the thermal and mass friction field (Oulaid, Benhamou, & Galanis, 2010). Compared to these papers, the direction of the air flow has a significant effect on the heat and mass transfer. Ghrissi et al. studied the effect of parameters on mass and heat transfer in an air channel with a saturated wall. They found that the inlet air in winter condition affects the heat and mass transfer tremendously at the interface than in summer conditions (Ghrissi et al., 2022). Therefore, it is important to consider different weather

conditions in the study of the effect of humid air on the heat and mass transfer in air cavity with evaporation or condensation at the wall.

According to the above statement, previous study lacks in the study of the effect of humid air in the air cavity between the claddings and wall sheathings on heat and mass transfer in a cavity with evaporation or condensations. This research studies the heat and mass transfer problem in air cavity with considering condensation or evaporation at the interface between the film and air. To analyze this, the partial differential equations are solved using the SIMPLER algorithm with considering the axial diffusion terms. The effect of inlet air conditions (the inlet air temperature, inlet air vapor content, and Reynolds numbers) on the axial evolutions of the transverse velocity at the interface, average air temperature, average air vapor content, friction factors, the sensible and latent Nusselt number, and the Sherwood number are investigated. The results of heat and mass transfer analysis approve the significant effects of convection on the comprehensive performance of building envelopes with sidings. These findings can potentially improve the accuracy and creditability of future related analysis and provide practical guidance on engineering designs of building envelopes of this type especially with the results of parametric analysis.

5.1. Problem Formulation

Atmosphere air, with uniform conditions such as the dry bulb temperature T_0, the relative humidity ϕ_0, and the velocity U_0, enters the air cavity behind siding. The height of the air cavity between the siding and wall sheathing is 2.5m, and the width is 1cm that is standard for most rainscreen application for siding assemblies in the United States. The thin film of liquid water covers in siding and wall sheathing. The air flow is assumed as the laminar flow, with considering

steady state conditions. The density in the body force is considered to be a linear function of temperature and mass fraction.

With the problem and coordinate system defined as Figure. 27, the continuity, momentum, energy, and concentration equations governing the system can be written, respectively, in the following form (Xu, Feng, & Zhang, 2017)

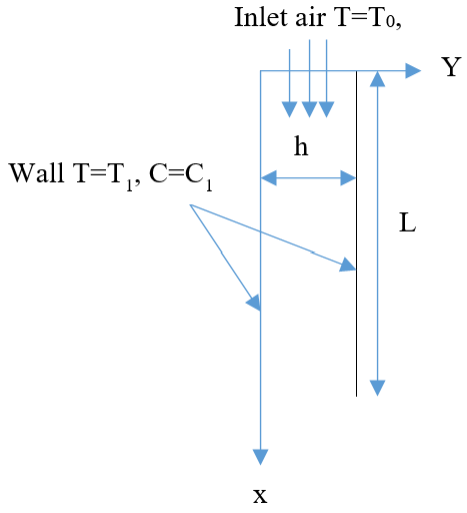

Figure 27. Physical model and coordinate system

$$\frac{\partial U}{\partial X}+\frac{\partial Y}{\partial Y}=0 \tag{76}$$

$$\rho\left(U\frac{\partial U}{\partial X}+V\frac{\partial U}{\partial Y}\right)=-\frac{\partial P}{\partial X}+\mu\frac{\partial^2 U}{\partial X^2}+\mu\frac{\partial^2 U}{\partial Y^2}+\rho g\beta(T-\bar{T})+\rho g\beta^*(C-\bar{C}) \tag{77}$$

$$\rho\left(U\frac{\partial V}{\partial X}+V\frac{\partial V}{\partial Y}\right)=-\frac{\partial P}{\partial y}+\mu\frac{\partial^2 V}{\partial X^2}+\mu\frac{\partial^2 V}{\partial Y^2} \tag{78}$$

$$U\frac{\partial T}{\partial X}+V\frac{\partial T}{\partial Y}=\frac{k}{\rho C_p}\left(\frac{\partial^2 T}{\partial X^2}+\frac{\partial^2 T}{\partial Y^2}\right) \tag{79}$$

$$U\frac{\partial C}{\partial X}+V\frac{\partial C}{\partial Y}=D_m\left(\frac{\partial^2 C}{\partial X^2}+\frac{\partial^2 C}{\partial Y^2}\right) \tag{80}$$

where, U and V are the velocity components along X and Y axis, respectively; ρ is the air flow density which is assumed constant in the flow field; p is the air pressure; g is the

acceleration due to gravity; β and β^* are the coefficients of thermal expansion and mass fraction expansion, respectively; T is the fluid temperature; $\bar{T}$ is the average of temperature at the wall sheathing and brick veneer; C is the fluid concentration; $\bar{C}$ is the average of concentration at the wall sheathing and brick veneer; μ is the dynamic viscosity of fluid; k is the thermal conductivity; C_p is the specific heat at constant pressure; D_m is the coefficient of mass diffusivity.

The boundary conditions of the flow field are defined as follows:

At the wall ($Y = 0$ or $Y = h$)

$$U = 0,\ V = Ve,\ T = T_1,\ C = C_2 \qquad \text{at } Y = 0 \quad (81)$$

$$U = 0,\ V = Ve,\ T = T_1,\ C = C_1 \qquad \text{at } Y = h \quad (81)$$

At the inlet ($X = 0,\ 0 < Y < h$)

$$U = U_0,\ V = 0,\ T = T_0,\ C = C_0 \qquad \text{at } X = 0 \quad (83)$$

At the outlet ($X =$ L , $0 < Y < h$)

All axial derivatives are zero

where the transverse velocity at the interface:

$$Ve = -Dm/v/(1 - w_w)(\frac{\partial C}{\partial Y})_{Y=0}$$

or

$$Ve = -1/Sc/(1 - w_w)(\frac{\partial C}{\partial Y})_{Y=0} \quad (84)$$

Heat transfer between the wet wall and the air:

$$q_t = k(\frac{\partial T}{\partial Y})_{Y=0} + \rho D h_{fg} \left(\frac{\partial C}{\partial Y}\right)_{Y=0} /(1 - w_w) \quad (85)$$

Nusselt number

$$Nu_t = q_t Dh/k(T_w - \bar{T}) \quad (86)$$

$$Sh = Dh * \frac{h}{D} \quad (87)$$

5.2. Numerical Solution

The method of control volume is adopted to solve the partial differential equations. The Simple algorithm is used to solve the velocity-pressure coupling. Convergence of this iterative procedure is declared when

$$Max\left(\frac{\varphi_{i,j}^{n+1}-\varphi_{i,j}^{n}}{\varphi_{i,j}^{n+1}}\right) < 10^{-5} \tag{88}$$

The non-uniform grid is adopted in both the streamwise and transverse directions. The node density near the inlet and the walls are greater. Figure 28 shows the effect of the number of nodes on the calculated results of average temperature in the air cavity for the same conditions. It shows that the average temperature profile in the cavity with the different number nodes are very close to each other, and the relative difference is within 1% on the average temperature in the air cavity. Therefore, 100×70 discretization is sufficiently accurate. Therefore, 100 x 70 nodes are used to calculate all the results in this thesis.

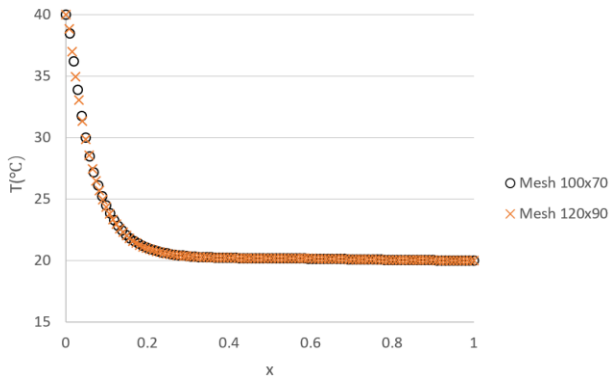

Figure 28. Effect of discretization on the average temperature in the air cavity along x direction

The numerical model in this chapter is validated with the results from the literature (Oulaid et al., 2010). Figure 29 shows that the agreement between this study and Oulaid et al.'s study is good. This result indicates that the numerical model developed above can be used to analyze the problem in this paper.

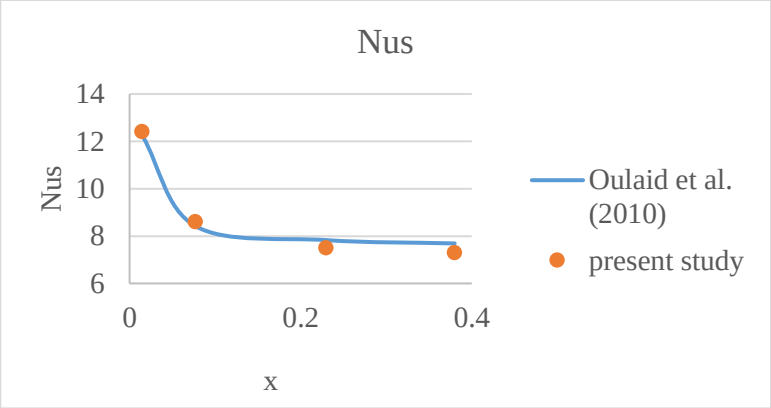

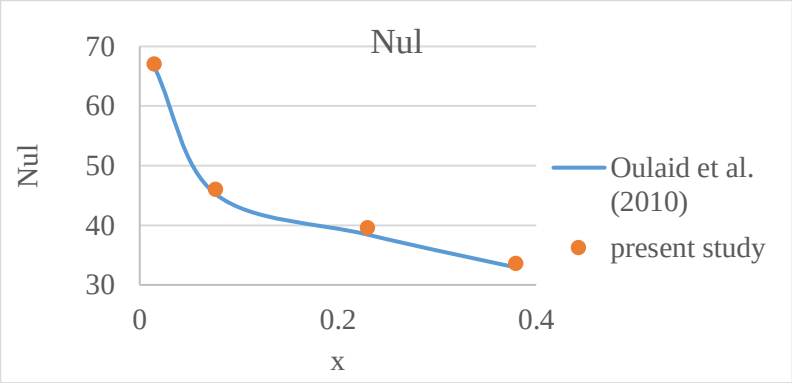

Figure 29. Validation of the Nusselt number

5.3. Results and Discussion

Table 3. Parameters for cases under study

Case	T_0 (℃）	Φ_0(%)	W_0 (g/kg)
1	30	10	2.6
2	30	55	14.56
3	30	70	18.65
4	10	10	0.75
5	40	10	4.56

In this paper, the Reynold number is fixed as 1000, the mass friction at the wall is calculated at the fixed temperature at the wall as 20◦C assuming the state of the air-vapor mixture at the wall as an ideal gas mixture. The five cases of the inlet moisture conditions are listed in Table 3. Grashof numbers determine the buoyance force acting on the direction of gravity and

aiding the entering flow. When the inlet temperatures in the table are higher than the wall temperature, the thermal Grashof numbers are negative, and the buoyance force caused by the temperature differential opposes the inlet flow. Meanwhile, the mass diffusion Grashof numbers are depended on the mass friction listed in Table 3. The mass diffusion Grashof numbers for case 1, 4 and 5 are positive, that for case 2 is nearly to zero, and that for case 3 is negative. Therefore, the mass diffusion buoyance forces aid the flow in the case 1, 4 and 5. On the contrary, the mass diffusion buoyance force opposes the flow in the case 3. Compared to the results, it helps to determine the effect of the buoyance force on the flow filed.

5.3.1. Effects on vapor velocity at the interface

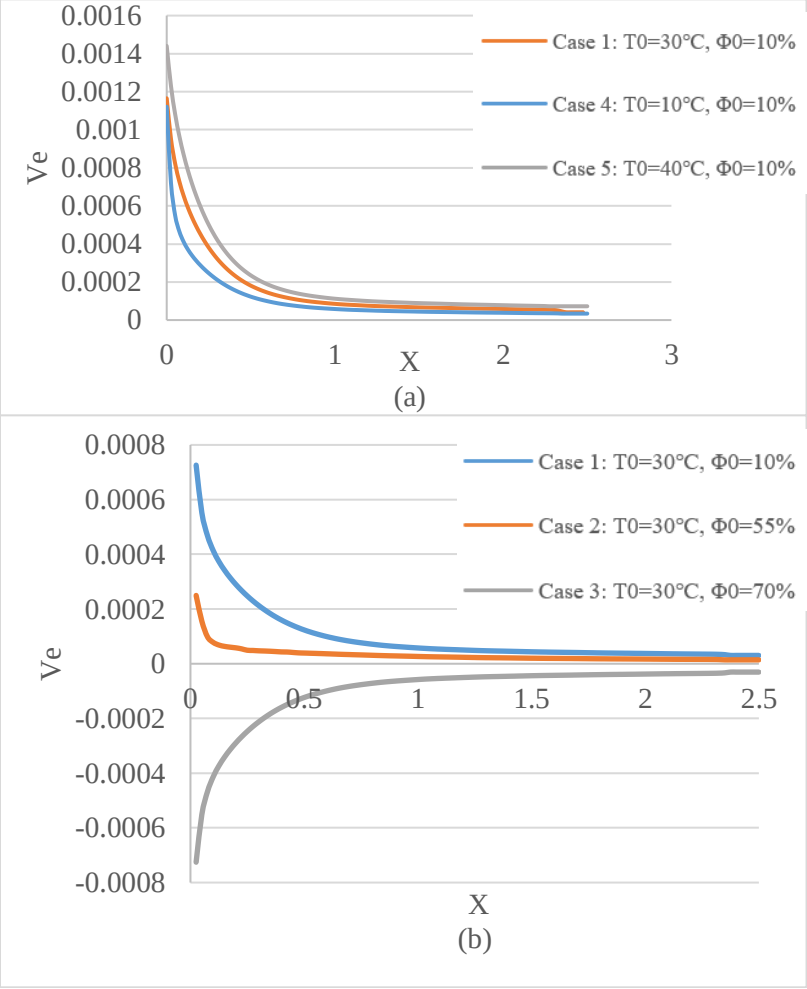

Figure 30. Axial evolution of the dimensionless transverse vapor velocity at the interface

Figure 30. shows the effects of temperature T_0 and humify ratio Φ_0 on the axial evolution of the dimensionless transverse vapor velocity at the interface. Figure 30 (a). is noted that the transverse vapor velocity at the interface decreases, then converges to the zero as x increases. Meanwhile, as the temperature increases, the dimensionless transverse vapor velocity increases. Figure 30 indicates that the transverse vapor velocity of the case 3 (T_0 =30℃and Φ_0 =70%) is negative, and the other cases' transverse vapor velocities are positive. Positive transverse vapor velocity means the moisture is evaporated and transferred to the airflow. On the contrary, negative transverse vapor velocity indicates the moisture is condensed and transferred to the wall. In case 2 (T_0 =30℃and Φ_0 =55%), the transverse vapor velocity is nearly to zero, which indicates there is no phase change and mass transfer between the flow and the wall. These results are consistent with the mass frictions at the wall and the flow. When the mass friction at the wall is larger than the flow (cases 1, 4, and 5), the moisture vapor at the wall transfers to the flow. On the contrary, when the mass friction at the wall is smaller than the flow (case 3: T_0 =30℃and Φ_0 =70%), the moisture vapor transfers to the opposite direction. Meanwhile, when the mass friction at the wall equals to the flow (case 2: T_0 =30℃and Φ_0 =55%)), there is no mass transfer between the wall and flow.

5.3.2. Effects on average mass friction in the cavity

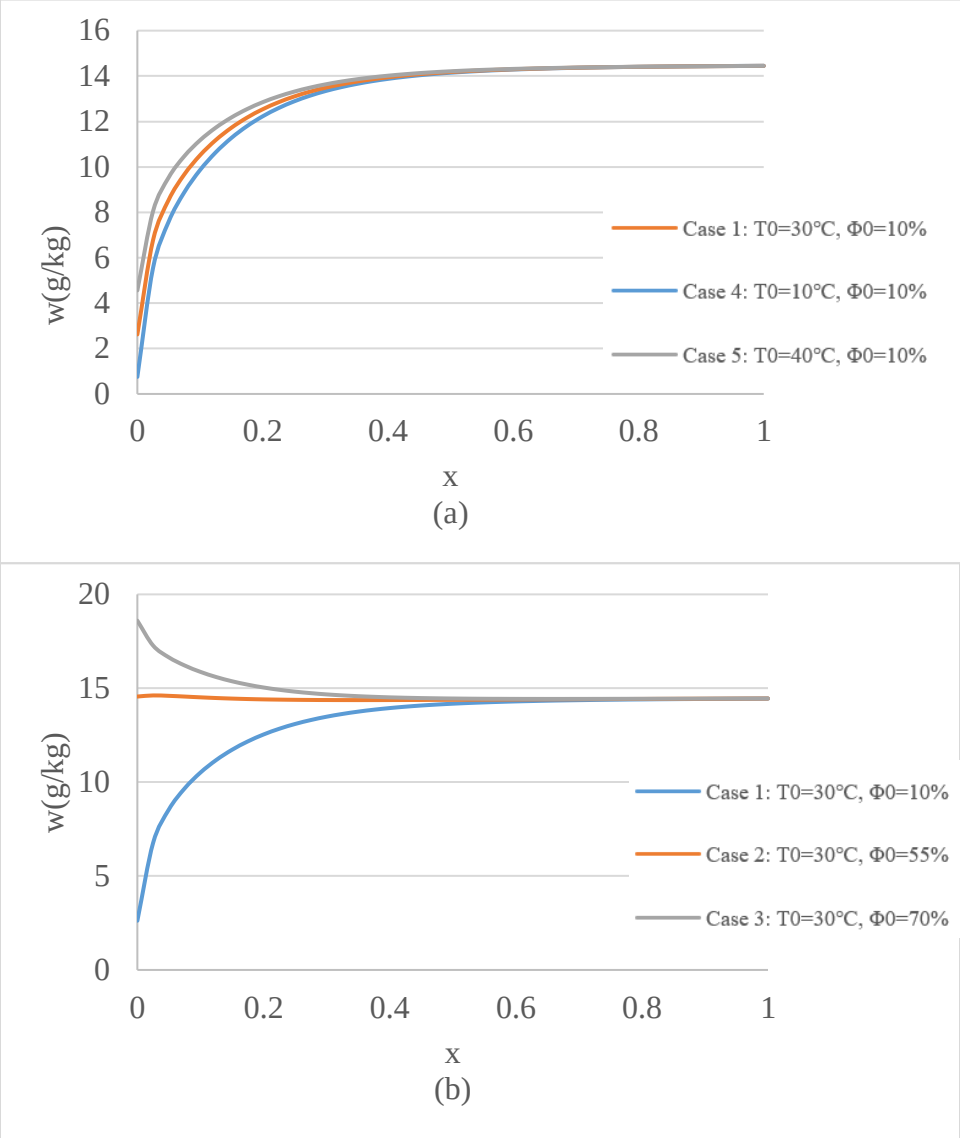

Figure 31. Axial evolution of the average mass friction

Figure 31 depicts the effects of temperature T_0 and humify ratio Φ_0 on the axial evolution of average mass friction. Figure 31 (a). shows that the average mass friction increases, then converged to the certain value as x increases. Meanwhile, as the temperature increases, the average mass friction increases. Figure 31 (b). shows in case 3 the average mass friction decreases with x, and in case 2 the average mass friction stays constant. Meanwhile, as the humidity ratio

increases, the average mass friction increases. All the cases indicated that the flow in the air cavity tended to the wall conditions at the outlet of the cavity, which is consistent with that transverse vapor velocity at the interface near the outlet of air cavity equals to zero.

5.3.3. Effects on average air temperature in the cavity

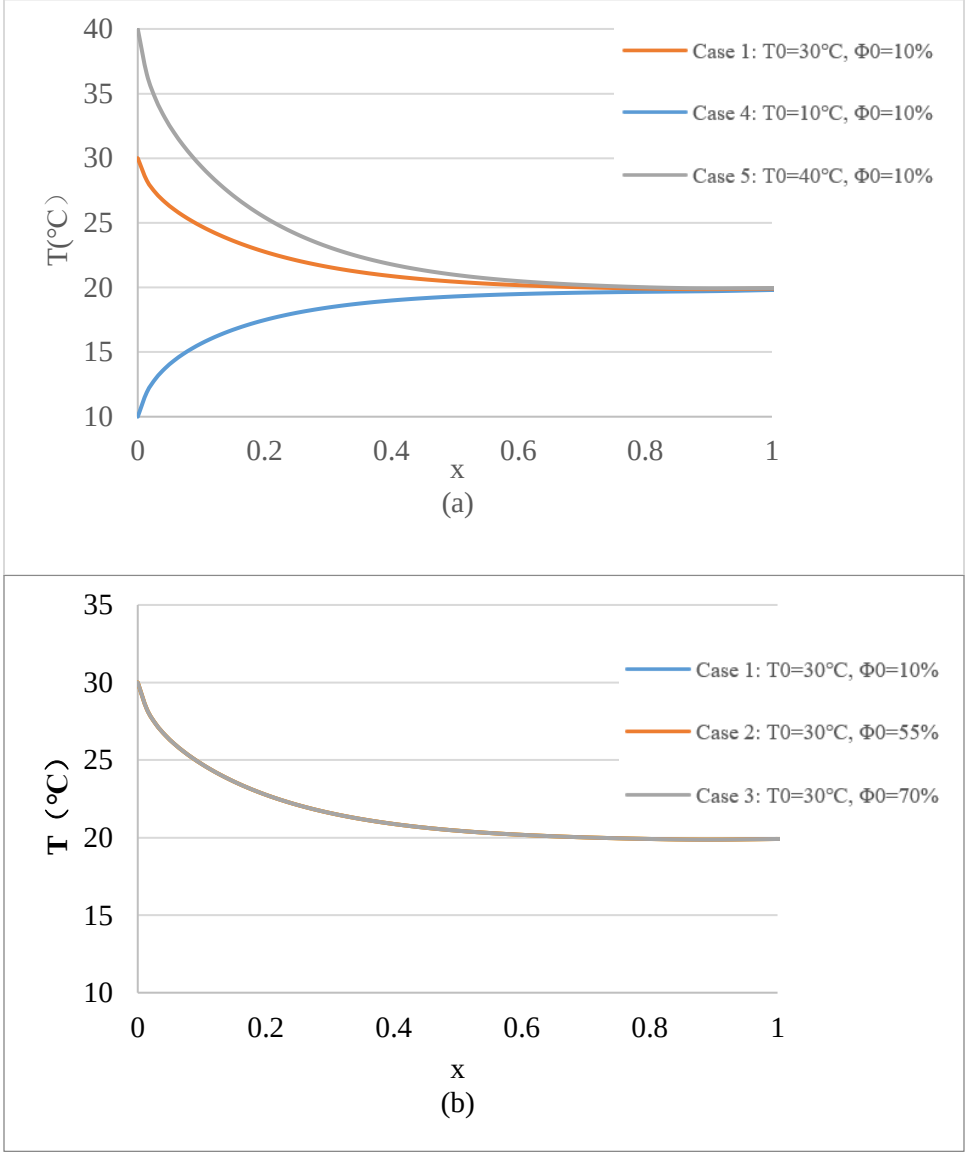

Figure 32. Axial evolution of the average air temperature

Figure 32 shows the effects of temperature T_0 and humify ratio Φ_0 on the axial evolution of average air temperature. Figure 32 (a). shows that when the inlet air temperature is above the wall temperature, the average air temperature decreases, then converges to the certain value as x

increases. On the contrary, when the inlet temperature is below the wall temperature, the average air temperature increases, then converges to the wall temperature as x increases. Meanwhile, as the inlet temperature increases, the average air temperature increases. Figure 32 (b). shows in cases 1 to 3 the average air temperature decreases with x. Meanwhile, as the inlet humidity ratio increases, the average air temperature keeps constant, which indicated that the inlet humidity ratio has a little effect on the average air temperature. All the cases indicated that the air temperature in the air cavity tended to the wall conditions at the outlet of the cavity, which is consistent with that transverse vapor velocity at the interface near the outlet of air cavity equals to zero.

5.3.4. Effects on axial evolution of the sensible Nusselt number

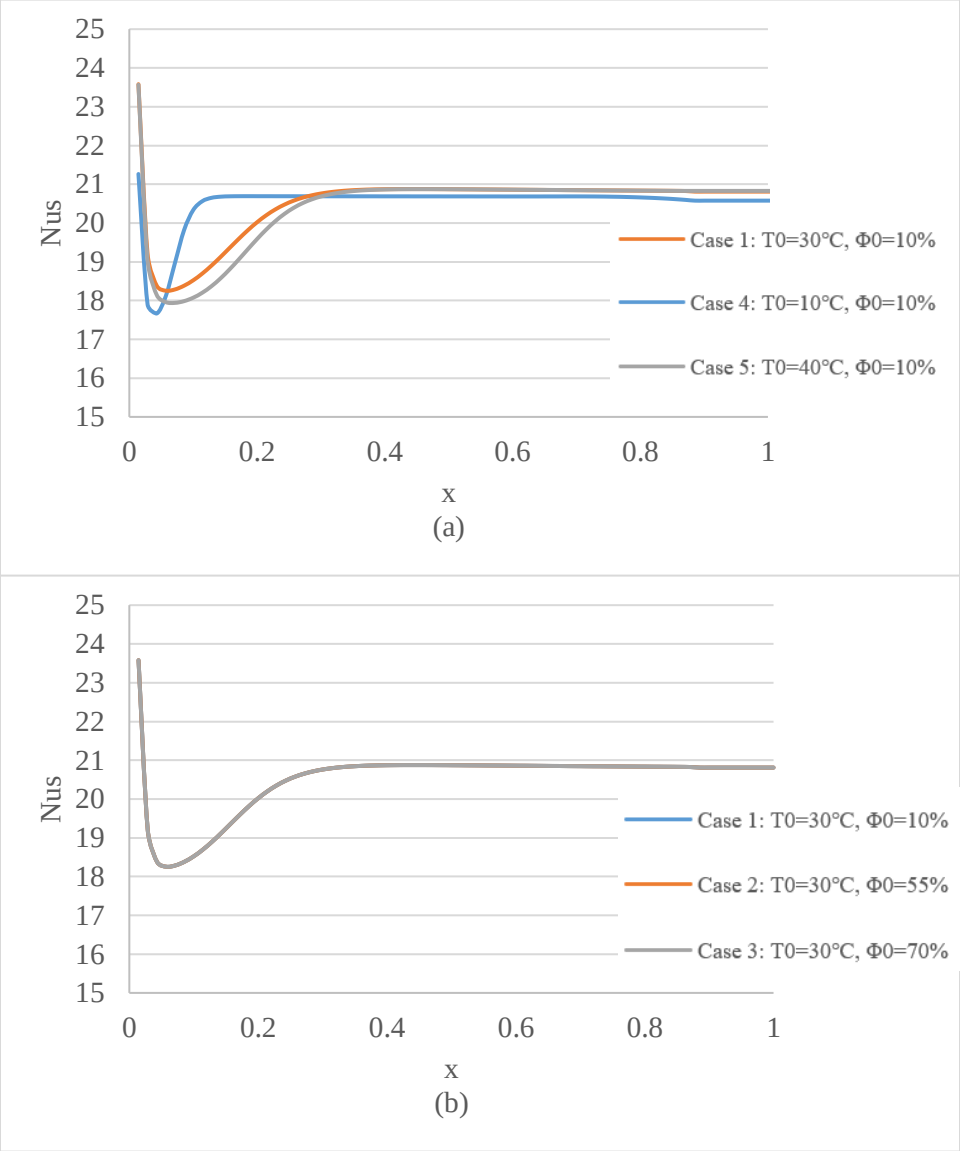

Figure 33. Axial evolution of the sensible Nusselt number

Figure 33 presents the effect of temperature T_0 and humidity ratio Φ_0 on the sensible Nusselt number. Nusselt number is always positive whether evaporation or condensation occurs. Figure 33 shows that Nus first decreases quickly, then increases, finally converges to the certain value with x increases. Moreover, the effect of temperature and humidity ratio on the sensible Nusselt is not significant when the thermal Grashof number and mass diffusion Grashof number

is the same for all the cases, which agrees with the results indicated by the Hammou et al. (2004) (Hammou et al., 2004).

5.3.5. Effects on axial evolution of the friction coefficient

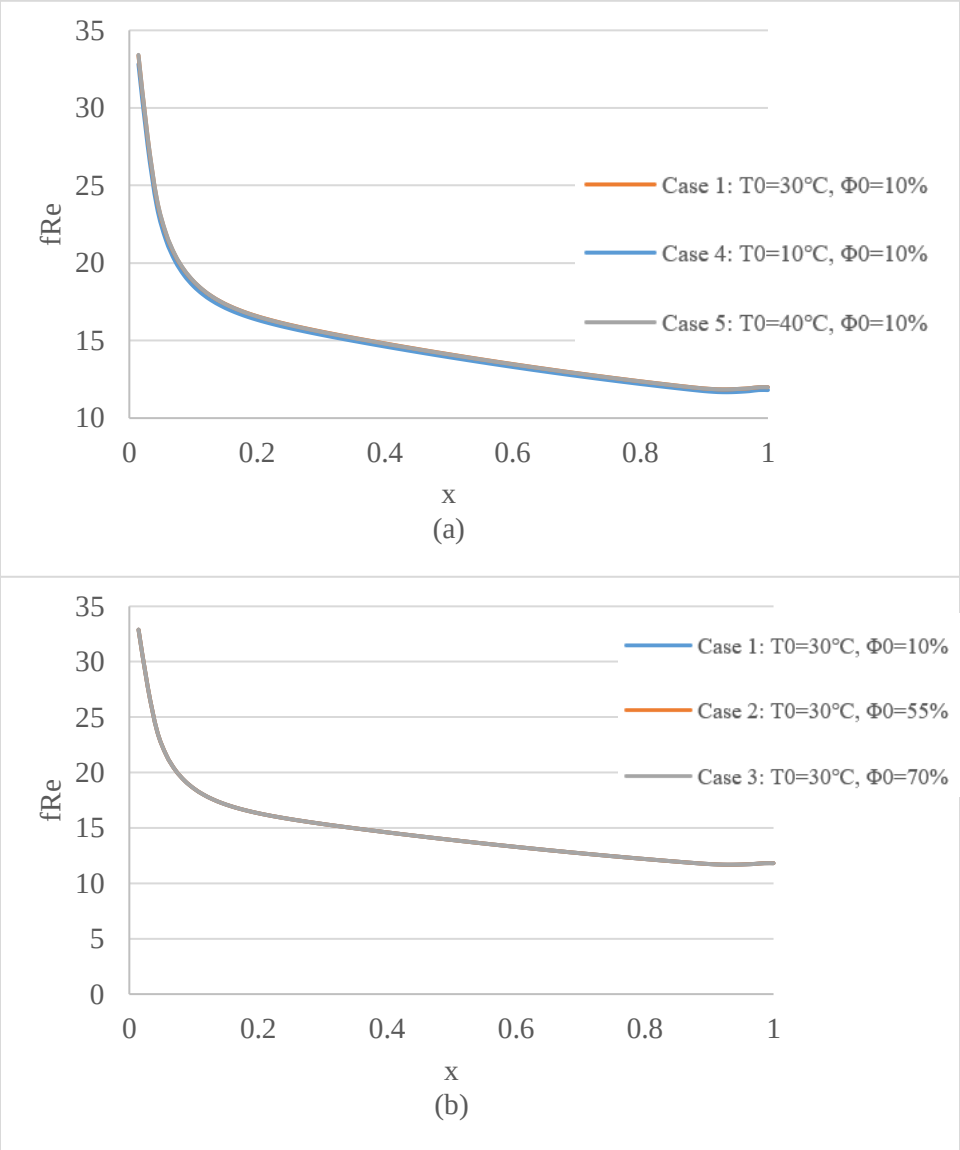

Figure 34. Axial evolution of the friction coefficient

Figure 34 presents the result of the axial evolution of axial evolution of the friction coefficient. It shows that the fRe first decreases then converges to the certain value with x increase. Both figures show that temperatures and humidity ratio have little effect on the axial evolution of the friction coefficient. This result agrees with Hammou et al.'s result (2004), when

the solutal Grashof number and thermal Grashof number are the same with all the cases (Hammou et al., 2004).

5.3.6. Effects on axial evolution of Sherwood number

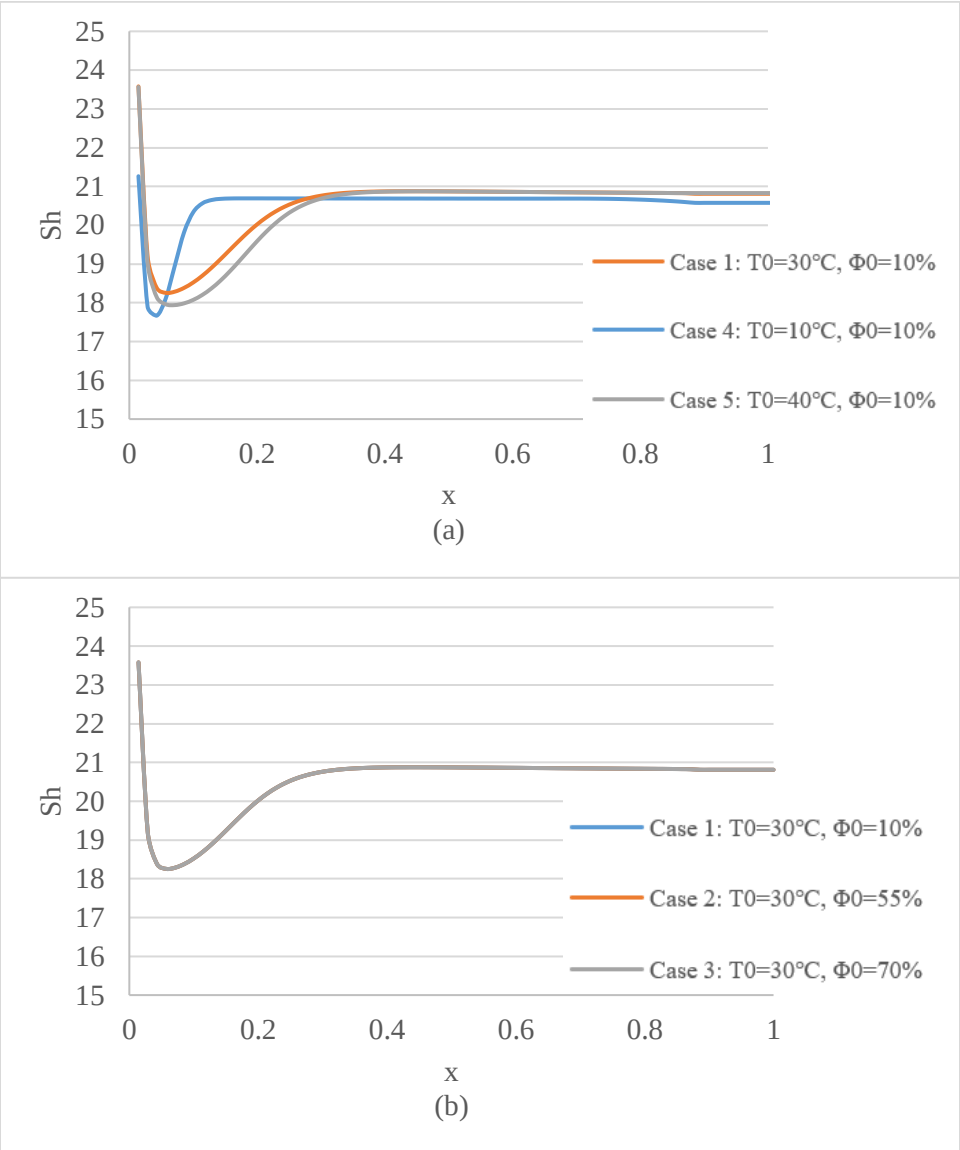

Figure 35. Axial evolution of Sherwood number

Mass transfer is represented by the Sherwood number. Figure 35 shows the effect of temperature T_0 and humidity ratio Φ_0 on the Sherwood number. According to the Eq.87, Sherwood number is always positive whether evaporation or condensation occurs. Figure 36 shows that Sh first decreases quickly, then increases, finally converges to the certain value with x

increases. In all cases, Sh tends towards to the same value, which agrees with the results reported by Hammou et al.(2004) (Hammou et al., 2004).. Compared to the sensible Nusselt number, it found that the distribution of Sh and Sensible Nusselt number are the same. Moreover, the effect of temperature and humidity ratio on the Sherwood number is not significant when the thermal Grashof number and mass diffusion Grashof number is the same for all the cases, which agrees with the results indicated by the Hammou et al. (2004) (Hammou et al., 2004).

5.3.7. Axial evolution of the latent Nusselt number

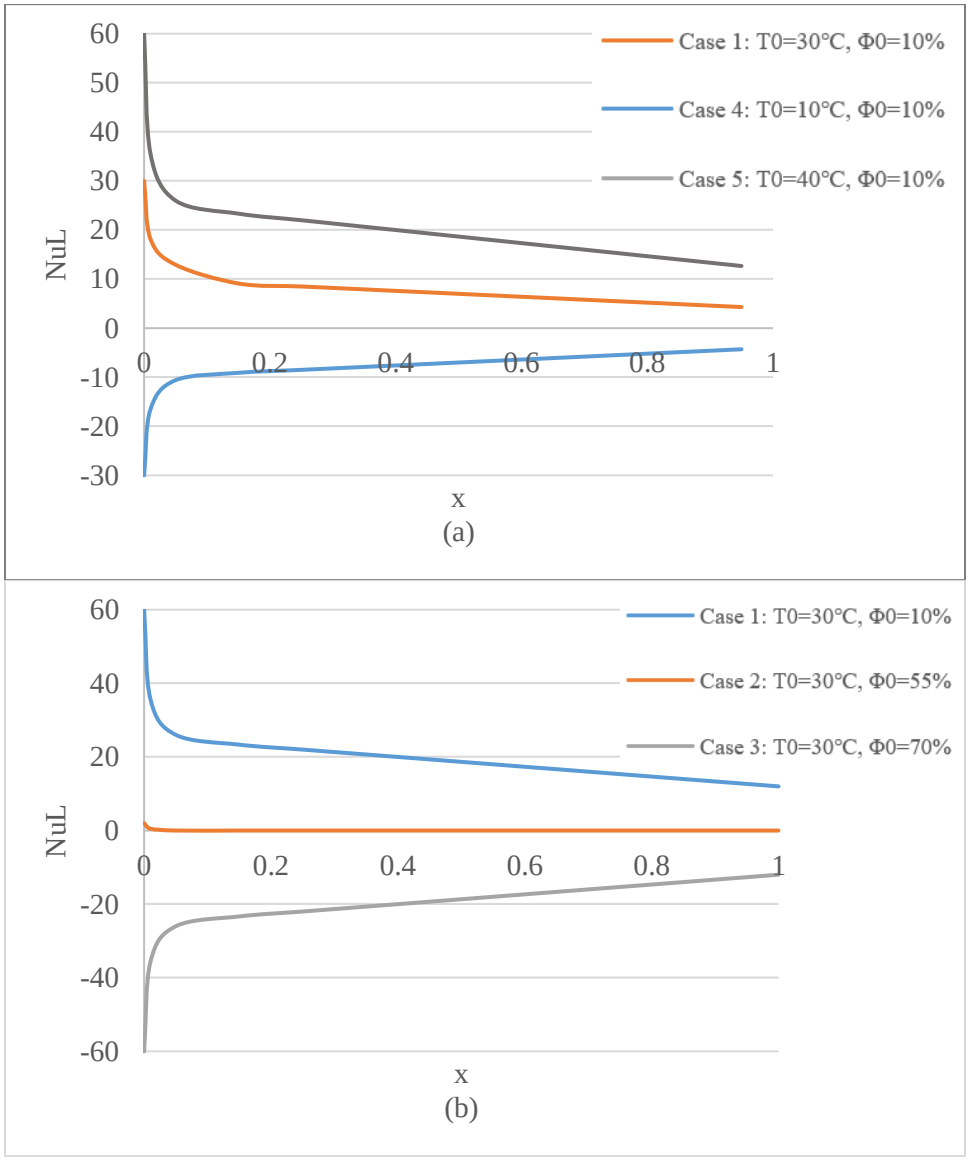

Figure 36. Axial evolution of the latent Nusselt number

Figure 36 show the effect of temperature T0 and humidity ratio Φ0 on the latent Nusselt number. According to the Eq.86, positive value of the latent Nusselt number means the evaporation of vapor at the wall while negative value of the latent Nusselt number indicates the condensation occurs. When the inlet air vapor content is close to the film vapor content, there is no mass transfer. Therefore, the value of the latent Nusselt number in the case 3 equals to zero as shown in Figure (b). As a while, when the inlet air vapor content is larger than the film water content, the inlet air vapor near the wall will condense. Therefore, NuL for case 3 (humidity ratio is 70%) is negative. When the inlet air vapor content is less than the film water content, NuL for case 1 (humidity ratio is 20%) is positive. That is because the film water vapors and flows into the air stream. According to the Eq. 86, when inlet air temperature is less than wall temperature, NuL value is negative. NuL decreases as the humidity ratio increases, while NuL decrease as inlet air temperature increases when the inlet air temperature is larger than the wall temperature. Moreover, when inlet air temperature is larger than the film water conditions, the Nul decreases as x increase while NuL increases as x increase when inlet air temperature is less than the film water temperature. Moreover, NuL increases as x increase when inlet air water content is larger than film water content while NuL decreases as x increase when inlet air water content is less than film water content.

Compared to the results between the latent Nusselt number and the sensible Nusselt number, firstly this paper finds that the latent Nusselt number can be positive or negative while the sensible Nusselt number always be positive. Secondly inlet air temperature and inlet air humidity ratio have a significant influence on latent Nusselt number and a small influence on the sensible Nusselt number.

5.3.8. Axial velocity profile

Figure 37 shows the results of the axial velocity profiles at the location of x=0.2. Figure 37 shows that at the center of the cavity, the axial velocity reaches the maximum values, and the axial velocity near the wall is close to zero. Meanwhile, the axial velocity keeps constant as the humidity ratio increase, which indicates that the humidity ratio has little effect on the axial velocity profiles. Figure 37 (a) shows the axial velocity decrease with the increase of inlet air temperature. Figures 37 indicates that the effect of humidity ratio and inlet air temperature on the axial velocity is small.

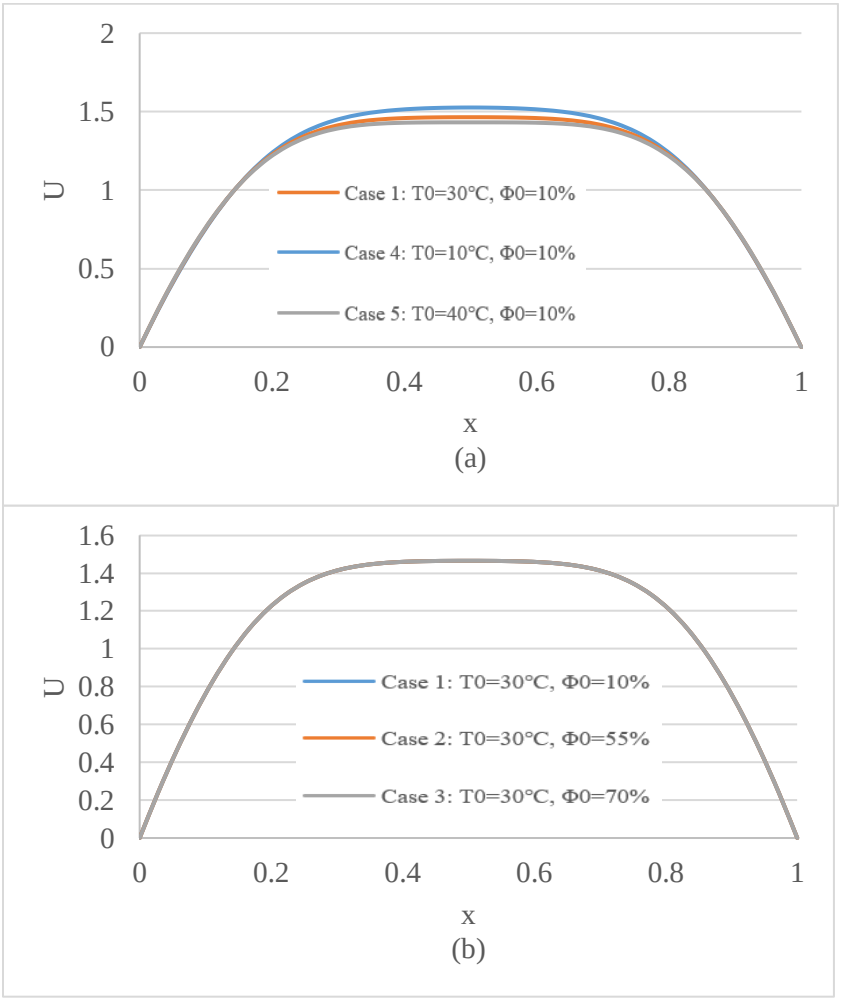

Figure 37. Axial velocity profiles at the location x=0.2

5.3.9. Effect of the Reynolds number

Four different values of the inlet air velocity are carried out which corresponds to four different values of the Reynolds number (from 1000 to 4000 with a step of 1000) to analyze the effect of inlet air velocity on the temperature and the moisture transfer. Inlet air temperature and relative humidity are 30℃ and 10%, respectively.

Figure 38 is noted that the average air temperature in the cavity decreases, then converges to the wall temperature as x increases. Meanwhile, as the increase of Reynold number, the average air temperature in the cavity increase. This result indicates the inlet velocity has an important effect on the average air temperature in the cavity. Moreover, all the cases indicated that the air temperature in the air cavity tended to the wall conditions at the outlet of the cavity, which is consistent with that transverse vapor velocity at the interface near the outlet of air cavity equals to zero.

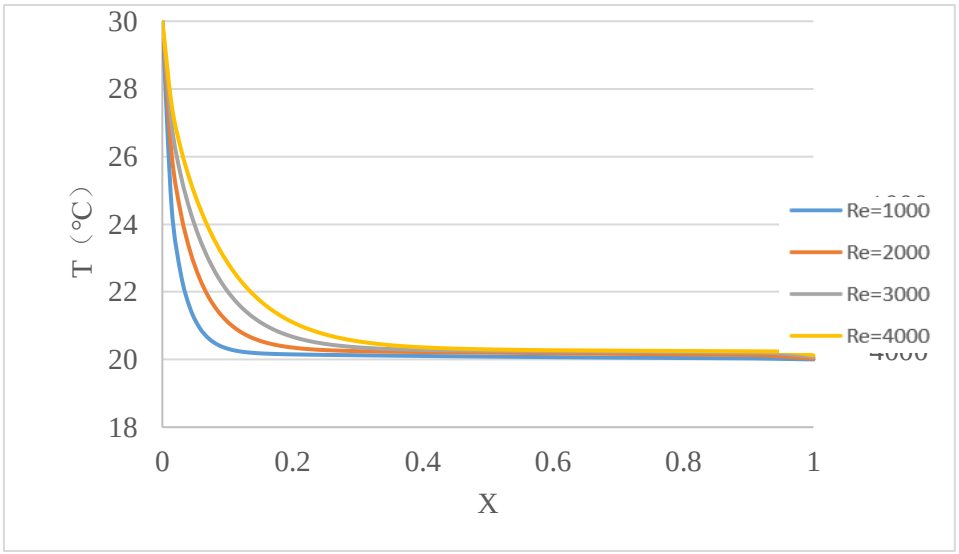

Figure 38. Effect of Reynolds number on the average temperature in the cavity

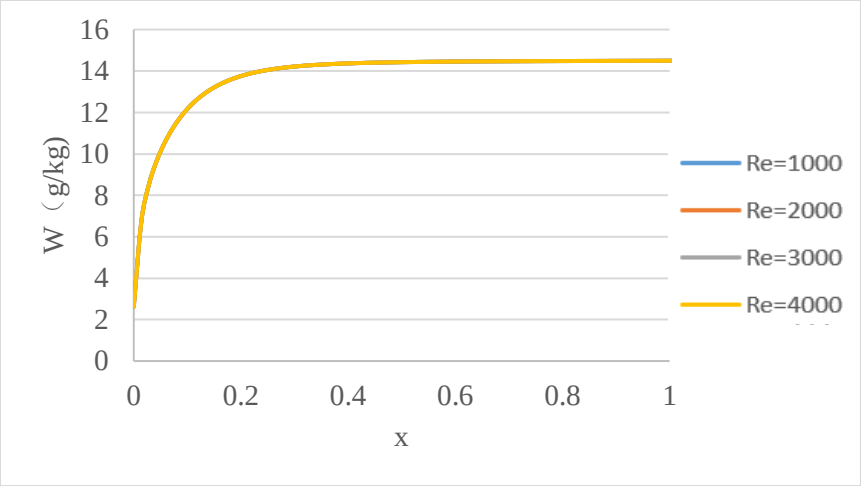

Figure 39. Effect of Reynolds number on the average mass friction in the cavity

Figure 39 shows the effects of Reynold number on the axial evolution of average mass friction. Figure 39 shows that the average mass friction increases, then converged to the certain value as x increases. Meanwhile, as the Reynold number increases, the average mass friction keeps constant. This result indicates that the inlet air velocity has little effect on the average mass friction in the cavity.

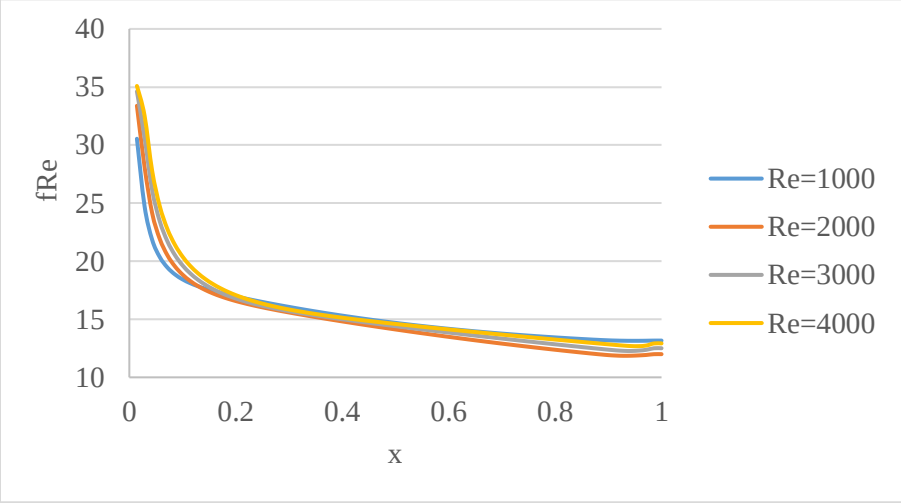

Figure 40. Effect of Reynolds number on the axial evolution of axial evolution of friction coefficient

Figure 40 shows the effects of Reynolds numbers on the axial evolution of axial evolution of the friction coefficient. It shows that the fRe first decreases monotonically as the air flow

moves downstream. Meanwhile, as the Reynolds number increase, the friction coefficient has a little change. However, compared to the effects of humidity ratio, the effects of Reynold number on the axial evolution of friction coefficient are relative larger.

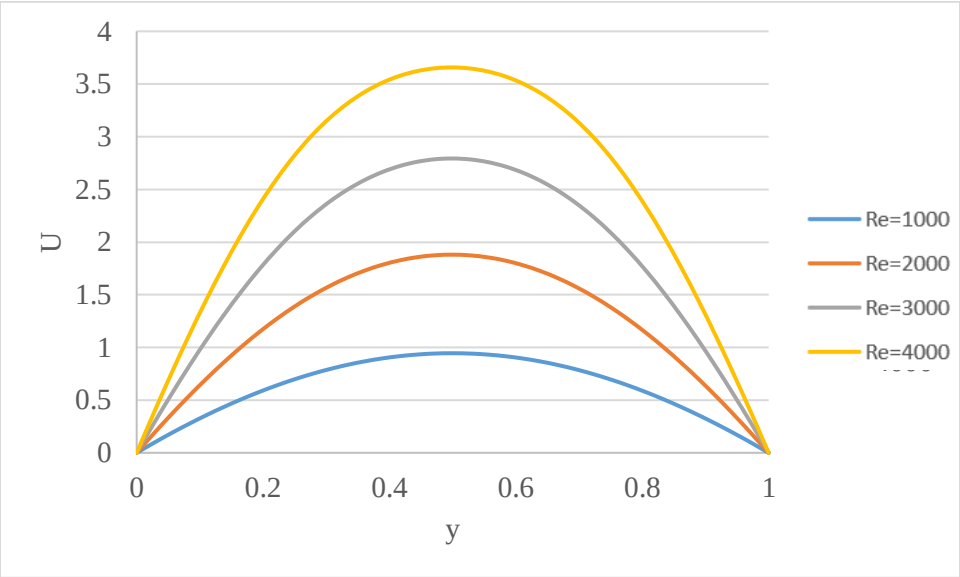

Figure 41. Effect of Reynolds number on the axial velocity in the cavity

Figure 41 shows the effects of Reynold number on the axial velocity in the cavity at the location of x=0.2. It is noted that the average axial velocity increases to the maximum value at the center of the cavity then decreases to zero as y increases. Meanwhile, as the Reynold number increases, the axial velocity increases. This result indicates that the Reynolds number has a significant effect on the axial velocity in the cavity.

5.3.10. Summary

This section presents the results of heat and mass transfer with phase change in the air cavity and investigated the effects of inlet air conditions (inlet air temperature, inlet air humidity ratio, and Reynolds number or the inlet air velocity) on the important metrics related to the performance of building envelope. It shows that the inlet air temperature has a significant effect on the axial evolution of the average temperature and latent Nusselt number while the inlet air

humidity ratio has an important effect on the axial evolution of vapor velocity at the interface and water content, and the latent Nusselt number. Moreover, these both parameters (inlet air temperature, inlet air humidity ratio) have a small effect on the axial evolution of the Sherwood number, the sensible Nusselt number, and the friction factors when the mass diffusion Grashof number and thermal Grashof number keeps constant. These results help to verify the importance of considering its influence in future design and analysis.

5.4. Conclusion

Considering the limitations of existing studies on the air cavity between the siding and wall sheathings for the energy performance of building envelope, this study investigated the effect of humid air in the air cavity on the heat and mass transfer with phase changes such as condensation or evaporation. This study redefines the heat and mass transfer problem in air cavity with humid air with considering condensation or evaporation at the interface between the film and air. To analyze this, the partial differential equations are solved using the SIMPLER algorithm with considering the axial diffusion terms. The main results of this research are listed as follows:

1) When inlet air vapor content is less than the water content at the wall, condensation will take place. On the contrary, evaporation will occur.
2) The sensible Nusselt numbers always be positive while the latent Nusselt numbers can be positive or negative. When the no mass transfer between the air and the water at the wall, the Nusselt number will be zero. Moreover, the inlet air temperature and inlet humidity ratio has an significant effect on the latent Nusselt number and a small effect on the sensible Nusslet number when the thermal Grashof number and mass diffusion Grashof number keeps constant.

3) The inlet air temperature has a significant effect on the axial evolution of the average temperature and latent Nusselt number while the inlet air humidity ratio has an important effect on the axial evolution of vapor velocity at the interface and water content, and the latent Nusselt number
4) Inlet air temperature and inlet air humidity ratio have a small effect on the axial evolution of the Sherwood number, the sensible Nusselt number, and the friction factors when the mass diffusion Grashof number and thermal Grashof number keeps constant

This study is an essential supplement of the state of the art which lacks an extensive analysis of the effects of humid air on heat and mass transfer in the air cavity between the siding and wall sheathings with phase change (condensation or evaporation) at the wall. The outcome of this study provides valuable guidance on the thermal performance evaluation of air cavity and has the potential of improving the design of siding for the overall energy performance of building envelope.

6. AIR CAVITY DEPTH IN MASS AND HEAT TRANSFER WITH HUMID AIR IN AIR CAVITY BEHIND CLADDINGS FOR BUILDING ENVELOPES

The largest end-energy use in the United States is the building sector, consuming approximately 41% of total energy and 72% of all electricity generated in 2016, and three fifths of this consumption can be attributed to building envelopes (Science & Council, 2008). It is becoming more common for exterior wall design to include air cavities behind exterior claddings, and many new wall assemblies with air cavities have been developed in recent years, such as active façade, double (or double-skin) envelope (Barbosa & Ip, 2014; Souza, Souza, & Rodrigues, 2018), rainscreen wall (Ge & Ye, 2007; Kumar, 2000; Marinosci, Semprini, & Morini, 2014) , ventilated façade (Aparicio-Fernández, Vivancos, Ferrer-Gisbert, & Royo-Pastor, 2014; Gagliano, Nocera, & Aneli, 2016; Patania, Gagliano, Nocera, Ferlito, & Galesi, 2010; Suárez et al., 2011), and ventilated wall (John Straube & Finch, 2009; Van Belleghem et al., 2015). Properly designed air-spaces in the enclosure systems provide a viable means to improve building energy efficiency (e.g., by reducing buildings' cooling load from solar radiation in the summer (Astorqui & Porras-Amores, 2017)), and wall systems with cladding ventilation strategies have also been proposed for the next generation of zero energy buildings (Astorqui & Porras-Amores, 2017).

In addition to the thermal performance benefit, air cavities behind claddings can provide a feasible way to reduce the building's moisture-related issues: rain penetration, frost damage, rotting, corrosion, mold growth, and discoloration of building materials. Properly designed cladding with air cavities can prevent both bulk water and capillary moisture flow into the wall sheathing (or even the inner wall), provide a drainage for incidental rainwater or condensation water, and remove evaporated / desorbed moisture from the inner wall or absorptive cladding through ventilation. While the capillary break and drainage functions are obvious, research about

the drying effects of ventilation have had contradictory findings. Field and laboratory research has shown (Finch & Straube, 2007c; Mayer & Künzel, 1983; Popp & Mayer, 1981) that the use of ventilated air spaces behind claddings has the potential to increase drying and reduce wetting from absorptive claddings and sun-driven moisture. However, some mentioned that the ventilated air layer behind claddings does not significantly accelerate drying of a capillary veneer wetted by rain. In the study of full-scale insulated wall assemblies with stucco cladding (Lawton et al., 1999), the authors concluded that drying was slow for all wall types and that the ventilated rainscreen wall design did not enhance drying of water that penetrates into the stud cavity.

Although the cavity ventilation was reported in that study ((Lawton et al., 1999)) not providing a benefit to moisture reduction, it is well accepted that higher ventilation rates behind the cladding will increase the drying rate of an initially wetted wall (Finch & Straube, 2007a; Ge & Ye, 2007). A larger ventilation rate can result from a higher cavity height. In addition, the larger opening areas allow for a greater amount of air flow through the cavity due to a lower pressure resistance (JF Straube & Burnett, 1998), increasing the drying potential at a given driving pressure. Previous research suggests that the depth of the cavity be more important than the size of vents (or cavity openings)(Salonvarra et al., 2007). A deeper cavity increases the drying potential due to higher air flow through the cavity, while it also reduces the drying rate due to the lower ventilation rate with a reduced stack effect. An optimal cavity depth therefore needs to be determined, and it is dependent on factors such as climatic conditions as well as the physical characteristics of cavity.

Different tools are proposed to study the moisture and thermal behavior of the air cavity behind the claddings, such as DELPHIN, MATCH, MOIST, WUFI and UMIDUS. Those tools are limited to 1D model and assume a homogeneous convective resistance along the element

geometry. Furthermore, they can not well predict the hygrothermal building performance without considering the thermal bridge and rising damps. The Computational Fluid Dynamics (CFD) as a common used tool can simulate the hygrothermal performance more accurate with taking into account the external climate conditions. For example, Van Belleghem et al. proposed a coupled computational Fluid Dynamics and Heat, Air, and Moisture model (Van Belleghem et al., 2015). However, the heat, air and moisture transportation in the cavity has limitations, due to the complexity of the building physical problems. On the other hand, most of the studies neglected the effect of humid air in the cavity on the mass and heat transfer for the building envelopes. Once the humid air enters the air cavity, it may be condensed or vapored under the certain climates. It further affects the thermal behavior of the wall for the buildings. As mentioned in Chapter 5.1 Introduction, this paper found that many researchers have investigated the effects of humid air in the channel with evaporation or condensations at the wall in other areas, and they found that the phase change of moisture has a significant influence in heat and mass transfer in the channel. Therefore, study of the effect of air cavity depth on mass and heat transfer with phase change in the air cavity behind claddings is necessary.

Aiming at improving the performance of energy analysis on building envelope especially that regarding the humid air in the cavity, the present study improves the heat and mass transfer problem in the air cavity considering the effects of condensation or evaporation of humid air and depth of the air cavity in the air cavity based on Chapter 5. The effect of inlet air conditions (the inlet air temperature, inlet air vapor content) on the axial evolutions of the transverse velocity at the interface, average air temperature, average air vapor content, the sensible and latent Nusselt number, and the Sherwood number are investigated. The findings can potentially improve the

accuracy and creditability of future related analysis and provide practical guidance on engineering designs of building envelopes of this type especially with the results of parametric analysis.

6.1. Problem Formulation

In this paper, the cladding system in a one-story residential building was studied as an example. The height of the air cavity between the siding and wall sheathing is 2.5m, and the width is h cm. Assuming the air with the dry bulb temperature T_0, the relative humidity ϕ_0, and the velocity U_0, enters the air cavity behind siding. The thin film of liquid water covers in siding and wall sheathing. The air flow is assumed as the laminar flow, with considering steady state conditions. The density in the body force is considered to be a linear function of temperature and mass fraction.

With the problem and coordinate system defined in Chapter 5 as Figure 27, the continuity, momentum, energy, and concentration equations governing the system can be written, respectively, in the following form:

$$\frac{\partial U}{\partial X}+\frac{\partial Y}{\partial Y}=0 \tag{89}$$

$$\left(U\frac{\partial U}{\partial X}+V\frac{\partial U}{\partial Y}\right)=-\frac{\partial P}{\partial X}+\frac{2r}{Re}\left(\frac{\partial^2 U}{\partial X^2}+\frac{\partial^2 U}{\partial Y^2}\right)-\frac{2r}{Re}(Gr_T T+Gr_c \mathrm{C}) \tag{90}$$

$$(U\frac{\partial V}{\partial X}+V\frac{\partial V}{\partial Y})=-\frac{\partial P}{\partial y}+\frac{2r}{Re}(\frac{\partial^2 V}{\partial X^2}+\frac{\partial^2 V}{\partial Y^2}) \tag{91}$$

$$U\frac{\partial T}{\partial X}+V\frac{\partial T}{\partial Y}=\frac{2r}{PrRe}(\frac{\partial^2 T}{\partial X^2}+\frac{\partial^2 T}{\partial Y^2}) \tag{92}$$

$$U\frac{\partial C}{\partial X}+V\frac{\partial C}{\partial Y}=\frac{2r}{ScRe}(\frac{\partial^2 C}{\partial X^2}+\frac{\partial^2 C}{\partial Y^2}) \tag{93}$$

where, U and V are the velocity components along X and Y axis, respectively; p is the air pressure; r is aspect ratio (h/L); Re is Reynolds number.Gr_T and Gr_C are thermal Grashof number and solutal Grashof number, respectively; T is the fluid temperature; C is the fluid concentration; Pr is Prandtl number; Sc is Schmidt number.

The boundary conditions of the flow field are defined as follows:

At the wall ($Y = 0$ or $Y = r$)

$$U = 0,\ V = Ve,\ T = 1,\ C = 1 \qquad \text{at } Y = 0 \qquad (94)$$

$$U = 0,\ V = Ve,\ T = 1,\ C = 1 \qquad \text{at } Y = r \qquad (95)$$

At the inlet ($X = 0,\ 0 < Y < r$)

$$U = 1\ V = 0,\ T = 0, \qquad \text{at } X = 0 \qquad (96)$$

At the outlet ($X =$ L , $0 < Y < h$)

All axial derivatives are zero

where the transverse velocity at the interface:

$$Ve = -2r(w_w - w_0)/ReSc/(1 - w_w)\ (\frac{\partial C}{\partial Y})_{Y=0} \qquad (97)$$

Heat transfer between the wet wall and the air is t:

$$q_t = k(\frac{\partial T}{\partial Y})_{Y=0} + \rho D h_{fg} \left(\frac{\partial C}{\partial Y}\right)_{Y=0} /(1 - w_w) \qquad (98)$$

Nusselt number

$$Nu_t = q_t Dh/k(T_w - \bar{T}) \qquad (99)$$

$$Sh = Dh * \frac{h}{D} \qquad (100)$$

6.2. Results and Discussion

The method used in this chapter is the same as Chapter 6. 100 x 70 nodes are used to calculate all the results in this thesis as shown in Chapter 5, where r=h/L=0.01538. The validations are implemented in Chapter 5.

This section presents and discusses the results of the air cavity depth in mass and heat transfer with the humid air obtained by solving the governing equations with specified boundary conditions using control volume method. This study analyzes cases with different values of

cladding depth to investigate the effects of their variations on the distribution of velocity, temperature, mass fraction, skin friction, Nusselt number, and Sherwood number. When analyzing the effects of a certain variable, the values of other variables are set as constant. The distributions of velocity, temperature, etc. are presented along the wall sheathing (x) and its normal direction (y) respectively.

In this paper, the Reynold number is fixed as 1000, the mass friction at the wall is calculated at the fixed temperature at the wall as 20◦C assuming the state of the air-vapor mixture at the wall as an ideal gas mixture. The inlet temperatures are assumed as 10◦C and 30◦C. the humidity ratios are assumed as 10% and 70%.

Table 4. Parameters for cases under study

Case	T0 (℃）	Φ0(%)	W0 (g/kg)
1	30	10	2.6
2	30	70	18.65
3	10	10	0.75

6.2.1. Effects on vapor velocity at the interface

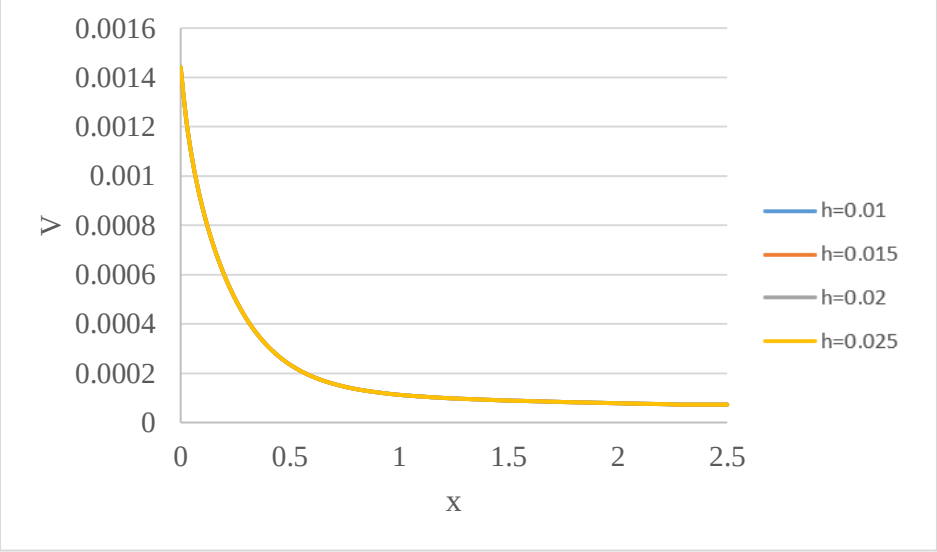

Figure 42. Axial evolution of the dimensionless transverse vapor velocity at the interface with T_0=30 ℃, Φ_0=10%.

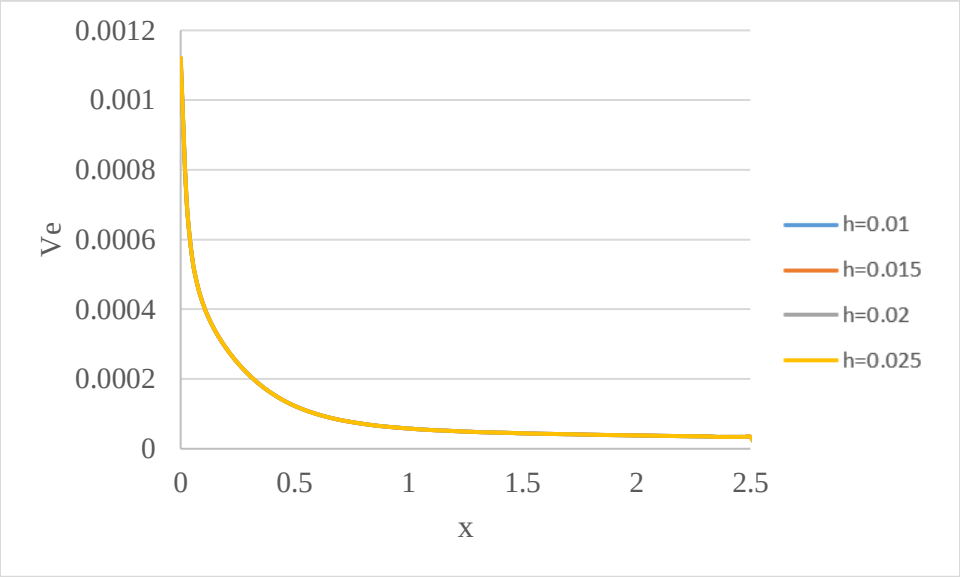

Figure 43. Axial evolution of the dimensionless transverse vapor velocity at the interface with T_0=10 ℃, Φ_0=10%.

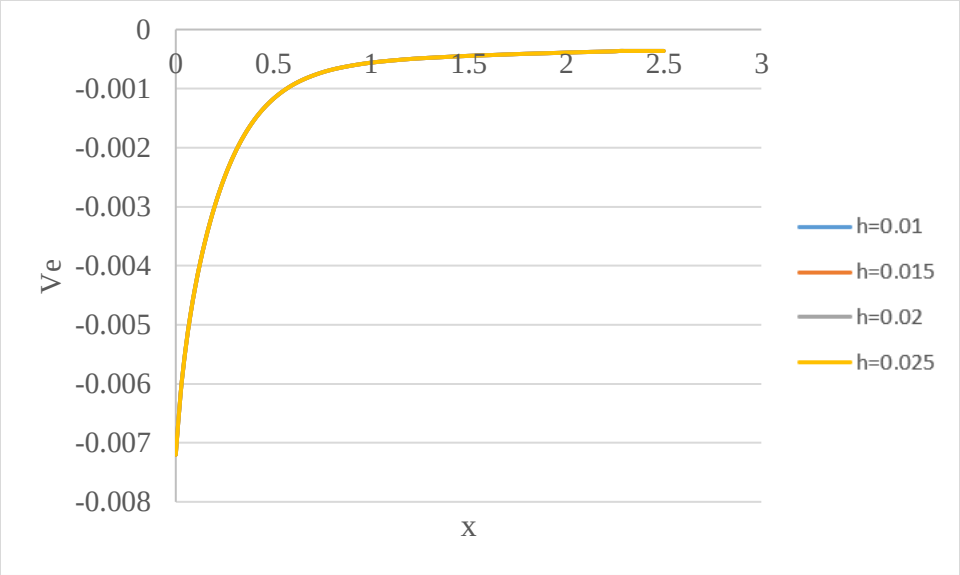

Figure 44. Axial evolution of the dimensionless transverse vapor velocity at the interface with T_0=30 ℃, Φ_0=70%.

Figures 42 to 44 show the effects of the cavity depth on the axial evolution of the dimensionless transverse vapor velocity at the interface with different conditions. Figure 42 and Figure 43 show that the transverse vapor velocity at the interface decreases, then converges to the

zero as x increase. Meanwhile, all the values of the transverse velocity are positive that means moisture is evaporated and transferred to the airflow. On the contrary, Figure 44 shows that the transverse vapor velocity at the interface increases, then converges to zero as x increases. The values of the transverse velocity are negative, which means moisture is condensed and transferred to the wall. The values of the transverse velocity are positive, which means moisture at the wall is evaporated and transferred to the flow. These results are consistent with the results in Chapter 5. Meanwhile, the effects of the cavity depth on the transverse velocity at the interface is very small, and it can be neglected.

6.2.2. Effects on average mass friction in the cavity

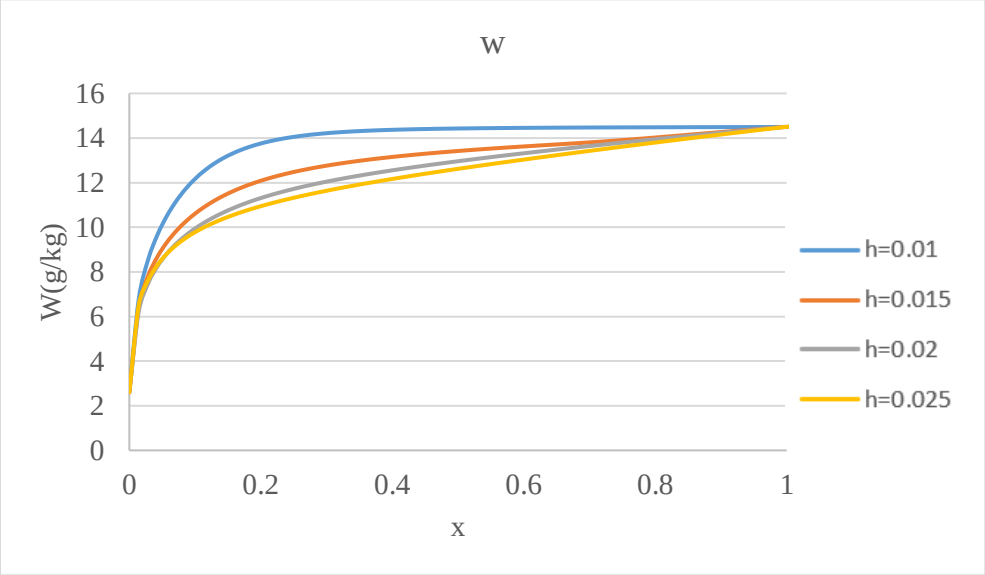

Figure 45. Axial evolution of the average mass friction with T_0=30 ℃, Φ_0=10%.

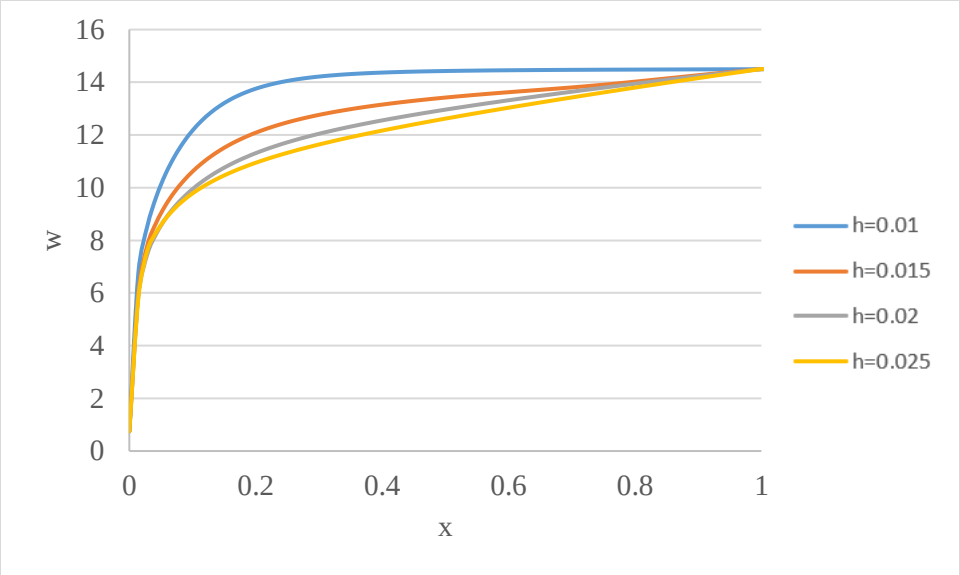

Figure 46. Axial evolution of the average mass friction with T_0=10 ℃, Φ_0=10%

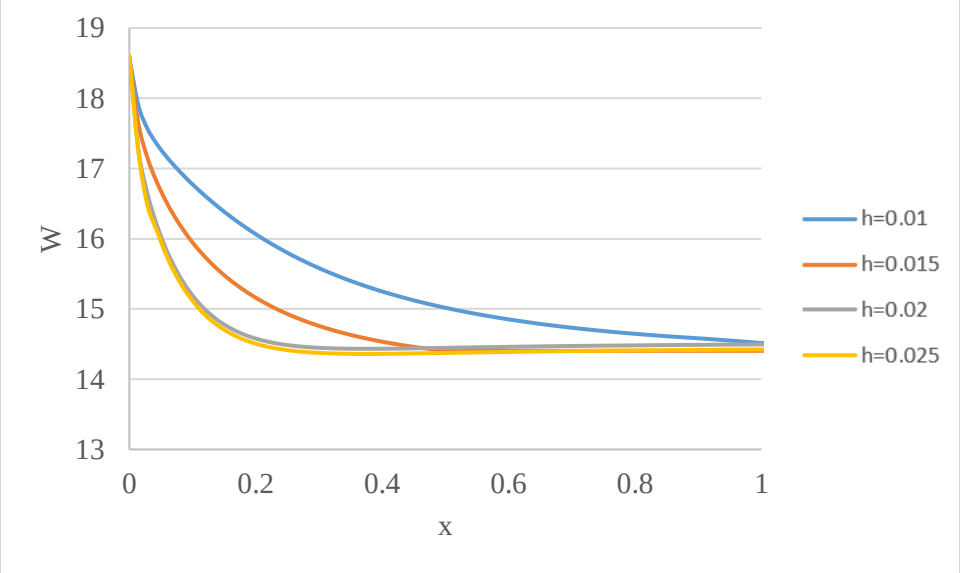

Figure 47. Axial evolution of the average mass friction with T_0=30 ℃, Φ_0=70%

Figures 45 to 47 describe the influences of air cavity depth on the axial evolution of the average mass friction in the cavity with different conditions. Figure 45 and Figure 46 show that the average mass friction increases, then converges into a certain value as x increases. On the contrary, Figure 47 presents that the average mass friction decreases, then converges into the certain value as x increases. These results are consistent with the result shown in Chapter 5. On

the other hand, at the same location, the average mass friction decreases as the air cavity depth increases. However, when the air cavity depth reaches a certain value, the average mass friction changes much smaller as the air cavity depth changes. It indicates that when the air cavity depth reaches a certain value, the mass friction in the cavity keeps constant at a certain location even with the air cavity depth continuing to increase. This depth can be opposed as the optimal cavity depth to keep the cavity having less moisture.

6.2.3. Average air temperature in the cavity

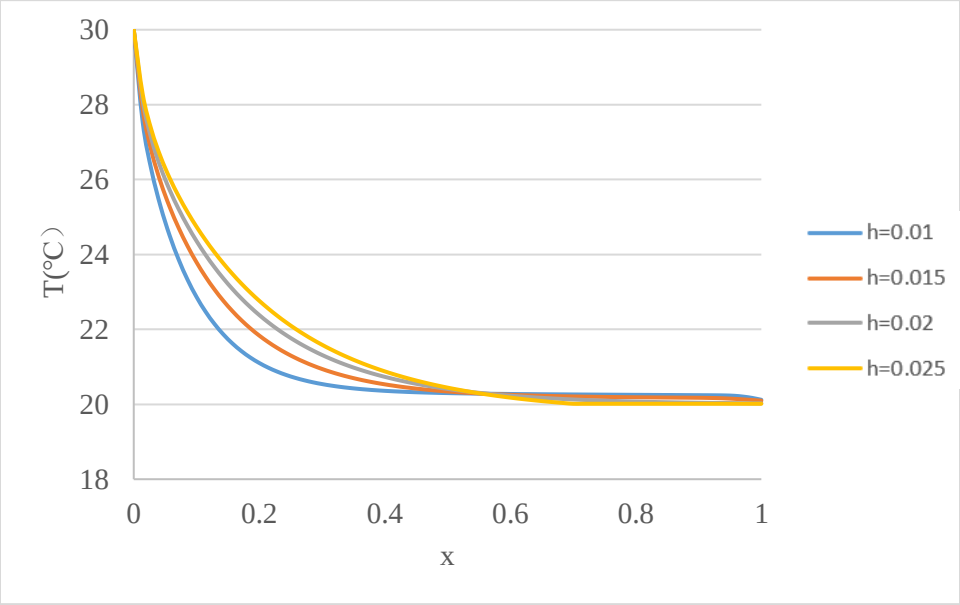

Figure 48. Axial evolution of the average air temperature in the cavity with T_0=30 ℃, Φ_0=10%.

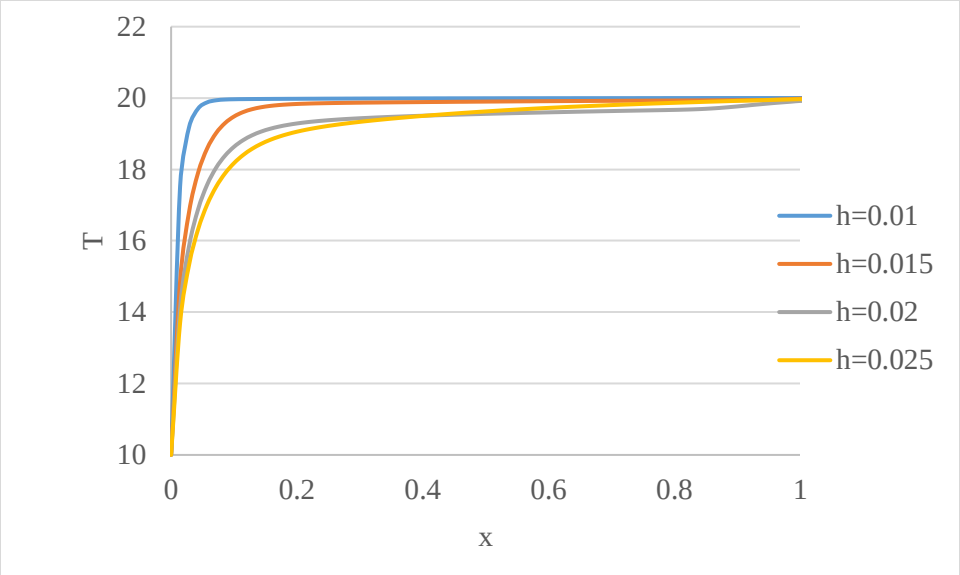

Figure 49. Axial evolution of the average air temperature in the cavity with T_0=10 ℃, Φ_0=10%

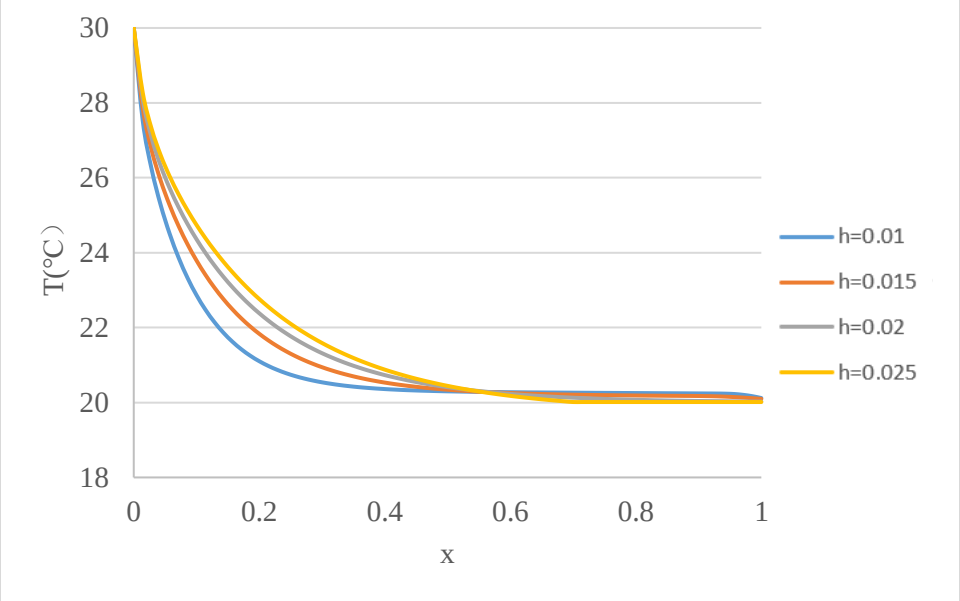

Figure 50. Axial evolution of the average air temperature in the cavity with T_0=30 ℃, Φ_0=70%

Figures 48 to 50 show the effects of the cavity depth on the axial evolution of the average air temperature in the air cavity with different conditions. Figure 48 and Figure 49 indicate that the average temperature decreases, then converges to the certain value (wall temperature) as x increases, and the temperature increases with the increase of the cavity depth. On the contrary,

Figure 50 indicates that the average temperature increases, then converges to the certain value (wall temperature) as x increases, and the temperature decreases with the increase of the cavity depth. These figures show that the depth has a significant effect on the axial evolution of the average temperature in the cavity.

6.2.4. Effects on axial evolution of the sensible Nusselt number

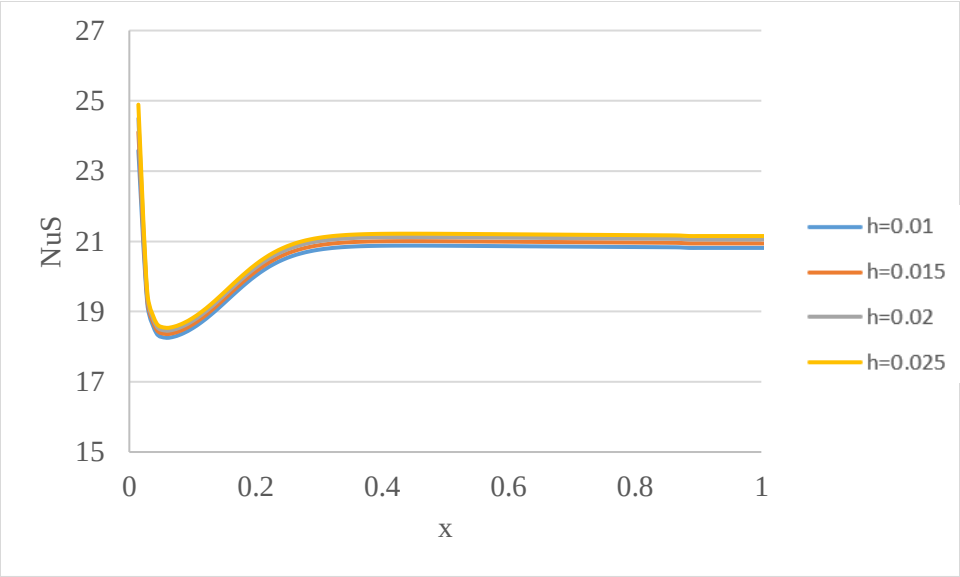

Figure 51. Axial evolution of the sensible Nusselt number with T_0=30 °C, Φ_0=10%.

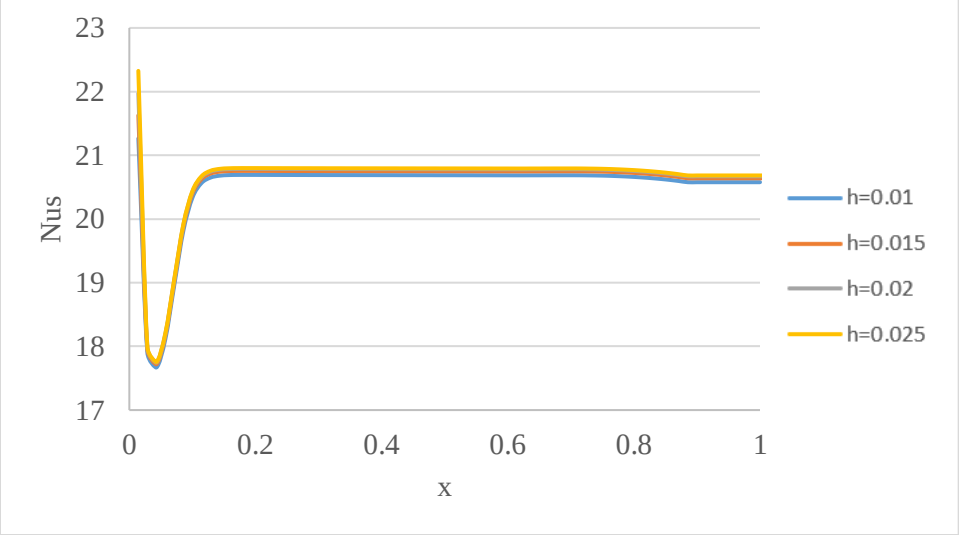

Figure 52. Axial evolution of the sensible Nusselt number with T_0=10 °C, Φ_0=10%.

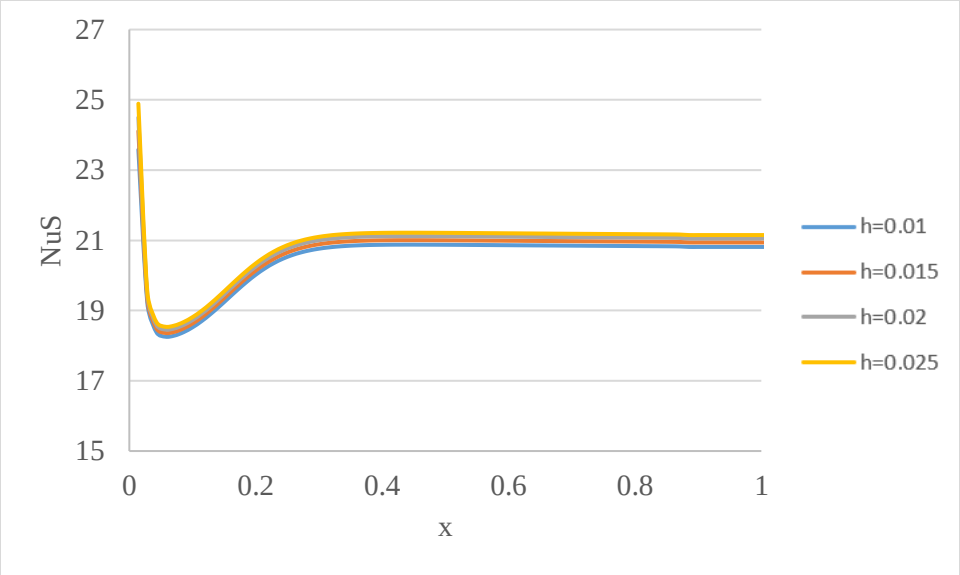

Figure 53. Axial evolution of the sensible Nusselt number with T_0=30 °C, Φ_0=70%.

Figures 51 to 53 show the effect of the cavity depth on the sensible Nusselt number with different conditions. Nusselt number is always positive whether evaporation or condensation occurs. Figures 51 to 53 show that Nus first decreases quickly, then increases, finally converges to the certain value with x increases. Moreover, the effect of the cavity depth on the sensible Nusselt is not significant when the thermal Grashof number and mass diffusion Grashof number is the same for all the cases, which agrees with the results indicated by Chapter 5 in this paper and the Hammou et al. (2004).

6.2.5. Effects on axial evolution of Sherwood number

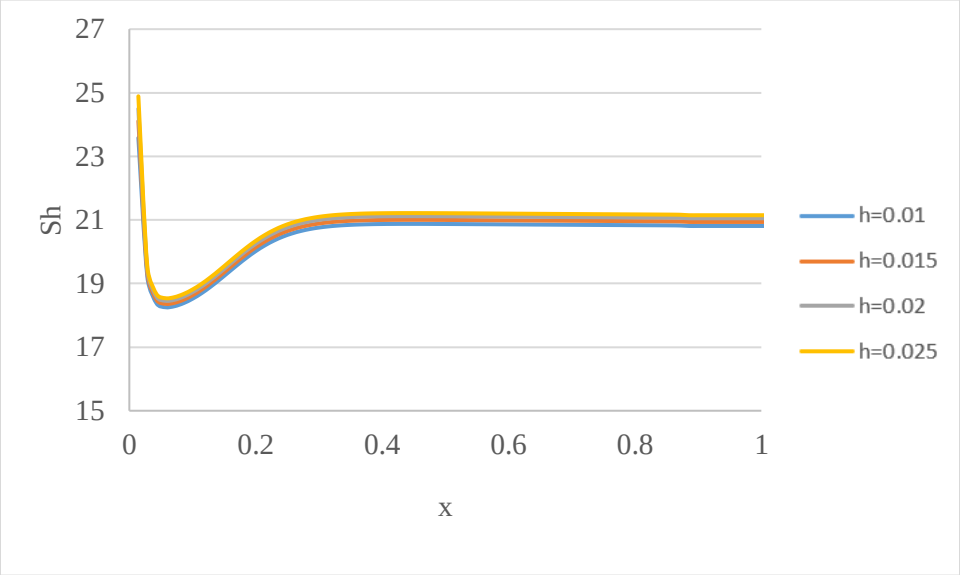

Figure 54. Axial evolution of Sherwood number with T_0=30 °C, Φ_0=10%.

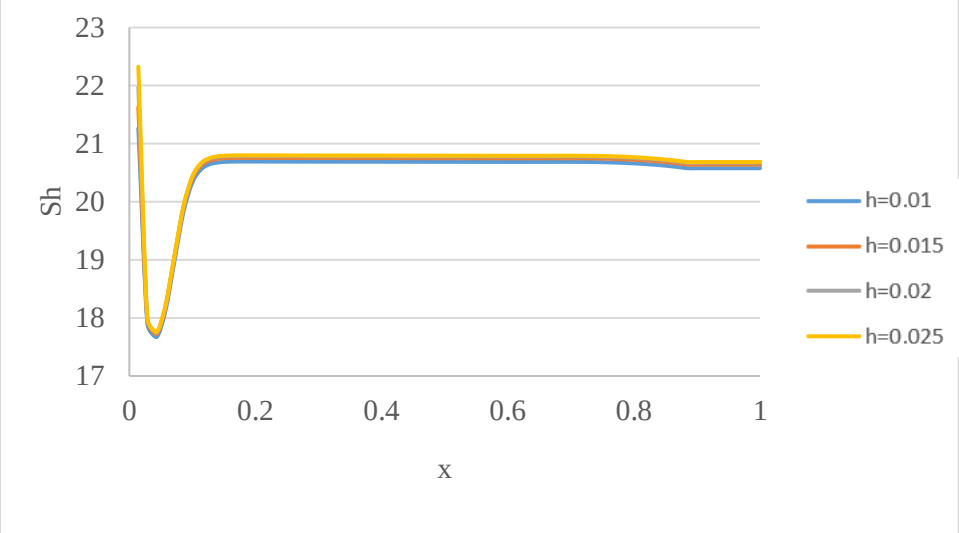

Figure 55. Axial evolution of Sherwood number with T_0=10 °C, Φ_0=10%.

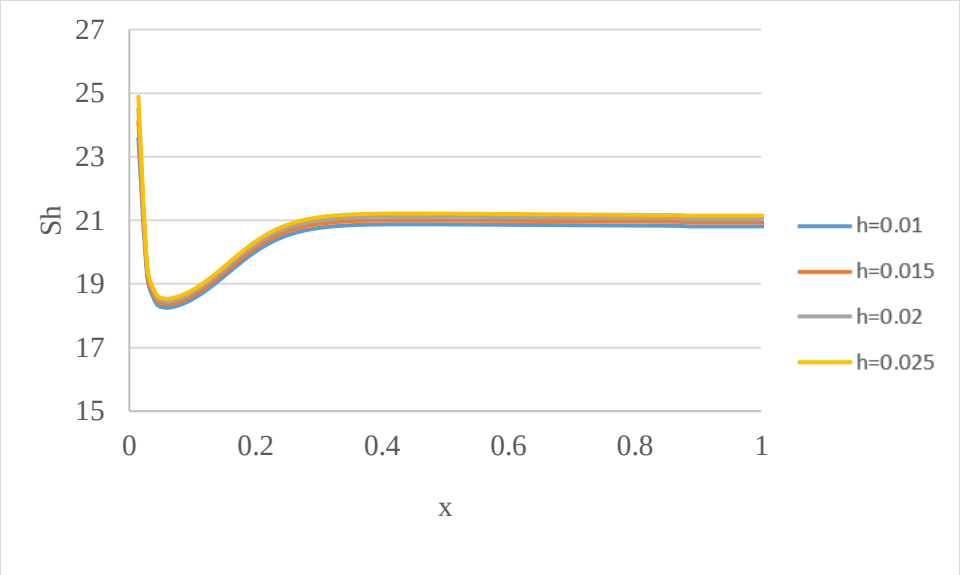

Figure 56. Axial evolution of Sherwood number with T_0=30 ℃, Φ_0=70%.

According to the Eq.87, Sherwood number is always positive whether evaporation or condensation occurs. Figures 54 to 56 are noted that Sh first decreases quickly, then increases, finally converges to the certain value with x increases. In all cases, Sh tends towards to the same value, which agrees with the results reported by Hammou et al.(2004). Compared to the sensible Nusselt number, it found that the distribution of Sh and Sensible Nusselt number are the same. Moreover, the effect of the cavity depth on the Sherwood number is not significant when the thermal Grashof number and mass diffusion Grashof number is the same for all the cases.

6.2.6. Axial evolution of the latent Nusselt number

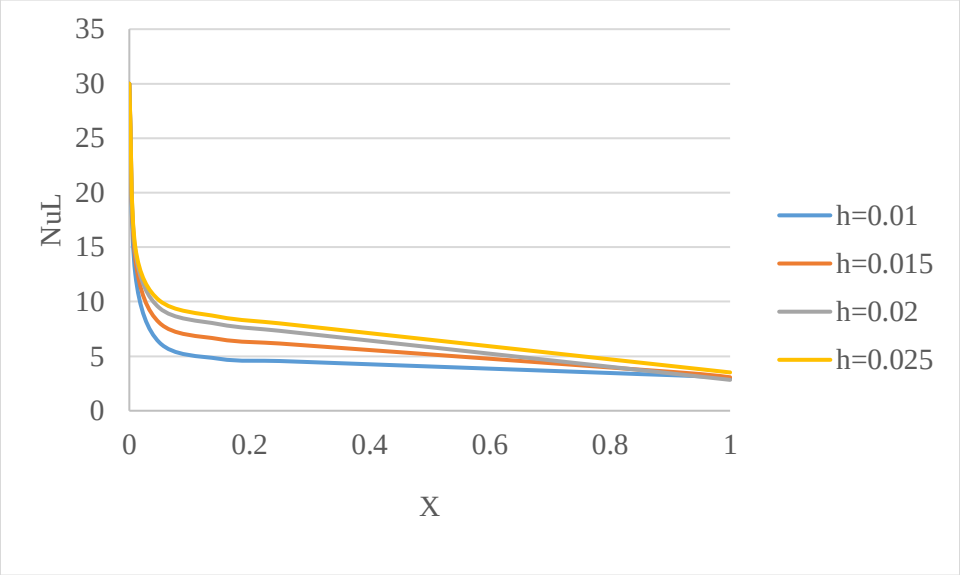

Figure 57. Axial evolution of the latent Nusselt number with T_0=30 °C, Φ_0=10%.

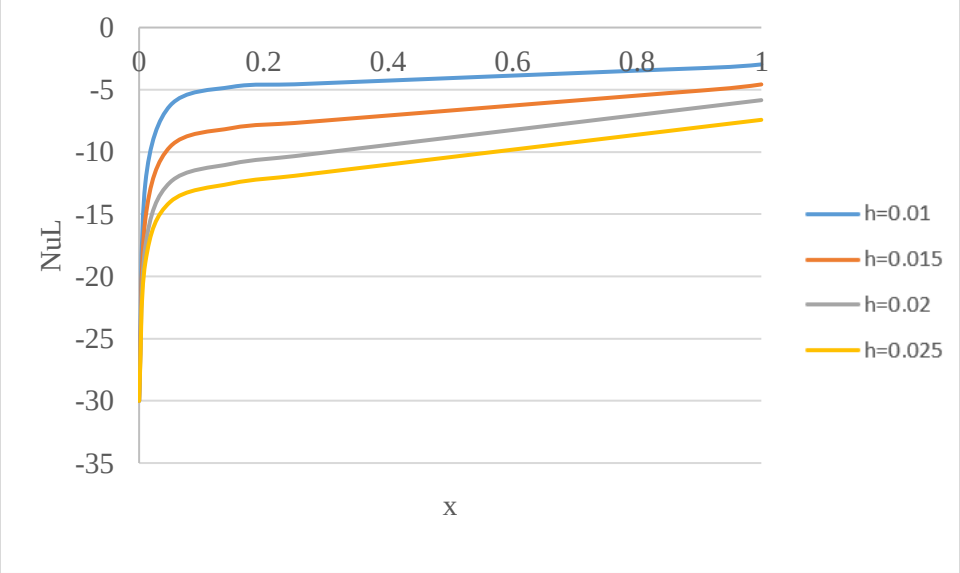

Figure 58. Axial evolution of the latent Nusselt number with T_0=10 °C, Φ_0=10%.

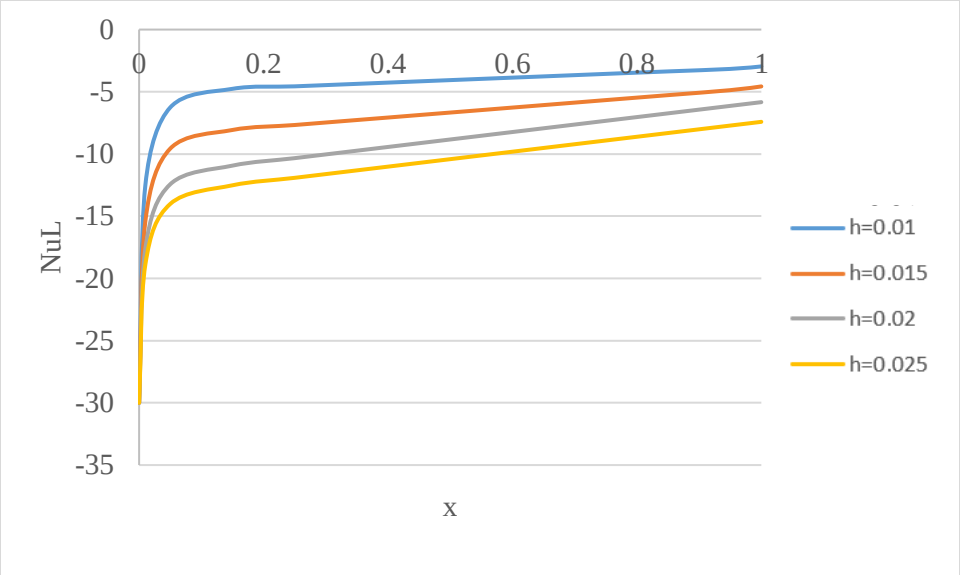

Figure 59. Axial evolution of the latent Nusselt number with T_0=30 ℃, Φ_0=70%.

Figures 57 to 59 describe the effect of cavity depth on the latent Nusselt number. According to Eq.86, NuL is positive when the inlet air vapor content is less than the film water content positive in Figure 58. That is because the film water vapors and flows into the air stream. On the contrary, when the inlet air vapor content is larger than the film water content, the inlet air vapor near the wall will condense. Therefore, NuL in Figure 59 (humidity ratio is 70%) is negative. Additionally, NuL value is positive when inlet air temperature is larger than wall temperature. Therefore, the NuL are positive in Figure 57 (T0=30 ℃ and Φ0=10%). It indicated that the effect of the cavity depth on the Nusselt number is more significant than sensible Nusselt number.

6.2.7. Summary

This section investigates the effects of the cavity depth with different conditions (inlet air temperature, inlet air humidity ratio) on the important metrics related to the performance of building envelope. It shows that the cavity depth has a significant effect on the axial evolution of the average temperature, the average mass friction, and latent Nusselt number. while the cavity

depth with different conditions (inlet air temperature, inlet air humidity ratio) have a small effect on the axial evolution of the Sherwood number, the sensible Nusselt number. These results help to verify the importance of considering its influence in future design and analysis.

6.3. Conclusion

This chapter investigated the effect of the cavity depth with different conditions (inlet temperature and inlet humidity ratio) on the heat and mass transfer with phase changes such as condensation or evaporation. To analyze this, the partial differential equations are solved based on the method in Chapter 5 with considering the axial diffusion terms. The main results of this research are listed as follows:

1) The air vapor will condense at the wall when inlet air vapor content is less than the water content at the wall. On the contrary, the film water vapors and flows into the air stream.
2) The cavity depth has a significant effect on the axial evolution of the average mass friction, the average temperature and latent Nusselt number while it has small effect on the axial evolution of vapor velocity at the interface and the latent Nusselt number.

These findings can not only improve the drying performance of siding through ventilated air as well as helping improve the thermal performance of the siding. Moreover, this paper provides design guidance for the new siding system.

7. CONCLUSIONS

The hygrothermal performance of air cavity for building envelopes are comprehensively investigated in this dissertation. The interaction of the heat, air and moisture is interest. Vinyl siding wall systems and masonry wall systems are the two focuses of the study because of their widespread use. The most important conclusions based on vinyl siding and masonry wall systems are briefly summarized as follows.

This dissertation firstly studies the drying potential of a siding system through the air flow rate within the cavities and investigates the effects of depth of air cavity in mixed convection behind vinyl siding for building envelopes based on perturbation technique. The results show that

1) the geometry of air cavity behind claddings has a major role in the air flow resistant compared to other factors such as wall friction
2) the effects of the geometry of air cavity on the overall performance of building envelopes are significant.
3) Depths of air cavity play a key role in determining the drying performance of siding systems. The temperature in the air cavity and the rate of heat transfer (Nusselt number) are more affected by the inlet temperature and the air cavity depth than the inlet moisture content. On the contrary, the mass friction and the rate of mass transfer (Sherwood number) are less affected by the inlet temperature than the inlet moisture.

Considering the limitations of existing studies on the air cavity between the cladding and wall sheathings for the energy performance of building envelope, this research then studies the heat and mass transfer problem in air cavity with considering condensation or evaporation at the interface between the film and air. The SIMPLER algorithm with the axial diffusion terms is adopted to solve the partial differential equations. The main results are listed as follow:

1) The air vapor will condense at the wall, when inlet air vapor content is less than the water content at the wall. On the contrary, the film water vapors and flows into the air stream.
2) The sensible Nusselt numbers always be positive while the latent Nusselt numbers can be positive or negative. The inlet air temperature and inlet humidity ratio have a significant effect on the latent Nusselt number and a small effect on the sensible Nusslet number when the thermal Grashof number and mass diffusion Grashof number keeps constant.
3) The inlet air temperature has a significant effect on the axial evolution of the average temperature and latent Nusselt number while the inlet air humidity ratio has an important effect on the axial evolution of vapor velocity at the interface and water content, and the latent Nusselt number.
4) The cavity depth has a significant effect on the axial evolution of the average mass friction, the average temperature and latent Nusselt number while it has small effect on the axial evolution of vapor velocity at the interface and the latent Nusselt number.

This dissertation is an essential supplement of the state of the art which lacks an extensive analysis of the effects of an extensive analysis of the effects of geometric irregularities, mix convection and humid air on heat and mass transfer in the air cavity between the claddings and wall sheathings. The outcome of this study provides valuable guidance on the thermal performance evaluation of air cavity and has the potential of improving the design of claddings for the overall hygrothermal performance of building envelope.

8. FUTURE WORK

Based on the conclusions drawn in this dissertation, ideas for future research are presented as follows. They are proposed to extend the work that has been done in this dissertation.

1) The future research will redefine drying potential of air cavity between different types of claddings and wall sheathings with the consideration of the air cavity depth related to the shape irregularity and the effect of the inlets and outlet uncertainty.
2) In order to simplify the computation procedure, this thesis create 2 D models to analyze the specific problems. In the future, 3D models will be built.
3) This dissertation studies the heat and mass transfer problem in air cavity behind brick claddings by considering condensation or evaporation at the interface between the film and air. It does not consider the effects of the shape irregularity. In the future, the effects of humid air in the cavity on mass and heat transfer with phase change at the wall with considering the effect of the geometry will be investigated.

REFERENCES

Aparicio-Fernández, C., Vivancos, J.L., Ferrer-Gisbert, P., Royo-Pastor, R. (2014). Energy performance of a ventilated façade by simulation with experimental validation. Applied Thermal Engineering, 66(1-2), 563-570. https://doi.org/10.1016/j.applthermaleng.2014.02.041

Astorqui, J. S. C., & Porras-Amores, C. (2017). Ventilated Façade with double chamber and flow control device. Energy and Buildings, 149, 471-482. https://doi.org/10.1016/j.enbuild.2017.04.063

Balocco, C. (2009). Transient Simulation of a Naturally Ventilated Façade in a Mediterranean climate. Paper presented at the Proceedings of the COMSOL Conference, Milan.

Barbosa, S., & Ip, K. (2014). Perspectives of double skin façades for naturally ventilated buildings: A review. Renewable and Sustainable Energy Reviews, 40, 1019-1029. https://doi.org/10.1016/j.rser.2014.07.192

Bassett, M., McNeil, S. (2020). Measured ventilation rates in water managed wall cavities. In Research in Building Physics and Building Engineering (pp. 403-410): CRC Press.

Beirão, S., Ribeiro, A., Lourenço, M., Santos, F., & Nieto de Castro, C. (2012). Thermal conductivity of humid air. International Journal of Thermophysics, 33(8), 1686-1703. https://doi.org/10.1007/s10765-012-1254-5

Bureau, U. S. C. (2011). Principal type of exterior wall material of new single-family houses completed. https://www.census.gov/const/C25Ann/sftotalexwallmat.pdf

Cherif, A. A., Daïf, A. (1999). Etude numérique du transfert dechaleur et de masse entre deux plaques planes verticalesen présence dun film de liquide binaireruisselant sur lune des plaques chauffée. International Journal of Heat and Mass Transfer, 42(13), 2399-2418. https://doi.org/10.1016/S0017-9310(98)00339-1

Chew, M., Tan, S., Kang, K. (2005). Contribution analysis of maintainability factors for cladding facades. Architectural Science Review, 48(3), 215-227. https://doi.org/10.3763/asre.2005.4828

Cho, K. J., Kim, M.U., Shin, H. D. (1998). Linear stability of two-dimensional steady flow in wavy-walled channels. Fluid dynamics research, 23(6), 349. https://iopscience.iop.org/article/10.1016/S0169-5983(98)00003-3/pdf

Davidovic, D., Srebric, J., Burnett, E. F. (2006). Modeling convective drying of ventilated wall chambers in building enclosures. International Journal of Thermal Sciences, 45(2), 180-189. https://doi.org/10.1016/j.ijthermalsci.2005.06.002

Desta, T. Z., Langmans, J., Roels, S. (2011). Experimental data set for validation of heat, air and moisture transport models of building envelopes. Building and Environment, 46(5), 1038-1046. https://doi.org/10.1016/j.buildenv.2010.11.002

El-Sadi, H., Haghighat, F., Fallahi, A. (2010). CFD analysis of turbulent natural ventilation in double-skin façade: Thermal mass and energy efficiency. Journal of Energy Engineering, 136(3), 68-75. https://doi.org/10.1061/(ASCE)EY.1943-7897.0000026

Eldabe, N., El-Sayed, M., Ghaly, A., Sayed, H. (2008). Mixed convective heat and mass transfer in a non-Newtonian fluid at a peristaltic surface with temperature-dependent viscosity. Archive of Applied Mechanics, 78(8), 599-624. https://doi.org/10.1007/s00419-007-0181-6

Finch, G., Straube, J. (2007a). Ventilated wall claddings: review, field performance and hygrothermal modeling. Paper presented at the Proceedings of the Thermal Performance of the Exterior Envelopes of Whole Buildings X International Conference, Clearwater Beach, FL, USA.

Finch, G., Straube, J. (2007b). Ventilated wall claddings: review, field performance and hygrothermal modeling. Proceedings of the thermal performance of the exterior envelopes of whole buildings X, Clearwater, FL, 2.

Finch, G., Straube, J. (2007c). Ventilated wall claddings: Review, field performance, and hygrothermal modeling. Paper presented at the Proceedings of the Thermal Performance of the Exterior Envelopes of Whole Buildings X International Conference, Clearwater Beach, FL, USA.

Gagliano, A., Nocera, F., Aneli, S. (2016). Thermodynamic analysis of ventilated façades under different wind conditions in summer period. Energy and Buildings, 122, 131-139. https://doi.org/10.1016/j.enbuild.2016.04.035

Ge, H., Ye, Y. (2007). Investigation of ventilation drying of rainscreen walls in the coastal climate of British Columbia. Proceedings of the thermal performance of the exterior envelopes of whole buildings X, Clearwater, FL, 2.

Ghaddar, N., Korczak, K., Mikic, B., Patera, A. (1986). Numerical investigation of incompressible flow in grooved channels. Part 1. Stability and self-sustained oscillations. Journal of Fluid Mechanics, 163, 99-127. https://doi.org/10.1017/S0022112086002227

Ghaddar, N., Magen, M., Mikic, B., Patera, A. (1986). Numerical investigation of incompressible flow in grooved channels. Part 2. Resonance and oscillatory heat-transfer enhancement. Journal of Fluid Mechanics, 168, 541-567. https://doi.org/10.1017/S0022112086000502

Ghrissi, W., Promis, G., Langlet, T., Douzane, O., Chouikh, R., Guizani, A. (2022). Study of the influence of input parameters in an air channel on mass and heat transfer phenomena within a wall saturated with water: Application to the renovation of old wet buildings.

Journal of Building Performance Simulation, 15(1), 81-96. https://doi.org/10.1080/19401493.2021.1994651

Gradeck, M., Hoareau, B., Lebouché, M. (2005). Local analysis of heat transfer inside corrugated channel. International Journal of Heat and Mass Transfer, 48(10), 1909-1915. https://doi.org/10.1016/j.ijheatmasstransfer.2004.12.026

Hammou, Z. A., Benhamou, B., Galanis, N., Orfi, J. (2004). Laminar mixed convection of humid air in a vertical channel with evaporation or condensation at the wall. International Journal of Thermal Sciences, 43(6), 531-539. https://doi.org/10.1016/j.ijthermalsci.2003.10.010

Hansen, M. H., Nicolajsen, A. (2002). On the influence of cavity ventilation on moisture content in timber frame walls. Paper presented at the Proceedings of the 6th Symposium on Building Physics in the Nordic Countries.

Hatami, M. (2017). Nanoparticles migration around the heated cylinder during the RSM optimization of a wavy-wall enclosure. Advanced Powder Technology, 28(3), 890-899. https://doi.org/10.1016/j.apt.2016.12.015

Hatami, M., Zhou, J., Geng, J., Song, D., Jing, D. (2017). Optimization of a lid-driven T-shaped porous cavity to improve the nanofluids mixed convection heat transfer. Journal of Molecular Liquids, 231, 620-631. https://doi.org/10.1016/j.molliq.2017.02.048

Hazleden, D., Morris, P. (2001). Evaluation of Vapor Diffusion Ports on Drying of Wood-frame Walls under Controlled Conditions. Forintek Canada Corp. report for project 3134. Vancouver. British Columbia.

Hens, H. (1984). Buitenwandoplossingen voor de residentiële bouw: De Spouwmuur.

Hinojosa, J., Orozco, D., Xaman, J. (2020). Experimental and Numerical Study of a Ventilated Room with Located Heat Sources. Journal of Energy Engineering, 146(4), 04020024. https://orcid.org/0000-0002-6311-3163.

Holmes, J. D. (1980). Mean and fluctuating internal pressures induced by wind. In Wind Engineering, Elsevier, 430-450. https://doi.org/10.1016/B978-1-4832-8367-8.50046-2

Hutcheon, N. B., Handegord, G. O., Hutcheon, N. B. (1983). Building science for a cold climate: Wiley Toronto.

Idelchik, I. E. (1986). Handbook of hydraulic resistance. Washington.

Jung, E. (1985). Dauerstandverhalten von Verblendziegelmauerwerk unter Witterunsbeansphruchung und Auswirkungen von Kerndamm-Maznahmen. Baust offindustrie(6), 185-188.

Karagiozis, A. N., Kuenzel, H. M. (2009). The effect of air cavity convection on the wetting and drying behavior of wood-frame walls using a multi-physics approach. Journal of ASTM International, 6(10), 1-15. https://10.1520/JAI101455

Kie, J. C., Moon-Uhn, K., Hyun, D. S. (1998). Linear stability of two-dimensional steady flow in wavy-walled channels. Fluid dynamics research, 23(6), 349. https://iopscience.iop.org/article/10.1016/S0169-5983(98)00003-3/meta

Kumar, K. S. (2000). Pressure equalization of rainscreen walls: a critical review. Building and Environment, 35(2), 161-179. https://doi.org/10.1016/S0360-1323(99)00015-3

Künzel, H. M. (1995). Simultaneous heat and moisture transport in building components. One- and two-dimensional calculation using simple parameters. IRB-Verlag Stuttgart, 65.

Langmans, J., Roels, S. (2015). Experimental analysis of cavity ventilation behind rainscreen cladding systems: A comparison of four measuring techniques. Building and Environment, 87, 177-192. https://doi.org/10.1016/j.buildenv.2015.01.030

Lawton, M. D., Brown, W., Lang, A. (1999). Stucco-clad wall drying experiment. CHMC Research Report.

Lawton, M. D., Brown, W., Lang, A. (2001). Stucco-clad wall drying experiment. Paper presented at the Proceedings of the Thermal Performance of the Exterior Envelopes of Whole Buildings VIII International Conference, Clearwater Beach, FL, USA.

Li, S., Karava, P. (2014). Energy modeling of photovoltaic thermal systems with corrugated unglazed transpired solar collectors–Part 2: Performance analysis. Solar Energy, 102, 297-307. https://doi.org/10.1016/j.solener.2013.12.041

Li, S., Karava, P., Currie, S., Lin, W. E., Savory, E. (2014). Energy modeling of photovoltaic thermal systems with corrugated unglazed transpired solar collectors–Part 1: Model development and validation. Solar Energy, 102, 282-296. https://doi.org/10.1016/j.solener.2013.12.040

Li, S., Karava, P., Savory, E., Lin, W. E. (2013). Airflow and thermal analysis of flat and corrugated unglazed transpired solar collectors. Solar Energy, 91, 297-315. https://doi.org/10.1016/j.solener.2013.01.028

Losses Due to Sudden Contraction, (2022) [cited 2022 10/23]; Available from: https://nptel.ac.in/courses/112104118/lecture-14/14-7_losses_sudden_contract.

Losses due to sudden enlargement, (2022) [cited 2022 10/23]; Available from: https://nptel.ac.in/courses/112104118/lecture-14/14-6_losses_sudden_enlarg.htm.

Lstiburek, J., Karagiozis, A., Ueno, K. (2002). Feasibility of Establishing Criteria for Permeable Envelope and/or Non-Mechanical Ventilation for Detached Single One or Two Family

Residential Construction (Final Paper). Building Science Corporation's Final Paper to the Minnesota Department of Administration of Building Codes and Standards Division.

Mamourian, M., Shirvan, K. M., Ellahi, R., Rahimi, A. (2016). Optimization of mixed convection heat transfer with entropy generation in a wavy surface square lid-driven cavity by means of Taguchi approach. International Journal of Heat and Mass Transfer, 102, 544-554. https://doi.org/10.1016/j.ijheatmasstransfer.2016.06.056

Marinosci, C., Semprini, G., Morini, G. (2014). Experimental analysis of the summer thermal performances of a naturally ventilated rainscreen façade building. Energy and Buildings, 72, 280-287. https://doi.org/10.1016/j.enbuild.2013.12.044

Mayer, E., Künzel, H. (1983). Untersuchungen über die notwendige Hinterlüftung an Aubenwandbekeidung aus grobformatigen Bauteilen. Franhofer Institut für Bauphysick, Forschungsbericht B Ho, 1, 83.

Mitchell, J. W., Braun, J. E. (2012). Principles of heating, ventilation, and air conditioning in buildings: John Wiley & Sons.

Canada Mortgage and Housing Corporation, H., Straube, J., Burnett, E. F. (1995). Vents, Ventilation Drying and Pressure Moderation: CMHC.

Nieto, F., Hernández, S., Jurado, J. (2009). Optimum design of long-span suspension bridges considering aeroelastic and kinematic constraints. Structural and Multidisciplinary Optimization, 39(2), 133-151. https://doi.org/10.1007/s00158-008-0314-8

Nore, K. (2010). Hygrothermal performance of ventilated wooden cladding. Doctoral Thesis, Norwegian University of Science and Technology, Trondheim, Norway http://hdl.handle.net/11250/231575

Nwaji, G. N., Okoronkwo, C. A., Ogueke, N. V., Anyanwu, E. E. (2021). Transient Simulation of a Building-Integrated Hybrid Solar Collector/Nocturnal Radiator with In-Built Thermal Storage for Space Cooling in Owerri, Nigeria. Journal of Energy Engineering, 147(2), 04021003. https://orcid.org/0000-0002-0982-1847

Oh, J. H., Kopp, G. A., Inculet, D. R. (2007). The UWO contribution to the NIST aerodynamic database for wind loads on low buildings: Part 3. Internal pressures. Journal of Wind Engineering and Industrial Aerodynamics, 95(8), 755-779. https://doi.org/10.1016/j.jweia.2007.01.007

Ouf, M. M., O'Brien, W., Gunay, H. B. (2018). Improving occupant-related features in building performance simulation tools. Paper presented at the Building Simulation. https://doi.org/10.1007/s12273-018-0443-y

Oulaid, O., Benhamou, B., Galanis, N. (2010). Flow reversal in combined laminar mixed convection heat and mass transfer with phase change in a vertical channel. International

journal of heat and fluid flow, 31(4), 711-721. https://doi.org/10.1016/j.ijheatfluidflow.2010.04.007

Patania, F., Gagliano, A., Nocera, F., Ferlito, A., Galesi, A. (2010). Thermofluid-dynamic analysis of ventilated facades. Energy and Buildings, 42(7), 1148-1155. https://www.sciencedirect.com/science/article/pii/S037877881000037X

Popp, W., Mayer, E. (1981). Untersuchungen über die Belüftung des Luftraumes hinter vorgesetzten Fassadenbekleidungen aus kleinformatigen Elementen: Informationsverbundzentrum Raum und Bau der Fraunhofer-Gesellschaft.

Pressnail, K., Timusk, J., Kan, L., Dong, B., Kan, V. (2003). In search of a wall for all seasons: controlling sun-driven moisture. Paper presented at the Proceedings of the 9th Canadian Conference on Building Science and Technology, Vancouver.

Radhi, H. (2010). On the optimal selection of wall cladding system to reduce direct and indirect CO2 emissions. Energy, 35(3), 1412-1424. https://doi.org/10.1016/j.energy.2009.11.026

Rahiminejad, M., Khovalyg, D. (2021). Review on ventilation rates in the ventilated air-spaces behind common wall assemblies with external cladding. Building and Environment, 190, 107538. https://doi.org/10.1016/j.buildenv.2020.107538

Rashidi, M. M., Nasiri, M., Khezerloo, M., Laraqi, N. (2016). Numerical investigation of magnetic field effect on mixed convection heat transfer of nanofluid in a channel with sinusoidal walls. Journal of Magnetism and Magnetic Materials, 401, 159-168. https://doi.org/10.1016/j.jmmm.2015.10.034

Salonvarra, M., Karagiozis, A. N., Pazera, M., Miller, W. (2007). Air cavities behind claddings-what have we learned. Paper presented at the Thermal Performance of the Exterior Envelopes of Whole Buildings Tenth International Conference.

Science, N., Council, T. (2008). Federal Research and Development Agenda for Net-Zero Energy, High Performance Green Buildings. In: Committee on Technology, Office of the President of the United States ….

Souza, L., Souza, H., Rodrigues, E. (2018). Experimental and numerical analysis of a naturally ventilated double-skin façade. Energy and Buildings, 165, 328-339. https://doi.org/10.1016/j.enbuild.2018.01.048

Srinivas, S., Gayathri, R., Kothandapani, M. (2011). Mixed convective heat and mass transfer in an asymmetric channel with peristalsis. Communications in Nonlinear Science and Numerical Simulation, 16(4), 1845-1862. https://doi.org/10.1016/j.cnsns.2010.08.004

Stazi, F., Ulpiani, G., Pergolini, M., Di Perna, C., D'Orazio, M. (2020). The role of wall layers properties on the thermal performance of ventilated facades: Experimental investigation

on narrow-cavity design. Energy and Buildings, 209, 109622. https://doi.org/10.1016/j.enbuild.2019.109622

Straube, J., Burnett, E. (1995). Vents, ventilation, and pressure moderation. University of Waterloo Building Engineering Group Report for Canada Mortgage and Housing Corp, Ottawa.

Straube, J., Burnett, E. (1998). Vents, ventilation and masonry veneer wall systems. Paper presented at the Proceedings of the Eighth Canadian Masonry Symposium, Jasper, Alta., Canada.

Straube, J., Burnett, E. F. (1999). Rain control and design strategies. Journal of Thermal Envelope and Building Science, 23(1), 41-56. https://doi.org/10.1177/109719639902300

Straube, J., Finch, G. (2009). Ventilated Wall Claddings: review, field performance, and hygrothermal modeling. Building Science Corporation, 1-25.

Straube, J., Smegal, J. (2007). The role of small gaps behind wall claddings on drainage and drying. Paper presented at the Proceedings of 11th Canadian Conference on Building Science and Technology.

Straube, J. F. (1999). Moisture control and enclosure wall systems: University of Waterloo.

Suárez, C., Joubert, P., Molina, J. L., Sánchez, F. J. (2011). Heat transfer and mass flow correlations for ventilated facades. Energy and Buildings, 43(12), 3696-3703. https://doi.org/10.1016/j.enbuild.2011.10.002

Takaoka, M., Sano, T., Yamamoto, H., Mizushima, J. (2009). Convective instability of flow in a symmetric channel with spatially periodic structures. Physics of fluids, 21(2), 024105. https://doi.org/10.1063/1.3067870

Tan, R. C. (1989). Some acceleration methods for iterative computer of derivatives of eigenvalues and eigenvectors. International journal for numerical methods in engineering, 28(7), 1505-1519. https://doi.org/10.1002/nme.1620280704

TenWolde, A., Carll, C., Malinauskas, V. (1995). Airflows and moisture conditions in walls of manufactured homes. Airflow performance of building envelopes, components, and systems, ASTM STP, 1255, 137-155.

Uvsløkk, S. (1988). The importance of wind barriers for insulated wood frame constructions. In Proceedings of the Symposium and Day of Building Physics, 24-26.

Vajravelu, K., Sastri, K. (1978). Free convective heat transfer in a viscous incompressible fluid confined between a long vertical wavy wall and a parallel flat wall. Journal of Fluid Mechanics, 86(2), 365-383. https://doi.org/10.1017/S0022112078001172

Van Belleghem, M., Steeman, M., Janssens, A., De Paepe, M. (2015). Heat, air and moisture transport modelling in ventilated cavity walls. Journal of Building Physics, 38(4), 317-349. https://doi.org/10.1177/1744259114543

Van Straaten, R. (2004). Measurement of Ventilation and Drying of Vinyl Siding and Brick Clad Wall Assemblies. UWSpace. http://hdl.handle.net/10012/909

Van Straaten, R. A. (2017). Pressure Equalization of Wind-Induced Pressures on Residential Vinyl Siding Cladding in Full-Scale. Electronic Thesis and Dissertation Repository. 4940. https://ir.lib.uwo.ca/etd/4940

Vickery, B. (1985). Gust factors for internal pressures in low-rise buildings. Paper presented at the Tenth Canadian Congress of applied mechanics: CANCAM'85. Proceedings.

White, F. M. (1979). Fluid mechanics, 1999. Me Graw-Hill.

Womble, J., Yeatts, B., Cermak, J., Mehta, K. (1995). Internal wind pressures in a full and small-scale building. Paper presented at the Proc., 9th Int. Conf. on Wind Engineering.

Xie, W., Xi, G. (2017). Geometry effect on flow fluctuation and heat transfer in unsteady forced convection over backward and forward facing steps. Energy, 132, 49-56. https://doi.org/10.1016/j.energy.2017.05.072

Xu, Q., Feng, J., Liu, L., Zhou, J., Ye, G., Chang, C. (2019). Analysis of mechanical-fluid-thermal performance of heat pipeline system with structural deformation effects. International Journal of Heat and Mass Transfer, 128, 12-23. https://doi.org/10.1016/j.ijheatmasstransfer.2018.08.122

Xu, Q., Feng, J., Zhang, S. (2017). Combined effects of different temperature and pressure loads on the “L”-type large-diameter buried pipeline. International Journal of Heat and Mass Transfer, 111, 953-961. https://doi.org/10.1016/j.ijheatmasstransfer.2017.04.067

Yan, W., Lin, T. (1989). Effects of wetted wall on laminar mixed convection in a vertical channel. Journal of Thermophysics and Heat Transfer, 3(1), 94-96. https://doi.org/10.2514/3.56231

Yan, W. M. (1993). Mixed convection heat and mass transfer in a vertical channel with film evaporation. The Canadian Journal of Chemical Engineering, 71(1), 54-62. https://doi.org/10.1002/cjce.5450710108

Yang, R. (1989). Shape design sensitivity analysis with frequency response. Computers & Structures, 33(4), 1089-1093. https://doi.org/10.1016/0045-7949(89)90445-8

Yang, YT., Chen, PJ. (2015). Numerical optimization of turbulent flow and heat transfer characteristics in a ribbed channel. Heat Transfer Engineering, 36(3), 290-302. https://doi.org/10.1080/01457632.2014.916158